PUBLISHED BY THE ACADEMY OF SCIENCES OF ALBANIA

JNTS

JOURNAL OF NATURAL AND TECHNICAL SCIENCES

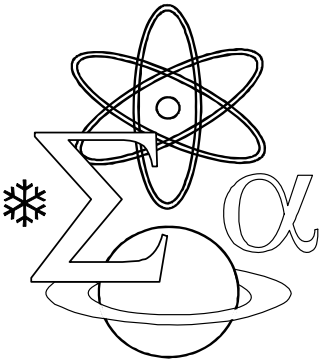

2014, Vol. XIX (1)

FOREWORD

Welcome to the latest issue of the Journal of Natural and Technical Sciences (*JNTS*) for 2014, which has been previously titled Albanian Journal of Natural and Technical Sciences (*AJNTS*) from 1996 to 2013.

I am delighted to welcome the new Editorial Board:

We are very much looking forward to working with all those who are interested in the area of scientific research, building on the outstanding achievements of the forthcoming years.

Our principal aim is to make *JNTS* a prominent international journal, specializing in the rapid publication of innovative, high-quality research articles in the realm of natural and technical sciences. It is our mission now to take the journal forward and to encourage the submission of presently under-represented disciplines.

As the scope of the journal is broad, we also seek to attract submissions that relate to issues of societal interest and development of the country such as quality of life, climate change, pollution, environment and conservation of biodiversity, water resources, health, food security, etc., in support of global agendas that are seminal to natural and technical sciences comprising earth sciences, biology, molecular biotechnology, nanotechnology, chemistry, mathematics, physics, engineering, medicine etc.

We as scientists work beyond frontiers when it comes to issues of common interest. Consequently, we have already started by changing the title of the journal (from 1996 to 2013), a decision approved by all the Members of the Editorial Board. From now on the title of the journal will be *The Journal of Natural and Technical Sciences*.

To old and new readers alike, thank you for your support.

We welcome your papers and we aim to accommodate any wish you might have to help us further the interests of *the journal* and make it the premier journal concerned with all aspects of natural and technical sciences that illustrate the unifying concepts of science with evidence, either observational or theoretical, from any relevant field. We ask you to be part of the activities of the Editorial Board and work together to increase the quality of journal. Consequently, we invite you to write review articles on topics concerned with all aspects of natural and technical sciences. The journal particularly welcomes contributions that illustrate the unifying concepts of science with evidence, either observational or theoretical, from any relevant field.

It is an exciting beginning for the journal, and there is every indication that the forthcoming period will be even better. I look forward to more interesting papers for publication, and for your continuing support.

Academician Prof. Dr Salvatore Bushati
Editor-in- Chief
Academy of Sciences of Albania,
Head of the Section of Natural and Technical Sciences

ACKNOWLEDGEMENTS

The Editors of Journal of Natural and Technical Sciences owes a debt of a special gratitude to all the reviewers listed below for giving their time and expertise to review papers submitted for publication in all volumes of the journal from 2011 to 2013.

Adelaida Andoni
Adem Salillari
Adil Neziraj
Afrim Tabaku
Alban Ibraliu
Alfred Frashëri
Alfred Maliqi
Alketa Lame
Alma Shehu
Alqi Cullaj
Altin Mele
Andon Dodbiba
Andonaq Londo
Andrea Maliqari
Angjelin Shtjefni
Anila Godo
Anila Paparisto
Anila Tanku
Anyla Kasneci
Arben Pambuku
Arjan Beqiri
Arjana Ylli
Artan Tashko
Artur Baxhaku
Artur Tato
Aurel Nuro
Avni Meshi
Bashkim Resuli
Betim Byku
Betim Çiço
Bujar Seiti
Çerçiz Dyrmishi
Daut Veizi
Drini Salto
Dritan Prifti
Dritan Topi
Dhimitër Dhora
Dhimitër Haxhimihali
Dhimitër Kraja
Edion Arapi
Eduard Andoni
Efigjeni Kongjika
Elda Marku
Elinda Kajo
Elton Pasku
Elton Zaka
Eqerem Arkaxhiu
Erion Spahiu
Etleva Hamzaraj
Eva Gavani
Evan Rroco
Fatbardha Babani
Fatbardha Vinçani
Fatmir Hoxha
Fatos Ylli
Fejzi Kavaj
Fejzi Kolaneci
Fisnik Kadiu
Flora Qarri
Genti Guxho
Gëzim Shehu
Gjerogjina Kule (Lito)
Ibrahim Milushi
Idriz Jata
Ilia Ninka
Ilir Alliu
Ilirian Malollari
Ilo Mele
Ismet Beqiri
Jakup Agalliu
Jani Skrami
Jozefita Marku
Jul Bushati
Kapllan Sulaj
Kastriot Misja
Kledi Xhaxhiu
Klementina Puto
Kostandin Dollani
Kostandin Dollani
Kozeta Sevrani
Kristaq Bërxholi
Kujtim Fishka
Lauresha Shabani
Ligor Nikolla
Lila Shundi
Liljana Kola
Linda Fuga
Luljeta Bozdo
Luljeta Qafmolla
Luljeta Xhagolli
Llukan Puka
Margarita Ifti
Merita Nake
Mihallaq Qirja
Mimoza Hafizi

SOME RESULTS OF GREEN'S RELATIONS *L* AND *R* IN RINGS

Rigena SEMA and Petraq PETRO
Department of Mathematics, Faculty of Natural Sciences,
University of Tirana, Tirana, Albania

ABSTRACT

In this paper, firstly we show certain relations that hold between the equivalence classes of the relations L and R in a ring A and the respective equivalence classes of the Green's relations $L(\bullet)$ and $R(\bullet)$ defined on the multiplicative semigroup of the ring A. Further, using these relations we study a case when a minimal left [right] ideal remains the same in the multiplicative semigroup of the ring A. Lastly, we study the behavior of a ring which does not have the identity element and does not have zero divisors, also rings, which are and simple.
Keywords: Ring, division ring, semigroup, left ideal, right ideal, Green's relations

1. INTRODUCTION

By a ring we mean an associative ring, which does not necessary has an identity element. The Green's relations L and R in the rings are introduced by Petro (1981) and further are studied by Steinfeld (1988) and Petro (2002). These relations mimic the relations L and R in semigroups which are introduced and studied by James Aleksander Green (Green, 1951) from whom they got the name. This is the reason that the relations and in rings are called Green's relations in the rings. We will denote by L and R the Green's relations in a ring $(A,+,\bullet)$, meanwhile the Green's relations in the multiplicative semigroup $(A,\bullet)$ of this ring will be denoted by $L(\bullet)$ and $R(\bullet)$ to be distinguished from those of the ring $(A,+,\bullet)$. These two kinds of relations are determined by the equalities of the principal left ideals and the principal right ideals of the ring $(A,+,\bullet)$ and it's multiplicative semigroup $(A,\bullet)$. Firstly, in this paper we show the relation that exists between the equivalence classes under the Green's relations L and R of a ring and

respective equivalence classes under the relations $L(\bullet)$ and $R(\bullet)$ of the multiplicative semigroup of this ring. Further, by using these relations we show a sufficient condition for a minimal left [right] ideal of a ring to remain minimal in the multiplicative semigroup of this ring. Lastly, we study Green's relations in rings, which do not have an identity element and divisors of zero and L-simple rings and R-simple rings by preliminarily specifying them as rings which have only two equivalence classes. At the end of the paper an open problem is raised.

2. ***Preliminaries***

We give some notions and present some auxiliary results that will be used throughout the paper.

Let $(A,+,\bullet)$ be a ring and *B*, *C* two subsets of *A*. We note:

$$B+C=\{b+c\in A: b\in B, c\in C\}$$
$$BC=\left\{\sum_{i=1}^{n} b_i c_i \in A: b_i\in B, c_i\in C\right\}$$

For simplicity we will write *bC* instead of *{b}C* and *Bc* instead of *B{c}*.

The Green's relations L and R in a ring *A* (Petro, 2002) are defined as follows:

$$\forall (a,b)\in A^2, aLb \Leftrightarrow (a)_l=(b)_l,$$
$$\forall (a,b)\in A^2, aRb \Leftrightarrow (a)_r=(b)_r,$$

where $(a)_l$, $(b)_l$, $(a)_r$, $(b)_r$ are the principal left ideals and principal right ideals generated by the elements *a, b* of *A*, respectively. The equivalence class $\bmod L$ and the equivalence class $\bmod R$ containing the element *a* of *A* are denoted by L_a and R_a respectively.

It is easily seen that for every element *a* of a ring *A*, the set *Aa* is a left ideal of *A*, *aA* is a right ideal of *A* and the following equalities are true:

$$(2.1)\qquad (a)_l=Za+Aa,$$

$$(2.2)\qquad (a)_r=Za+aA.$$

If in the above definitions of Green's relations *L* and *R* in the ring *A*, we replace the ring *A* with an arbitrary semigroup *S* and the principal left [right] ideals $(a)_l$, $(b)_l$, $[(a)_r,(b)_r]$ we regard as principal left [right] ideals

generated by the elements *a, b* of semigroup *S*, then we have Green's relations in the semigroup *S*, which we will denote by the same symbol as Green's relations in the ring *A*. In this paper, to distinguish between the Green's relations L and R in the ring $(A,+,\bullet)$ from the Green's relations in the multiplicative semigroup $(A,\bullet)$ of this ring, these latter ones will be denoted by $L(\bullet)$ and $R(\bullet)$. Also, the equivalence classes of the element *a* of the multiplicative semigroup $(A,\bullet)$ of the ring $(A,+,\bullet)$ under the Green's relations $L(\bullet)$ and $R(\bullet)$ will be denoted by $L_a(\bullet)$ and $R_a(\bullet)$.

Proposition 2.1. (Howie, 1995). Let *S* be a cancellative semigroup (that is a semigroup in which, for all *a, b, c*, $ca = cb \Rightarrow a = b$ and $ac = bc \Rightarrow a = b$) and suppose that *S* has not an identity. Then $L = R = 1_A$.

Proposition 2.2. (Steinfeld, 1978). A ring *A* has no proper left [right] ideals if and only if it is either a division ring or a zero ring of some prime order.

3. ***Main results***

Let $(A,+,\bullet)$ be an arbitrary ring. We have the Green's relations *L* and *R* in the ring $(A,+,\bullet)$ and the Green's relations $L(\bullet)$ and $R(\bullet)$ in the multiplicative semigroup $(A,\bullet)$ of this ring. If the ring has an identity element, then from the equalities (2.1), (2.2) follows immediately that $L = L(\bullet)$ and $R = R(\bullet)$. Generally, from the equalities (2.1), (2.2) it is obvious that $L(\bullet) \subseteq L$ and $R(\bullet) \subseteq R$.

The following example shows that these inclusions may be strict ones.

Example 3.1. Let $S = \{0, e, a, b\}$ be the semigroup given by the following Cayly table (Clifford, 1978)

·	e	a	b	0
e	e	a	0	0
a	0	0	0	0
b	b	0	0	0
0	0	0	0	0

Consider the semigroup ring of semigroup *S*, over the ring of integers Z. In this ring we have:

$$-a \in L_a, -a \notin L_a(\bullet), -b \in R_a, -b \notin R_a(\bullet).$$

This example also shows that generally the Green's relations *L* and *R* in a ring are different from Green's relations $L(\bullet)$ and $R(\bullet)$ in the multiplicative semigroup of this ring. So, the Green's relations in a ring that we study in this paper are different from Green's relations in a ring defined as Green's relations in its respective semigroup (Nai-feng, 2002).

Theorem 3.2. Let $(A,+,\bullet)$ be a ring and *a* an element of *A*. Then *L*-class [*R*-class] L_a [R_a] is either a union of $L(\bullet)$-classes [$R(\bullet)$-classes] of the multiplicative semigroup $(A,\bullet)$ of the ring $(A,+,\bullet)$, which must have a single element, or $L_a = L_a(\bullet)$ [$R_a = R_a(\bullet)$].

Proof. There are two possible cases:

Case 1. Every $L_x(\bullet)$ class, which is inclused in L_a has only one element. Then we have:

$$L_a = \bigcup_{x \in L_a} L_x(\bullet).$$

Case 2. There is one class $L_b(\bullet)$, $b \in L_a$, which has at least two elements. Let *b* and *c* be two different elements of *A*, which belong to $L_b(\bullet)$. Then exist the elements *u, v* of *A* such as *b=uc* and *c=vb*. For every element $b \in L_a$, there exist integers k_1, k_2 and the elements u_1, u_2 of *A* such that:

$$d = k_1 c + u_1 c \text{ and } c = k_2 d + u_2 d.$$

By making suitable replacements, we have:

$$d = k_1 c + u_1 c = k_1 vb + u_1 vb = (k_1 v + u_1 v)b,$$
$$b = uc = u(k_2 d + u_2 d) = (k_2 u + uu_2)d,$$

which means that $dL(\bullet)b$. So, $d \in L_b(\bullet) \subseteq L_a(\bullet)$, and consequently $L_a \subseteq L_a(\bullet)$. Now, it's evident that $L_a = L_a(\bullet)$. The proof for the class R_a runs similarly. ■

Definition 3.3. Two elements *a,b* of the ring *A* are called right [left] divisors to each other if there are elements *c,d* of *A* such that *a=cb*[*a=bc*] and *b=da*[*b=ad*].

The elements *a* and *b* of the ring *A* are called divisors to each other when they are left divisors and right divisors to each other.

Corollary 3.4. Let *a* be a non-zero element of the ring $(A,+,\bullet)$. If the principal left [right] ideal $(a)_l[(a)_r]$ of the ring $(A,+,\bullet)$ is minimal and there is an element $b \neq a$ such that *a* and *b* are right [left] divisors to each other, then $(a)_l[(a)_r]$ is a minimal principal left [right] ideal of the multiplicative semigroup $(A,\bullet)$ of this ring.

Proof. It is easily seen that the elements $b \neq a$ belong to the $L(\bullet)$-class of the multiplicative semigroup $(A,\bullet)$ of the ring $(A,+,\bullet)$. From **Theorem 3.2**, we have these equalities:

$$L_a \bigcup 0 = (a)_l = L_a(\bullet) \bigcup 0.$$

In the other hand, if we denote $(a)_l^s$ the principal left ideal of the multiplicative semigroup $(A,\bullet)$ of the ring $(A,+,\bullet)$, which is generated by the elements $a \in A$, we have:

$$L_a(\bullet) \bigcup 0 = (a)_l^s \subseteq (a)_l = L_a(\bullet) \bigcup 0.$$

Hence, $(a)_l^s = (a)_l = L_a(\bullet) \bigcup 0$. Now, it is evident that $(a)_l$ is a minimal left ideal of the multiplicative semigroup $(A,\bullet)$ of the ring $(A,+,\bullet)$. ■

If an *L*-class has only one element *a*, then it is clear that $L_a - L_a(\bullet)$. The following proposition shows a case when the only *L*-classes and *R*-classes of the ring $(A,+,\bullet)$ that coincide with the respective $L(\bullet)$-classes and $R(\bullet)$-classes of the multiplicative semigroup $(A,\bullet)$ of this ring are those that have only one element.

Proposition 3.5. Let $(A,+,\bullet)$ be a ring without multiplicative identity and without zero divisors with at least two elements. Then the only *L*-classes [*R*-classes] in the ring $(A,+,\bullet)$ that coincide with the respective $L(\bullet)$-classes [$R(\bullet)$-classes] in the multiplicative semigroup $(A,\bullet)$ of this ring are those, which have only one element.

Proof. Since the ring $(A,+,\bullet)$ does not have divisors of zero, then the set $A^* = A \setminus 0$ is closed under the multiplication on the ring A and form a semigroup with respect to the multiplication induced in it. It is clear that the semigroup $(A^*,\bullet)$ does not have an identity and it is a cancellable semigroup. We see that for every element $a \neq 0$ of A, the class $L_a(\bullet)$ of the element a of the semigroup $(A,\bullet)$ coincide with the respective class of the semigroup $(A^*,\bullet)$, which has only one element, exactly the element a, by **Proposition 2.1**. From **Theorem 3.2**, we have $L_a = L_a(\bullet)$ if and only if L_a has one element. The proof for the relation R runs similarly. ■

From this proposition we obtain immediately the following corollary:

Corollary 3.6. Let $(A,+,\bullet)$ be a ring without zero divisors and without a multiplicative identity. The Green's relations L and R coincide with the Green's relations $L(\bullet)$ and $R(\bullet)$ in multiplicative semigroup $(A,\bullet)$ of the ring $(A,+,\bullet)$ if and only if $L = R = 1_A$, where 1_A is the identity relation in A.

Above we saw an extreme case when Green's relations L and R in a ring are the finest possible, which means that the equivalence class *modL* and the equivalence class *modR* has only one element.

Now, we will examine another extreme case, precisely the case when the Green's relations in a ring are the thickest possible, i.e. when every two non-zero elements of a ring are equivalent under this relations. In this case it is clear that for every $a \in A \setminus 0$, we have $L_a = R_a = A \setminus 0$.

We will call a ring A with at least two elements, L-simple [R-simple] ring if the only equivalence classes under these relations are 0 and $A \setminus 0$.

Utilizing **Proposition 2.2**, we get the following:

Proposition 3.7. For every ring A, with at least two elements the following conditions are equivalent:

1) The ring A is a division ring.
2) The ring A is not a zero-ring (with zero multiplication) and it is -simple.
3) The ring A is not a zero-ring and it is R-simple.

Proof. We will prove the equivalence of the proposition 1) and 2). The proof of equivalence $1) \Leftrightarrow 3)$ runs similarly.

Suppose that the ring A is a division ring. Then A is not a zero-ring and for every non zero element $a \in A$ we have:

$$A = Aa \subseteq (a)_l \subseteq A .$$

So,

$$\forall (a,b) \in A^* = A \setminus 0, (a)_l = A = (b)_l ,$$

and consequently the ring A is L-simple.

Conversely, suppose that the ring A is not a zero-ring and it is L-simple. Let a be an element different from zero of the ring A, which exist because the ring is not with zero multiplication. Since $L_a = A \setminus 0$, we have:

$$A = L_a \bigcup 0 \subseteq (a)_l \subseteq A .$$

So, the ring A does not have proper left ideals and by **Proposition 2.2** the ring is a division ring. ■

From the above proposition and the **Proposition 2.2** we get immediately this:

Corollary 3.8. For every infinite ring A, the following propositions are equivalents:

1) The ring A is a division ring.
2) The ring A is L-simple.
3) The ring A is R-simple.

From **Proposition 3.7** it follows immediately that if a ring $(A,+,\bullet)$ is L-simple [R-simple], then the relations $L[R]$ in the ring $(A,+,\bullet)$ coincide with Green's relations $L(\bullet)$ [$R(\bullet)$] in the multiplicative semigroup of this ring.

Conversely, if the multiplicative semigroup of the ring $(A,\bullet)$ is $L(\bullet)$-simple [$R(\bullet)$-simple], then the only equivalence $L(\bullet)$ [$R(\bullet)$]-classes are 0 and $A \setminus 0$, so it is evident that the ring $(A,+,\bullet)$ is L [R]-simple.

So in the second extreme case, when the Green's relations in a ring $(A,+,\bullet)$ are trivial, then they coincide with the respective Green's relations in the

multiplicative semigroup $(A,\bullet)$ of this ring and vice-versa. While in the first extreme case, we saw that this coincidence does not hold (we saw a special case when we have this coincidence).

So, it is natural to raise the following problem.

Problem. Find necessary conditions, sufficient conditions, necessary and sufficient conditions, so that if in the ring $(A,+,\bullet)$ the Green's relation $L(\bullet)$ [$R(\bullet)$] in the multiplicative semigroup $(A,\bullet)$ of this ring is the identy relation 1_A, then the relation *L* [*R*] is equal to 1_A.

REFERENCES

Cliford AH. 1978. Remarks on minimal quasi-ideals in semigroups. Semigroup Forum. **16(1),** 183-196, USA.

Green JA. 1951. On the structure of semigroups, *Annals of Mathematics*. **54 (1)**, 163-172, USA.

Howie JM. 1995. Fundamentals of semigroup theory, Oxford University Press, USA.

Nain-feng Zh. 2002. Green's equivalences on gamma rings. *Journal of Guizhou Natural University (Natural Sciences*).**20**,(**4**),. 44-46, China.

Petro P. 1982. Two Green's type theorems for rings, BSHN, **No.2**, 17-22, Albania.

Petro P. 2002, Green's relations and minimal quasi-ideals in rings, Communication in. Algebra **30** (**10**), pp. 4677-4686. USA.

Steinfeld O. 1978. Quasi-ideals in rings and semigroups, Disqusitiones Mathematicae Hungaricae **10** Akademiai Kiodo, Budapest, Hungary.

Steinfeld O. 1988. On canonical quasi-ideals in rings, Annales Universitatis. Scientarium, Budapesinensis de Rolando Eötvös Nominatae Sectio. Mathematica. 171-178, Hungary.

THE NUMERICAL SIMULATION OF NONLINEAR COBWEB MODEL IN MATLAB

Pranvera MULLAJ
Faculty of Economy, University of Tirana, Albania
Eglantina XHAJA and Fatmir HOXHA
Faculty of Natural Sciences, University of Tirana, Albania

ABSTRACT

The cobweb model or cobweb theory is an economic model that explains why prices might be subject to periodic fluctuations in certain types of markets. It describes cyclical supply and demand in a market where the amount produced must be chosen before prices are observed. The case when the supply and the demand are nonlinear functions is here reported. In addition, the stability of the system is analyzed via numerical simulations.
***Keywords**:* cobweb, nonlinear, demand, supply, stability, market

1. INTRODUCTION

The cobweb models describe the dynamics of the price in a market. Chiarella (1998), Hommes (1994) and Matsuomo (1999) reported on cobweb chaos. Finkenstadt (1995) applied the model when the supply is a linear function and the demand a nonlinear function. Hommes (1994), Jensen and Urban (1999), Ma and Mu (2007) and Pou (2000) used the linear function of the demand and nonlinear function of the supply. All the aforementioned papers report that the nonlinear cobweb model explains different fluctuations observed even in real economic data. The case when the supply and the demand are nonlinear functions is here reported.

2. A case of a nonlinear models

Suppose that the estate developers in the market belong to a benefit group that have a common benefit target. Usually the price p characterizes the nonlinear demand function $p = a - b\sqrt{Q}$, where *a, b* are positive constants, a is the maximum price in market and Q is the total amount in the market. The relations of these quantities are formalized as follows:

$$\kappa_1(t) = b_0 - b_1 p_1(t) + b_2 p_1^2(t),\ \kappa_2(t) = c_0 - c_1 p_2(t) + c_2 p_2^2(t) \quad (2.1)$$

where $b_0, b_1, b_2, c_0, c_1, c_2$ are positive constants, $p_1(t)$ is the land price in time period t, $p_2(t)$ is the housing price in time period *t*, $K_1(t)$ is the land demand in time period *t* and $K_2(t)$ is the housing demand in time period *t*. Due to the law of demand that the slope of demand curve is negative, the prices $p_1(t)$ and $p_2(t)$ must fulfil the inequalities: $2b_2 p_1(t) - b_1 < 0$ and $2c_2 p_2(t) - c_1 < 0$; $4b_2 b_0 - b_1^2 > 0$, $4c_2 c_0 - c_1^2 > 0$, so the signs of demand equations in formulae (2.1) are positive. Here, the land price and housing price are proportional, even though the housing market does not directly have any impact on land market. The land price is of great impact for the housing, which decreases as the land price increases. The real estate companies adjust the housing supply according to relative policies and the situation of housing price and land price. The supply formula is given as follows:

$$S_1(t) = e_0 + e_1 p_1(t) + e_2 p_1^2(t),\ S_2(t) = d_0 + d_1 p_2(t) + d_2 p_2^2(t) - d_3 p_1(t) \quad (2.2)$$

where $d_0, d_1, d_2, d_3, e_0, e_1, e_2$ are positive constants, $S_1(t)$ is the land supply in time period t, and $S_2(t)$ is the housing supply in the time period t. As $2e_2 p_1(t) + e_1 > 0$ and $2d_2 p_2(t) + d_1 > 0$, we must confirm that the slope of the supply curve is positive. In addition, we must confirm that it is in accordance with the supply law. Providers begin to supply the products only when

$$p_1(t) > \frac{-e_1 + \sqrt{e_1^2 - 4e_2 e_0}}{2e_2},\ p_2(t) > \frac{-d_1 + \sqrt{d_1^2 - 4d_2 d_0}}{2d_2}. \quad (2.3)$$

Let define,

$$Z(p) = K(p) - S(p). \quad (2.4)$$

$Z(p)$ is the demand function increasing with price, which denotes the difference between the demand and supply. When the price is low, we say that excess demand exist and when the price is high, excess supply exists, so p^* satisfies the equation $Z(p^*) = 0$ and p^* is called equilibrium point.

Substituting (2.1) and (2.2) in (2.4), we obtain:

$$\begin{aligned} Z(p_1(t)) &= b_0 - e_0 - (e_1 + b_1)p_1(t) + (b_2 - e_2)p_1^2(t), \; t = 0,1,2,\cdots \\ Z(p_2(t)) &= c_0 - d_0 - (d_1 + c_1)p_2(t) + (c_2 - d_2)p_2^2(t) + d_3 p_1(t). \end{aligned} \tag{2.5}$$

Since $Z(p)$ follows the law of demand, the following conditions hold:

$$\begin{aligned} b_2 - e_2 &> 0, \\ c_2 - d_2 &> 0, \\ 2(c_2 - d_2)p_2(t) - (d_1 + c_1) &< 0, \\ 2(b_2 - e_2)p_1(t) - (e_1 + b_1) &< 0. \end{aligned} \tag{2.6}$$

α_1 is the adjustment parameter of the land price, which denotes the adjustment degree of benchmark land price controlled by government through the land supply plan. α_2 is the adjustment parameter of housing price, the dynamic model of land price and housing price can be established as follows:

$$\begin{aligned} p_1(t) &= p_1(t-1) + \alpha_1 Z(p_1(t-1)), t = 0,1,2,\cdots \\ p_2(t) &= p_2(t-1) + \alpha_2 Z(p_2(t-1)). \end{aligned} \tag{2.7}$$

where α_1 and α_2 are positive constants.

1. The stability analysis

a. **Bifurcation and chaos**. From the expansion of formulae (2.7) is obtained:

$$\begin{aligned} p_1(t) &= p_1(t-1) + \alpha_1[b_0 - e_0 - (e_1 + b_1)p_1(t-1) + (b_2 - e_2)p_1^2(t-1)] \\ p_2(t) &= p_2(t-1) \\ &\quad + \alpha_2[c_0 - d_0 - (d_1 + c_1)p_2(t-1) + (c_2 - d_2)p_2^2(t-1) + d_3 p_1(t-1)] \\ &\quad t = 0,1,2,\cdots \end{aligned} \tag{3.1}$$

where $p_1(t)$ is the land price in time period t, $p_2(t)$ is the housing price in time period *t*.

Let,

$$u = \frac{\alpha_1(e_2-b_2)}{1+\alpha_1\sqrt{(e_1+b_1)^2-4(e_2-b_2)(e_0-b_0)}},$$
$$U = \frac{1}{2} - \frac{1}{2}\frac{1-\alpha_1(e_1+b_1)}{1+\alpha_1\sqrt{(e_1+b_1)^2-4(e_2-b_2)(e_0-b_0)}}, \quad (3.2)$$
$$x(t) = up_1(t) + U.$$

Another form of the first equation of (3.1) is:

$$x(t) = \lambda x(t-1)(1-x(t-1)), \quad (3.3)$$

where $\lambda = 1 + \alpha_1\sqrt{(e_1+b_1)^2 - 4(e_2-b_2)(e_0-b_0)}$. This is the general form of the discrete logistic equation. The stability of $x(t)$ varies along with variety of λ according to logistic rule.

If $\alpha_1 < 0$, then $\lambda < 1$ implies that exist only one fixed point in system (3.1), however $\alpha_1 < 0$ is insignificant.

If $0 \leq \alpha_1 < 2/\sqrt{(e_1+b_1)^2 - 4(e_2-b_2)(e_0-b_0)}$, then $1 \leq \lambda < 3$ implies that exist two fixed points in system (3.1) and bifurcation appears.

If, $2/\sqrt{(e_1+b_1)^2 - 4(e_2-b_2)(e_0-b_0)} \leq \alpha_1 \leq \sqrt{6}/\sqrt{(e_1+b_1)^2 - 4(e_2-b_2)(e_0-b_0)}$, then $3 \leq \lambda \leq 1+\sqrt{6}$ implies that exist 4 fixed points in system (3.1) and period-doubling bifurcation appears. When λ increases, the number of fixed points continues to grow until $\lambda = 3.5699$;

when $\alpha_1 = 2.5699/\sqrt{(e_1+b_1)^2 - 4(e_2-b_2)(e_0-b_0)}$, the value of $x(t)$ is not equal in every point that appeared before, the system enters chaos from period doubling bifurcation.

The same argument holds even for the second equation of formulae (3.1). Let $\alpha_1 = 0$:

When $0 < \alpha_2 < 2/\sqrt{(d_1+c_1)^2 - 4(d_0-c_0)(d_2-c_2)}$, bifurcation occurs.

When $2/\sqrt{(d_1+c_1)^2 - 4(d_0-c_0)(d_2-c_2)} \leq \alpha_2 \leq \sqrt{6}/\sqrt{(d_1+c_1)^2 - 4(d_0-c_0)(d_2-c_2)}$, period doubling bifurcation occurs.

When $\alpha_2 = 2.5699/\sqrt{(d_1+c_1)^2 - 4(d_0-c_0)(d_2-c_2)}$, system enters chaos.

b. **Stability analysis**. In the following we will discuss about the stability of the fixed

points of the dynamic system (3.1) through the analysis of the eigenvalues of the linear asymptotic equation of formulae (3.1). Four fixed points of difference function (3.1) are obtained

$$E_1\begin{cases} p_1 = \frac{b_1+e_1\pm\sqrt{(e_1+b_1)^2-4(e_2-b_2)(e_0-b_0)}}{2(b_2-e_2)} \\ p_2 = \frac{d_1+c\pm\sqrt{(d_1+c_1)^2-4(c_2-d_2)(c_0-d_0+d_3p_1)}}{2(c_2-d_2)} \end{cases} \tag{3.4}$$

if:

$$(e_1+b_1)^2-4(e_2-b_2)(e_0-b_0)\geq 0, \qquad (d_1+c_1)^2-4(c_2-d_2)(c_0-d_0+d_3p_1)\geq 0. \tag{3.5}$$

Lemma 3.1. The equilibrium

$$E_1\left(\frac{b_1+e_1\pm\sqrt{(e_1+b_1)^2-4(e_2-b_2)(e_0-b_0)}}{2(b_2-e_2)}, \frac{d_1+c\pm\sqrt{(d_1+c_1)^2-4(c_2-d_2)(c_0-d_0+d_3p_1)}}{2(c_2-d_2)}\right) \tag{3.6}$$

is an unstable equilibrium point. The proof of this Lemma can be found in (Ma and Mu, 2007).

2. Numerical simulations

To study the dynamics of system (3.1) it is suitable the use of the parameters with the following values:

$$b_0=1.2, b_1=2, b_2=1.6, c_0=4, c_1=1.6, c_2=0.04,$$
$$d_0=0, d_1=3, d_2=0.02, d_3=0.4, e_0=0.5, e_1=0.3, e_2=0.2. \tag{4.1}$$

Below is simulated the discrete logistic model (3.1) for different values of α_1, according to the analysis discussed in paragraph 3.1. For what is said above

$$\lambda = 1+\alpha_1\sqrt{(e_1+b_1)^2-4(e_2-b_2)(e_0-b_0)}.$$

The following cases could be distinguished:

Case 1.1: $\alpha_1 < 0, (\alpha_1 = -1)$ so $\lambda = 0.1705$. The values of the parameters from (4.1) are a means to address the following graph:

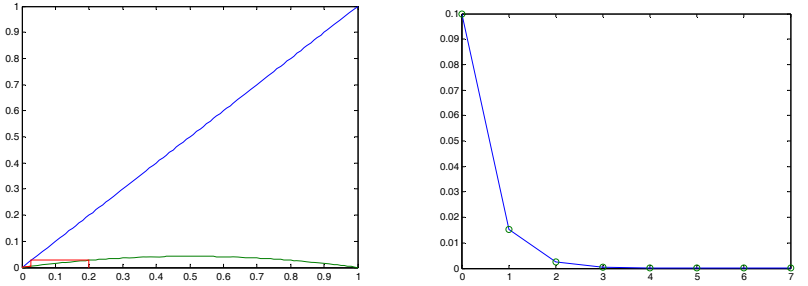

Figure 1.1 The approximation of cobweb model for $\lambda = 0.1705$, $x_0 = 0.1$, $n = 7$.

We can see from the graph that the system has only one fixed point.

Case 1.2: $0 \leq \alpha_1 < 2/\sqrt{(e_1 + b_1)^2 - 4(e_2 - b_2)(e_0 - b_0)}$, for the values of the parameters from (4.1) $0 \leq \alpha_1 < 1.7087, (\alpha_1 = 1)$, so $\lambda = 2.1705$ is obtained the following graph:

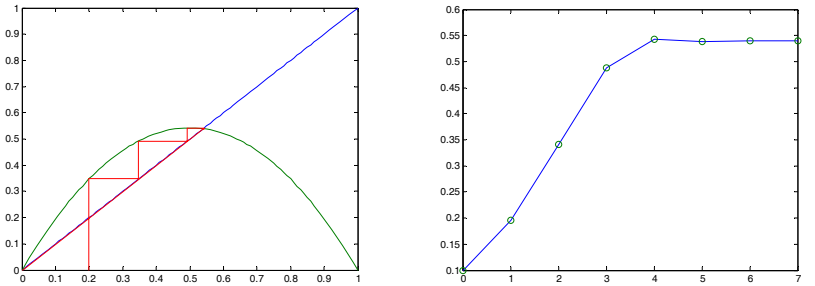

Fig. 1.2 The approximation of cobweb model for $\lambda = 2.1705$, $x_0 = 0.1$, $n = 7$.

We see that the system has two fixed points and bifurcation occurs.

Case 1.3:

$0 \leq \alpha_1 < 2/\sqrt{(e_1 + b_1)^2 - 4(e_2 - b_2)(e_0 - b_0)}$ $0 \leq \alpha_1 < 2/\sqrt{(e_1 + b_1)^2 - 4(e_2 - b_2)(e_0 - b_0)}$,

for the values of parameters from (4.1) $1.7087 \leq \alpha_1 < 2.0927, (\alpha_1 = 2)$, so $\lambda = 3.35$ is obtained the following graph:

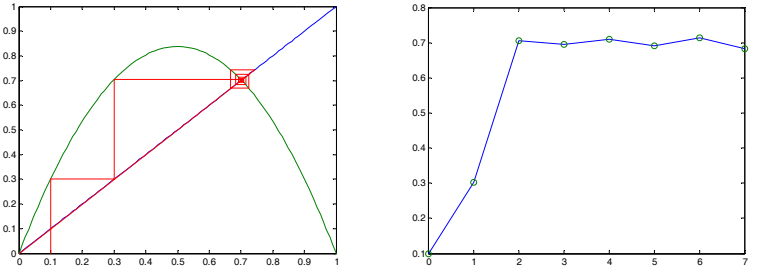

Fig. 1.3 The approximation of cobweb model for $\lambda = 3.35$, $x_0 = 0.1$, $n = 7$.

We see that the system enters chaos.

Case 2.1

Let see the simulation of the second equation of the formulae (3.1). Let $\alpha_1 = 0$:

When, $0 < \alpha_2 < 2/\sqrt{(d_1 + c_1)^2 - 4(d_0 - c_0)(d_2 - c_2)}$, for the values of the parameters of (4.1) $0 < \alpha_2 < 0.4381$ ($\alpha_2 = 0.2$) so $\lambda = 1.913$ bifurcation occurs.

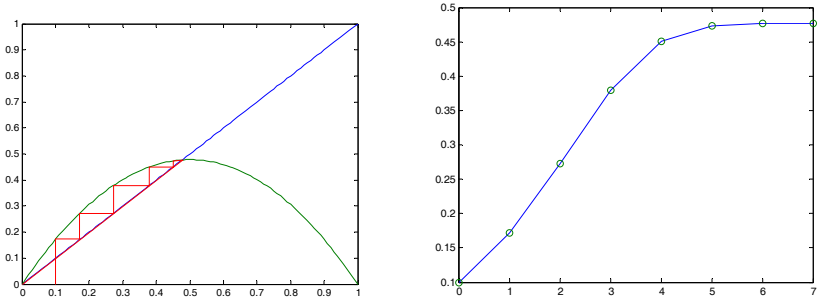

Figure 1.4 The approximation of cobweb model for $\lambda = 1.913$, $x_0 = 0.1$, $n = 7$.

Case 2.2

When $2/\sqrt{(d_1 + c_1)^2 - 4(d_0 - c_0)(d_2 - c_2)} \leq \alpha_2 \leq \sqrt{6}/\sqrt{(d_1 + c_1)^2 - 4(d_0 - c_0)(d_2 - c_2)}$, for the values of parameters of (4.1) $0.4381 < \alpha_2 < 0.5366$ ($\alpha_2 = 0.5$) so $\lambda = 3.2826$ period doubling bifurcation occurs.

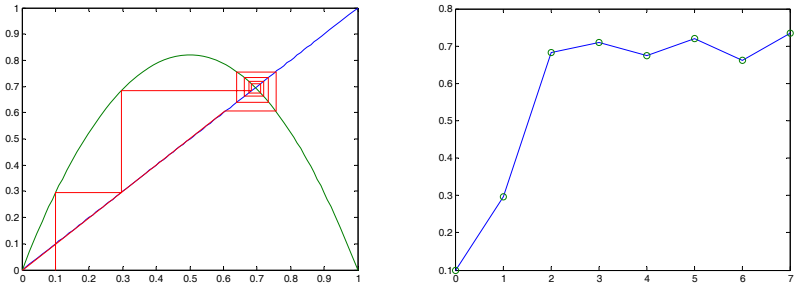

Figure 1.5 The approximation of cobweb model for $\lambda = 3.2826$, $x_0 = 0.1$, $n = 7$.

Case 2.3

When $\alpha_2 = 2.5699/\sqrt{(d_1 + c_1)^2 - 4(d_0 - c_0)(d_2 - c_2)}$, for the values of parameters of (4.1) $\alpha_2 = 2.5699/4.5651$ ($\alpha_2 = 0.5629$) so $\lambda = 3.5697$ system enters chaos.

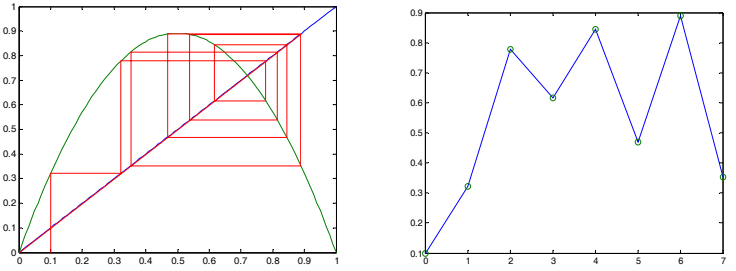

Figure 1.6 The approximation of cobweb model for $\lambda = 3.5697$, $x_0 = 0.1$, $n = 7$.

3. CONCLUSIONS

The present paper provides information about a nonlinear model for the real estate market based in the cobweb model. This is a model for nonlinear supply and demand functions. Numerical simulations are performed in Matlab. Results report that the land supply is of great impact for the real estate market. In addition, that small oscillations make possible that the market enters chaos. Combining land price with the housing price make passing from chaos in a stationary situation possible.

REFERENCES

Chiarella C. 1988. The cobweb model, its instability and the onset of chaos. *Economic Modeling*. **5, (4)** 377-384.

Finkenstadt B. 1995. Nonlinear Dynamics in Economics: A theoretical and Statistical Approach to Agricultural Markets, Lecture Notes in Economics and Mathematical Systems, no.426, Springer, Berlin, Germany.

Hommes CH.1994. Dynamics of the cobweb model with adaptive expectations and nonlinear supply and demand. *Journal of Economic Behaviour & Organization*. **24, (3),** 315-335.

Jensen RV, Urban R. 1984. Chaotic price behavior in a nonlinear cobweb model. *Economics Letters*. **15, (3-4),** 235–240.

Ma J, Mu L. 2007. Complex dynamics in a nonlinear cobweb model for real estate market, Discrete Dynamics in Nature and Society, art. ID. 29207.

Matsumoto A. 1999. Preferable disequilibrum in a nonlinear cobweb economy. *Annals of Operations Research*.**89,** 101-123.

Puu T.2000. Atractors, Bifurcations and Chaos: nonlinear Phenomena in Economics, Springer, Berlin, Germany, 2000.

IMPROVING THE CALCULATION RESULTS OF LATTICE SPACING FROM $Q\bar{Q}$ POTENTIAL

Dafina XHAKO, Rudina ZEQIRLLARI and Artan BORIÇI
Department of Physics, Faculty of Natural Sciences, University of Tirana, Albania

ABSTRACT

In the area of Lattice Quantum Chromodynamics, the potential between a static quark and antiquark that can be calculated from the Wilson loops is of considerable theoretical interest. High-Performance Computing Infrastructure for South East Europe's Research Communities (HP-SEE) has recently carried out project on the calculation of lattice spacing and the results are here reported. Parallel computing with FermiQCD software to recalculate the static quark-antiquark potential is here applied. Consequently, the method has been improved. Improvement concerns the symmetrisation of Wilson loops, as in the Euclidian space-time there is no specified direction for time or space and, the improvement of statistical errors of lattice spacing using weighted coefficients with Jackknife method. Simulation involving SU(3) gauge field configuration was used to obtain the quark-antiquark potential for different values of coupling constant and for 8^4, 12^4 and 16^4 lattice volume. The calculations are performed for 100 configurations, statistically independent, of the gauge fields of the lattice. The behaviour of calculated potential from quarks distance, shows that quarks are confined into hadrons. Here, the results of lattice spacing for different lattice volume and the respective statistical errors are reported. The calculated values of lattice spacing are compared with the values of lattice spacing from Sommer's parameterization and results show that they are within the range of errors found.
***Keywords**:* lattice spacing, quark-antiquark potential, symmetrisation of Wilson loops, weighted coefficients

1. INTRODUCTION

The lattice formulation, Lattice-QCD (Gattringer and Lang, 2009) is one of the most powerful non-perturbative methods to "solve" Quantum Chromodynamics theory. It is a lattice gauge theory formulated on a grid or lattice of points in space and time, where fields representing quarks are defined at lattice sites while the gluon fields are defined on the links

connecting neighboring sites. This formulation of QCD in discrete rather than continuous space-time naturally introduces a momentum cut off at the order 1/a, where a is the lattice spacing, which regularizes the theory. This approximation approaches continuum QCD as the spacing between lattice sites is reduced to zero. As a result lattice QCD is mathematically well-defined. Its power comes mainly from the possibility to evaluate physical quantities "exactly" via numerical simulations, yielding a method to test whether QCD provides the correct framework for describing strong interactions. The lattice spacing plays the role of the ultraviolet regulator, rendering the quantum field theory finite.

The potential between a static quark and antiquark defines the energy of gauge fields in the presence of two static color sources separated by a distance R. At large distances quark confinement shows up and perturbative methods are no longer able to describe the behavior of physical observables; in this context, lattice gauge theories play an important role. Lattice results can be used to investigate non-perturbative features of the static quark potential and to test the range of validity of perturbation theory, which is still an important phenomenological issue which has to be investigated more precisely. The Creutz and Moriarty (1982) computer experiment to measure the static quark-antiquark potential basically relates to quarks are confinement, so that the static potential exhibits a linear rise at large distances. Recent lattice studies (Schilling et al., 1993; Deldar, 2000; Bali, 2000; Paris et al., 1983) confirm the existence of the linear potential for the intermediate distances or the fundamental and higher representations in SU(3). Based on these measurements, quarks are confined in all representations of SU (3).

Basing on the aforementioned results, Xhako et al., (2012) calculated the static quark-antiquark potential in quenched approximation using high parallel calculation techniques for lattices with different volume. Results report that further improvement is needed, as the error of lattice spacing a is too small to justify the difference between $a\_$ calculated and a from Sommer's parameterization (Sommer, 1993). In the present investigation the calculation method of interquark potential is improved symmetrizing the Wilson loops because in the Euclidian space-time there is no specified direction for time or space. In addition, the statistical errors of lattice spacing are improved using weighted coefficients via the Jackknife method.

2.MATERIALS AND METHODS

Wilson loops were introduced by Wilson (1974) as an attempt to a non-perturbative formulation of quantum chromodynamics. The measurements on the lattice of the potential, related to Wilson loop measures, have parallel

histories laying in (Stack, 1983; Grifiths et al., 1983; Campbell et al., 1984; Campbell et al., 1988; Perantonis et al., 1989).

The potential is extracted from so called Wilson loops W(R,T), which are defined to be the trace of path-ordered products of link variables $U_\mu(n)$ along the path C(R,T). This loop construction corresponds to the world lines of a quark-antiquark pair at rest, separated by distance R from each other and "travelling" over time separation T. In Euclidian time, this observable will reveal the static "ground state" energy for large T values. To calculate the energy we start from the correlate function of quark antiquark operator for different time:

$$W(R,T) = \left\langle 0 \left| O_R(0) O_R(T)^* \right| 0 \right\rangle = \left\langle O_R(0) O_R(T)^* \right\rangle \quad (1)$$

when operator $O_R(T)$ is gauge invariant and is defined as:

$$O_R(T) = \bar{q}(T,0) U\big((T,0) \to (T,R)\big) q(T,R) \quad (2)$$

and $U\big((T,0) \to (T,R)\big)$ is gauge field that connect static quarks from point (T,0) to point (T, R). Finally the Wilson loops can be defined as:

$$W(R,T) = \mathrm{tr}\, U\big((0,0) \to (0,R)\big) U\big((0,R) \to (T,R)\big) U\big((T,0) \to (T,R)\big)^* U\big((0,0) \to (T,0)\big)^* \quad (3)$$

If we introduce in formula (3) a set of identity expressions $\sum_n |n><n| = I$ after several easy steps will have:

$$W(R,T) = \sum_n \left| \langle 0 | O_R(0) | n \rangle \right|^2 e^{-E_n(R)T}, \quad (4)$$

or it can be written as:

$$W(R,T) = \sum_n c_n e^{-V_n(R)T} \quad (5)$$

Where the ground state is $V_1(R) \equiv V(R)$ and the other values, for n>1, are the potentials of the excited states. So, mathematically we can locate the ground state if we take the limit of expression (5)

$$\lim_{T\to\infty} W(R,T) \cong c_1 e^{-V(R)T}, \qquad (6)$$

and than we can take logarithm of (6) in order to have the final expression for potential of ground state. As size of T in lattice simulation is practically limited, the effective potential calculatedly from

$$V(R)_{eff} = -\log \frac{W(R,T+1)}{W(R,T)} \qquad (7)$$

can be often used.

We started from a closed rectangular path C(R,T) with extension R x T in Fermiqcd software (Di Pierro, 2001; 2002; 2004) and wrote the full code that calculates different planar Wilson loops, for R = T = 1,..6. The simulation is made for 100 statistically independent gauge field backgrounds. The output of Wilson loops is than treated in Matlab software. For each R it is selected the value of effective potential for large time T when it is reached a "plateau". In the present paper, our previous method is improved taking in consideration the symmetrisation of the Wilson loops before calculation of the effective potential. In our previous work (Xhako et al., 2012), Wilson loops were taken arbitrary in the form W(R, T) when the first index was space index and the second one was time index. In fact, in Euclidian geometry there is no privileged direction for space or time. So, the symmetrisation is carried out by averaged W(R, T) and W (T, R) Wilson loops.

Finally, we fit the calculated values of the effective potentials according to the physical model (physically, this behavior implies the confinement of color in the flux tubes of the gluonic field) (Bali, 2000):

$$V(R)_{eff} = V_0 + KR + \frac{\alpha}{R} \qquad (8)$$

where α is a constant (the coefficient of the Coulomb-like term) and K the string tension parameter. We can take the representation of this model in lattice unit by multiplying with lattice spacing the equation (8):

$$\hat{V}(R)_{eff} = \hat{V}_0 + \hat{K}\frac{R}{a} + \frac{a}{R}\hat{\alpha} \qquad (9)$$

The coefficients of the model (9) are simply calculated in Matlab using matrix notation and solving a linear system as in (Xhako et al., 2012). We have calculated lattice spacing *a* basing on (Guagnelli et al., 1998). The

physical volume of the lattice (*L^4*) with length *L* is related to the lattice volume (*N^4*) with *N* point for direction by *L=aN*. In order to take physical length *L* of the lattice constant we changed the value of the parameter $\beta = 6/g^2$ (g is the QCD coupling) in each simulation with different lattice volume (8^4, 12^4, 16^4). The changed values of the coupling constant are taken from parameterization of the low-energy reference scale r_0 according to (Guagnelli et al., 1998). We have rewrite also the script in Matlab that calculate statistical errors of the parameters of the model with Jacknife method (Miller, 1974), but including weight coefficients of errors of the potential. The results are shown in Table 1 in the results section. Plotting the effective potential values for different R we have taken the graph of quark – antiquark potential.

3. RESULTS AND DISCUSSION

The simulations are made with Wilson action on 8^4, 12^4, 16^4 lattices at three lattice spacing for 100 SU(3) gauge field configurations and carried out on the BG-HPC cluster that is located in Bulgaria (part of HP-SEE project), using Fermiqcd software. In the following paragraph, the graph of quark antiquark potential for lattice 16^4 is reported.

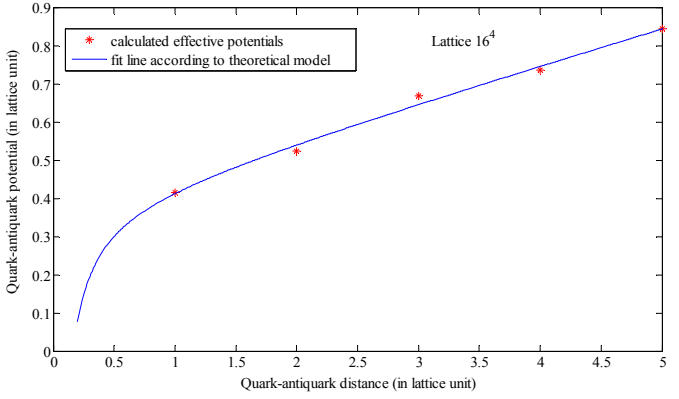

Fig. 1 Graph of quark-antiquark potential for beta=6, 16^4 lattice volume, in lattice unit.

From the behaviour of the potential from quark distance, for lattice volume 16^4, Fig.1, where the same behaviour it is taken for 8^4, 12^4—the quark-antiquark potential it is dominated by a Coulomb–like term at short distances with an R dependent coupling $V(R) \cong V_0 + \alpha / R$ for R small and by a linearly rising term at large distances $V(R) \cong V_0 + KR$ for R large, that

confirm the fact of confinement of quarks within hadrons as in (Parisi et al., 1983; Schilling 1993; Deldar 2000; Bali 2000). The recalculation values of the lattice parameter for different lattice volumes and their statistical error are in Table 1 reported.

Table 1. The values of lattice spacing *a* for different lattice volume with respective statistical errors

Lattice volume	Coupling constant β	Lattice spacing a from parameterization (in fm)	Calculated lattice spacing *a* (in fm)	Statistical error of *a*
8^4	5.7	0.1707	0.1735	0.0145(76)
12^4	5.85	0.1230	0.1273	0.0214 (38)
16^4	6	0.0931	0.0973	0.0594(74)

The standard method of computing quark-antiquark potential from planar Wilson loops has been investigated using parallel computation techniques involving Fermiqcd. Results report that the quark-antiquark potential is dominated by a Coulomb–like term at short distances for small R and by a linearly rising term for large R confirming the so called quark confinement, one of the most important properties of QCD in low energy regimes. The present paper aims at fostering the previous work done by the authors. In the present investigation results of the lattice spacing parameters for different lattice volume and their statistical errors are improved. Reported in Table 1, the values of lattice spacing for different lattice volume are calculated within the range of statistical error. The calculated values of lattice spacing compared with them from parameterization show that they are within the range of errors found. These values of lattice spacing can be used to set the scale of the theory, so with them we can convert quantity from lattice unit in physical unit.

ACKNOWLEDGMENTS

This paper reports on results of the project run by the High-Performance Computing Infrastructure for South East Europe's Research Communities (HP-SEE). Co-founded by the European, the project Commission (under contract number 261499) under the Seventh Framework Program (FP7). HP-SEE involves and addresses specific needs of a number of new multi-disciplinary international scientific communities (computational physics, computational chemistry, life sciences, etc.) and thus stimulates the use and expansion of the emerging new regional HPC infrastructure and its services. Further information is available at official website of the project (http://www.hp-see.eu/).

REFERENCES

Bali G. 2000. Casimir scaling of SU (3) static potentials. *Physical Riverview*. 1- 12. D62, 114503. Available on line : http://arxiv.org/pdf/hep-lat/0006022.pdf **.**

Campbell NA, Huntley A , Michael C. 1988. Heavy quark potentials and hybrid mesons from SU(3) lattice gauge theory. *Nuclear Physics B.* **306 (1)**, 51-62.

Campbell NA, Michael C, Rakow PEI. 1984. *Physics Letters B.* **139, 288.**

Creutz M, Moriarty KJM. 1982. Numerical studies of Wilson loops in SU(3) gauge theory in four dimensions. *Physical Review D.* **26 (8)**, 2166-2168. http://thy.phy.bnl.gov/~creutz/mypubs/pub061.pdf

Deldar S. 2000. Pure SU(3) potentials in the fat-centre-vortices model. *Physics Review D* 62, 34509

Di Pierro M. 2001. Parallel Programming with Matrix Distributed Processing. *Computer Physics Communcations* .**141**, 98-148.

Di Pierro M. 2002, FermiQCD: A tool kit for parallel lattice QCD applications. *Nuclear Physics B*- Proceedings. Supplement. **106-107**, 1034-1036 .

Di Pierro M, El-Khadra A, Gottlieb S, Kronfeld A, Mackenzie P, Okamoto M, Oktay M, Simone J, 2004, www.fermiqcd.net, *Nuclear Physics Proceedings Supplement*. 129:832-834.

Gattringer C, Lang CB. 2009. Quantum Chromodynamics on the Lattice. Springer. ISBN: 3642018491.343.

Grifiths LA, Michael C, Rakow PEI. 1984. The string tension from lattice QCD. *Physics Letters B* **129**, 288-292.

Guagnelli M, Sommer R, Wittig H. 1998. Precision computation of a low-energy reference scale in quenched lattice QCD. *Nuclear Physics B*. **535 (1-2)**, 389-402.

Miller RG.1974. The Jackknife- A Rivew. *Biometrika*. **61, (1),** 1-15**.**

Parisi G, Petronzio R, Rapuano F. 1983. Measurement of the String Tension Near the Continuum Limit. *Physics Letter B*. **128(6)**, 418-420.

Perantonis SJ, Huntley A, Michael C. 1989. Static potentials from pure SU (2) lattice gauge theory. *Nuclear Physics B*. **326 (2)**, 544-556. Available online: http://users.iit.demokritos.gr/~sper/PAPERS/1989J-PerantonisHuntleyMichael-NPB326.pdf

Schilling K, Bali GS. 1993. The Static Quark-Antiquark Potential: A ``Classical'' Experiment On The Connection Machine CM-2. *International Journal of Modern Physics C.* **4**,1167-1177

Sommer R. 1993 A New Way to Set the Energy Scale in Lattice Gauge Theories. *Nuclear Physics B*. **411**, 839-854.

Stack JD. 1983. *S*caling of the Quark-Antiquark Potential and Improved Actions in SU(2) Lattice Gauge Theory. *Physics Letters B.* **136,** 411-417.

Wilson KG. 1974. Confinement of Quarks. *Physics Review D*.**10**, 2445-2459.

Xhako D, Zeqirllari R, Borici A. 2012. Using Parallel Computing to Calculate Static Interquark Potential in LQCD**.** HP-SEE User Forum. Springer. ISBN 978-3-319-01519-4, DOI 10.1007/978-3-319-01520-0.

CONCENTRATION TRENDS OF PRIMARY AIR POLLUTANTS, THEIR PHOTOCHEMICAL TRANSFORMATIONS AND ENVIRONMENTAL IMPACT

Dhurata PREMTI and Ilirjan MALOLLARI
Department of Chemistry, Faculty of Natural Sciences,
University of Tirana, Albania

ABSTRACT

Concentration trends of primary air pollutants, their photochemical transformations and environmental impact is in the present paper investigated. Monitoring sites chosen within each zone reflect the risk of being exposed to elevated levels of primary air pollutants. The results are here reported and compared to the Upper and Lower Assessment Thresholds indicated in the EU Air Quality Framework Directive CAFE 2008/50. These thresholds indicate a potential risk of exceeding limit values fixed for protecting human health. They trigger specific monitoring requirements. Trends and behaviours in the datasets for each primary component and period of record were examined with monthly average concentration behaviour. These represented plots of average concentrations for each month available and aid in understanding average seasonal behavior of measured pollutants.
Keywords: Primary Pollutants; Photochemical Transformations; Concentration Trends

1. INTRODUCTION

The effects on health of transport-related air pollution have become one of the leading concerns about transport. Road transport will remain a significant contributor to air pollution in cities across the Albania as carbonaceous material is emitted. Few papers (Chu and Macias 1981) have reported that traffic-generated dust is of great impact for the human health. Exhaust emissions are an important source of traffic related pollution and several epidemiological and toxicological studies (Mol *et al*., 2010), have linked such emissions to adverse health effects. Road abrasion, tire wear and brake wear are non-exhaust traffic emissions which become relatively more important with progressive reductions in exhaust emissions (Bower 1997). Toxicological research increasingly indicates that such non-exhaust pollutants could be responsible for some of the observed health effects (Blanchard 1999). Coal combustion results in sulfate-contaminated particles

for which there is strong evidence of adverse effects from epidemiological studies. Health relevant sources also include power generation (oil and coal combustion), and metal industry. Based on most recent studies (Hak *et al*., 2009), exposure to particles from biomass combustion, most notably residential wood combustion during winter, may be associated not only with respiratory but also with cardiovascular health.

The pollutants in the present investigation measured consist of primary pollutants: nitrogen dioxide (NO_2), benzene (C_6H_6), sulfur dioxide, (SO_2) and ozone (O_3). Monthly measurements of total accumulated pollutant have been carried out at urban, rural, sub-urban and industrial sites in Albania, using diffusion tubes in June 2012, January 2008 and 2012.

Results report that nitrogen dioxide concentrations vary between rural, urban and traffic sites in a different manner from particle matter (PM) and ozone (O_3). Nitrogen dioxide concentrations are higher close to the sources and at traffic areas and decrease in urban background areas. The lowest concentrations are found in rural areas. While secondary PM and O_3 are formed regionally from precursor gases, chemical reactions are less likely to create NO_2. For most NO_X sources, the share of NO in NO_X emissions is much greater than that of NO_2, typically 10–20 times higher. The NO_2 concentration is then increased at the expense of NO, due to reactions with O_3. In traffic and urban areas with fresh inputs of NO, some of the O_3 present is depleted while oxidising NO to NO_2. In rural, areas relatively limited fresh NO emissions are available, except near highways and combustion plumes. The reaction between NO, NO_2 and O_3 leads to chemical equilibrium.

Photochemical Transformations

Photochemical reactions transform primary pollutants into secondary air pollutants. The oxidation of sulfur dioxide (SO_2) and nitrogen dioxide (NO_2) and their conversion to particulate sulfate, and gaseous and particulate nitrates are important characteristics of mainly urban air photochemistry. The environmental effects of these secondary pollutants are associated with acidification of precipitation, visibility reduction and have deleterious effects on human health, enhancing the negative effects of primary pollutants.

The rate of conversion of NO_x to NO_3 affects ozone formation and the ultimate fate of NO_x in the atmosphere. SO_2 is oxidized to sulfate and the oxidation rate determines its lifetime in the atmosphere (Atkinson *et al*., 1997). NO_x and SO_2 are oxidized to HNO_3 and H_2SO_4 in the atmosphere, which in turn form the nitrate NO_3^- and sulfate SO_4^{2-}.

Atmospheric oxidation of SO_2 occurs by homogeneous and heterogeneous paths and the oxidation rate increases as relative humidity increases through both paths involving OH production. A large fraction of SO_2 should react with

water vapor and be converted to SO_3 through heterogeneous reaction, and then is oxidized either by reaction with O_3 and H_2O_2 or by reaction with catalytic metals. Sulfate is generated as H_2SO_4 mist by the homogeneous nucleation processes in the H_2SO_4–H_2O system, followed by the transition to ammonium sulfate $(NH_4)_2SO_4$ and/or ammonium bisulfate NH_4HSO_4. The droplet phase reactions are important for the oxidation of SO_2 to sulfate in the atmosphere. SO_2 is oxidized to H_2SO_4 by homogeneous gas–phase reactions followed by condensation of the H_2SO_4 both onto pre-existing particles and into new particles with partial neutralization by ammonia (NH_3). SO_2 may react immediately with OH in the atmosphere to produce SO_3. The reaction rate of SO_3 with H_2O in the gas–phase was generally considered to be very fast. However the reaction of SO_3 with H_2O is quite slow in the gas–phase. The reaction rate constant of SO_3 with ammonia is more than 4 orders of magnitude larger than that of SO_3 with H_2O in the gas–phase. Sulfuric acid in the atmosphere can further react with ambient ammonia producing a (NH_4HSO_4) and the very weakly acidic $(NH_4)_2SO_4$ which is the most common form of SO_4^{2-} (Finlayson-Pitts and Pitts 2000).

The proportion of each of the aforementioned sulfate species in the atmosphere depends upon meteorological conditions and local concentrations of ammonia. If ammonia is scarce, sulfate will remain in more acidic forms such as ammonium bisulfate or sulfuric acid. Sulfate can primarily be found in fine particle.

NO_x are also emitted, or produced in, the troposphere. Nitric oxide (NO) is short lived because it oxidized to produce nitrogen dioxide (NO_2) which plays a major role in O_3 production. NO_x comprise a mixture mainly of NO and NO_2, prominent in air quality studies. As a precursor pollutant of O_3, NO_2 poses a threat to public health. Previous studies have shown, however, that NO_x emissions from anthropogenic sources exceed natural sources.

Vehicular traffic emissions are the main sources of NO_x in our country. High temperature causes the oxidation of atmospheric N_2, first to NO and then to NO_2, which plays a major role in the formation of ground–level O_3. The NO_x emitted from fossil fuel combustion has a lifetime of less than a day against oxidation to HNO_3 and peroxyacetylnitrate (PAN). The products of NO_x oxidation in the atmosphere include both gaseous and particulate nitrate. Nitric acid which is the most important transformation product of NO_x, is formed through either the homogeneous reaction of NO_2 with the OH radical, reaction of NO_3 with aldehydes or hydrocarbons or hydrolysis of N_2O_5 in the atmosphere. The gas–phase reaction of NO_2 with OH radicals is the dominant pathway for HNO_3 formation during daytime whilst, N_2O_5 hydrolysis and NO_3 free radical is believed to become an important source of HNO_3 during night. The fate of HNO_3 is controlled by the reaction with basic species such as NH_3 gas or with crustal minerals and sodium chloride particles, and dry

deposition. The prime influence upon HNO_3 concentrations is expected to be ambient temperature, relative humidity and NH_3 concentrations at sites where ammonium nitrate, (NH_4NO_3) is formed. HNO_3 can be transformed into aerosol by neutralization reactions (De More *et al*., 1997).

2. RESULTS AND DISCUSSIONS

Passive diffusive sampling, the experimental method in the present investigation used, relies on the diffusion of analytes through a diffusive surface onto an adsorbent. After sampling, the analytes are chemically desorbed by solvent extraction or thermally desorbed and analysed. Passive sampling is used as a screening method rather than a regulatory method, for which continuous monitors are needed. Trends and behaviours in the datasets for each primary component and period of record were examined with 'monthly average concentration' behaviour. These represented plots of average concentrations for each month available. These patterns aid in understanding average seasonal behavior in environmental data. The targets for NO_2 are defined by the two limit values for the protection of human health: i) the long term limit value, corresponding to the annual mean limit value of 40 μg/m^3 and, ii) the short term limit value, corresponding to the hourly mean limit value of 200 μg/m^3.

The annual mean limit value for NO_2 for the protection of human health is 40 μg/m^3 and had to be met in 2010. NO_2 annual mean exceedance are mostly attributed to local traffic, domestic heating, local industry and power generation, industrial emissions etc. (table 1).

Table 1. Annual limit value for the protection of human health (NO_2)

Threshold	Frequency	Value (μg/m^3)
Upper Assessment Threshold	not to be exceeded more than 18 times a year	32
Lower Assessment Threshold	not to be exceeded more than 18 times a year	26

The experimental data shown in figure 1 report that in almost half of urban areas such as Gjirokastra-city center; Saranda-district; Peshkopi-city center, there are increased concentration values from January 2008 to January 2012. In July 2008, the NO_2 levels were under the Lower Assessment Threshold

(LAT), varying from 4.5 μg/m^3 to 26 μg/m^3. High values of NO_2, over the UAT value were measured in Tirana-Directory of Public Health, Tirana-21 Dhjetori sites.

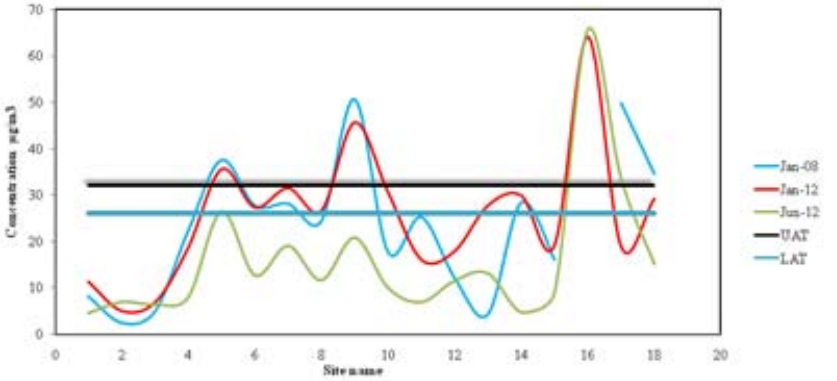

Fig 1. Concentration trends for nitrogen dioxide concentration in main sites, during January 2008, January 2012 and June 2012 (μg/m^3).

The variation of SO_2 values show it's oxidation process to sulfate and the oxidation rate determines its lifetime in the atmosphere, which in turn forms sulfate SO_4^{2-}. Atmospheric oxidation of SO_2 occurs by heterogeneous and homogeneous paths and the oxidation rate is increased with increasing relative humidity through both paths involving OH production. A large fraction of SO_2 should react with water vapor and be converted to SO_3 through heterogeneous reaction, and then is oxidized either by reaction with O_3 and H_2O_2 or by reaction with catalytic metals. The proportion of each of the above sulfate species in the atmosphere depends upon meteorological conditions and local concentrations of ammonia. If ammonia is scarce, sulfate will remain in more acidic forms such as ammonium bisulfate or sulfuric acid. Sulfate can primarily be found in fine particle.

SO_2 concentrations decreased from January 2008 to January 2012 in main urban centres (figure 2). In Fier sites, SO_2 concentrations are constantly high during most periods due to oil rafinery factories spread in sub-urban, and rural areas for this city. LAT and UAT are not passed for this primary pollutant (table 2).

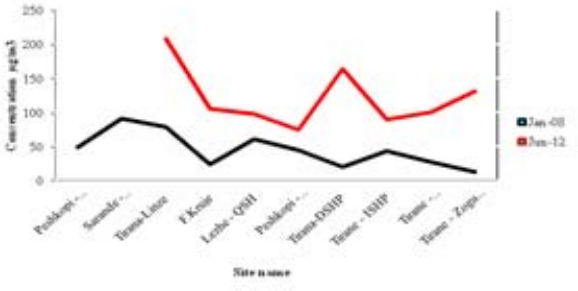

Fig 2. Concentration trends for sulfur dioxide concentration in main sites, during January 2008, January 2012 and June 2012 (μg/m^3).

Table 2. Annual limit value for the protection of human health (SO_2)

Threshold	Frequency	Value (μg/m^3)
Upper Assessment Threshold	Not to be exceeded more than 3 times a year	75
Lower Assessment Threshold	Not to be exceeded more than 3 times a year	50

The most severe pollution events occur when a combination of light winds and suppressed vertical mixing prevents the dispersion of pollutants from an urban center. The process of ozone formation typically requires several hours and occurs only at times of bright sunlight and warm temperatures. During June the average minimum-maximum temperature is 16^0C-28^0C while during January it is 2^0C-12^0C. For this reason, peak ozone values typically are found downwind of major cities rather than in the urban center (figure 3). During severe events with light winds, high ozone concentrations are more likely to occur closer to the city center. There are neither LAT nor UAT defined for this pollutant. In addition, the observed values can hardly be compared to any target value or long term objective (based on hourly values, 8 hour values or AOT).

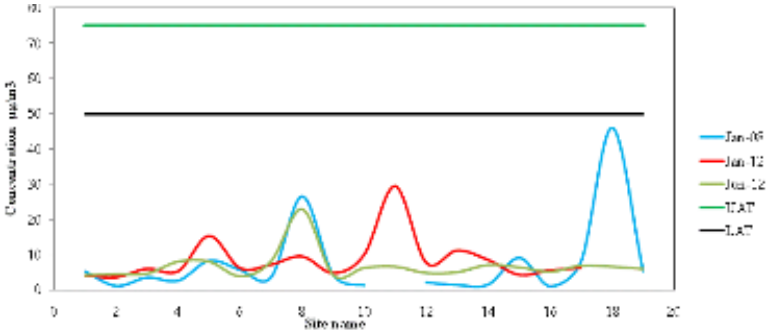

Fig. 3. Concentration trends for Ozone concentration in main sites, during January 2008 and June 2012 (μg/m^3).

Concentrations of benzene were highest at traffic stations, as gasoline is still one of the most important sources of benzene. Concentrations measured at traffic stations decreased steadily from January 2008 to January 2012 (figure 4). Benzene concentrations at urban and rural stations show lower decrease during the same period.

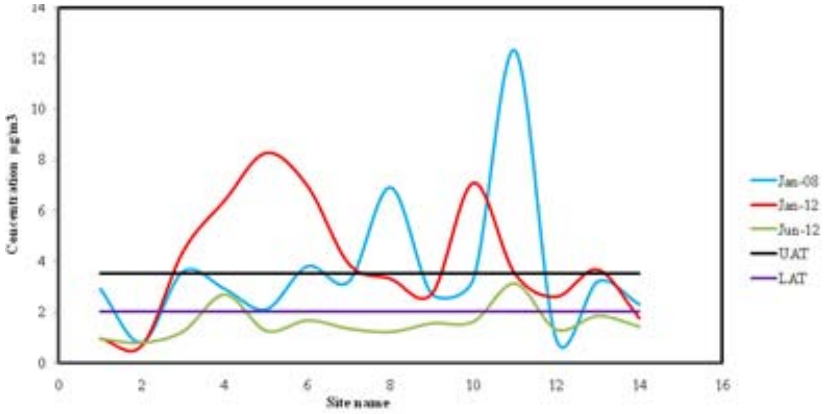

Fig. 4. Concentration trends for benzene concentration in main sites, during January 2008, January 2012 and June 2012 (μg/m^3).

There are several processes that have impact on the removal process of benzene in ambient air, like the photochemical degradation of benzene which also contributes to ozone formation, and the chemical reactivity of benzene is relatively low. An atmospheric lifetime of several days is sufficient for benzene to be transported over long distances.

In June 2008, levels of benzene were low due to high photochemical degradation and only 12 % of concentration values exceeded LAT and UAT

(table 3). In January 2008 and January 2012 respectively 85.7% and 78.6% of concentration values exceeded LAT while 21.4% and 50% exceeded UAT limit.

Table 3. Annual limit value for the protection of human health (C_6H_6)

Threshold	Frequency	Value (μg/m^3)
Upper Assessment Threshold	Annual average	3.5
Lower Assessment Threshold	Annual average	2

ACKNOWLEDGEMENTS

This work has been generously supported by the European Union under the framework project "Consolidating the Environmental Monitoring system in Albania" (EuropeAid/128449/C/SER/ALIPA 2008).

REFERENCES

Atkinson R, Baulch DL, Cox RA, Hampson RF, Kerr JA, Rossie MJ, Troe J. 1997. Evaluated Kinetic and Photochemical Data for Atmospheric Chemistry. Supplement V. IUPAC Subcommittee on Gas Kinetic Data Evaluation for Atmospheric Chemistry. *Journal of Physical Chemistry. Ref. Data,* **26***,* 521-1011.

Blanchard CL. 1999. Methods of attributing ambient air pollutants to emission sources. *Annual Review Energy Environment*. **24**: 329-365.

Bower J. 1997. Ambient air quality monitoring. In: Air Quality Management, R.E. Hester and R.M.Harrison (Eds.). *The Royal Society of Chemistry*. Cambridge*,* UK, 41-65.

Chu LC, Macias ES. 1981. Carbonaceous urban aerosol: Primary or secondary? In Atmospheric Aerosol: Source/Air Quality Relationships. E. S. Macias and P. K. Hopke, eds.,American Chemical Society, Washington, DC. 251-268.

Council Directive 2008/50/EC of the European Parliament and of the Council of 21st May 2008, on ambient air quality and cleaner air for Europe. *http://ec.europa.eu/environment/air/quality/legislation/directive.htm*

DeMore WB, Sander SP, Golden DM, Hampson RF, Kurylo MJ, Howard CJ, Ravishankara AR. Kolb CE, Molina MJ, 1997. "Chemical Kinetics and Photochemical Data for Use in Stratospheric Modeling," in *JPL Publication 97-4*, Jet Propulsion Laboratory, Pasadena, CA.

Finlayson-Pitts BJ, Jr Pitts JN. 2000. Chemistry of the upper and lower atmosphere – theory, experiments, and applications. *Academic Press*: San Diego, CA.

Hak C, Larssen S, Randall S, Guerreiro C, Denby B, Horálek J. 2009. Traffic and Air Quality. Contribution of Traffic to Urban Air Quality in European Cities. *ETC/ACC Technical Paper* 2009/12.

Mol WJA. Hooydonk PR, van and Leeuw, FAAM. 2010. The state of the air quality in 2008 and the European exchange of monitoring information in 2009. *ETC/ACC Technical paper* 2010/1.

RADON CONCENTRATION IN SOIL AND INDOOR IN QUATERNARY DEPOSITS

Safet DOGJANI
Institute of Geosciences, Energy, Water and Environment,
Polytechnic University of Tirana, Albania
Salvatore BUSHATI
Academy of Sciences of Albania

ABSTRACT

The present paper investigates on the radon concentration levels in the soil and indoor for the city of Fier, one of the main cities of Albania. Radon is a naturally occurring gas that results from the radioactive decay of uranium. Radon breaks down into odorless and colorless particles that are often present in the home. In addition, it is very dangerous for the health, as when inhaling it or its decay products, sensitive lung tissues are stricken causing damage that can lead to lung cancer. Consequently, an accurate assessment of radon level is very important. In the present investigation, radon concentration levels and soil permeability measurements have been made. Measuring time varied between 24 and 72 hours and active radon detectors were used. Results report that in the 52 sites where measurements were made, the level of radon concentration ranges from 2000 up to 43000Bq/m^3. In addition, 19 sites out of 52 are characterized by high soil permeability. Moreover, three categories of radon risk are here reported. In Fier, 11.54% of the territory is identified as high radon risk area.
Keywords: natural radioactivity, radon, permeability, Becquerel, Quaternary deposits, Fier.

1. INTRODUCTION

Radon is a *radioactive*, colorless, odorless and tasteless *noble gas*, occurring naturally as an indirect *decay product* of *uranium* or *thorium*. As radon itself decays, it produces new radioactive elements called radon daughters or decay products. Unlike the gaseous radon itself, radon daughters are solids and stick to surfaces, such as dust particles in the air. If such contaminated dust is inhaled, these particles can stick to the airways of the lung and increase the risk of developing lung cancer. Inhalation is the main route of radon gas entry into the body for radon and its decay products. Radon

decay products may attach to particulates and aerosols in the air we breathe (for example, cooking oil vapors). When they are inhaled, some of these particles are retained in the lungs.

Long-time exposure to environments with high levels of radon, the alpha particles from its radioactive decay directly strike sensitive lung tissue causing damage that can lead to lung cancer (UNSCEAR, 2000). UNSCEAR (2000) and USEPA (2012) stated that 70-75% of the total dose of radon gas that humans inhale comes from natural radioactive sources. There are many sources of indoor radon (Barnet and Neznal, 1994), but particularly from: i) air, ii) building materials and, iii) radon-contaminated drinking water used in bathroom showers and sprays, though this occurs only when the water comes from a private well. Geological environment is of great impact to the aforementioned sources. Because radon comes from rock and soil, it can be found anywhere. Radon is emitted from the ground and enters a home through cracks in walls, basement floors, foundations and other openings. Theoretically, under stationary conditions and in different depth, U (Ra), density, coefficient of radon gas emanation and porosity expressed in the following equation are of great impact for the volumetric activity level of radon concentration in soils (avRn).

$$avRn = a_{m} Ra^{226} \cdot \rho \cdot \frac{K_{em}}{P}$$

where: $a_{m} Ra^{226}$, radium content 226 in soil, Bq/kg

ρ, soil density, kg/m^3

$K_{em,}$ coefficient of Radon gas emanation

P, value of soil porosity

Results report that smokers who are also exposed to radon have a much higher risk of lung cancer. In addition, association between residential radon exposure and lung cancer is clear. USEPA (2012) estimated that the risk of lung cancer is 20/1000 if you have 1.3pCi/L of radon found. In addition, for the non-smokers the risk of lung cancer is 2/1000 if you have 1.3pCi/L of radon found. Consequently, recognizing concentration of this deadly gas in working environment and homes and minimizing its levels to natural background levels must be top priority for every institution.

2. MATERIALS AND METHODS

Twelve to fifteen field measurements for the volumetric activity level of Radon concentration in soils, AvRn were carried out at 52 lithologically and

tectonically different sites. In addition to lithological content and tectonic features, climatic conditions were different from one site to an other. All the aforementioned features are of great impact for the radon concentration (Barnet and Neznal 1994; Matolin et al., 2000). Soil permeability (K) was determined as well. All the measurements (12-15) were carried in a surface area of 250-300m^2.

Measuring time

The volumetric activity level of Radon concentration in soils, (a_vRn) was determined 6 minutes after sampling was carried out to avoid the impact of radon-220 as recommended in (Plch, 1996).

Sampling

Air samples were collected 0.8m from the earth surface due to climatic conditions.

Procedures for measuring

The volumetric activity level of Radon concentration in soils was measured using 1.2m long cylindrical steel tube with the diameter Ø, 12 mm and metal pinnacles at its bottom. The equipment drives in a depth of 0.80 m (Matolin et al., 2000; Plch, 1996). Fifty centimeters long, the metal pinnacles disconnects from the 5cm long tube and remains in the ground (lost tip).

Consequently, the air coming from the pores of soil gets into cylindrical tube. Once getting into the cylindrical tube, absorbed using a syringe, the air gets into the container MB145, of radon equipment Luk4. The method involves software and measures automatically radon concentration. Measuring error is ± 7% (Plch 1996). Data of gas concentration are expressed in Becquerel's per cubic meter (Bq/m^3), and are transferred to P.C., where selection for every measuring site is made.

Measurement of soil permeability

Gas permeability of soils and rocks is one of the most important factors which determine the possible radon sources of any given site and therefore one of the main parameters for final radon risk classification of building sites (Neznal et al., 1996). Measuring process takes place in the holes where data for the determination of a_vRn were collected, i.e., 0.8m from the surface. The RADON – JOK instrument was used for the determination of soil permeability.

Measurement of radon in indoor air

Here, the radon active detectors Fritra-2 are involved. Measuring time varied from 24 to 72 hours. Windows and doors remained closed while carrying out the short-term test.

Assurance quality

With regard to the assurance quality standard, the instruments in the present investigation used were calibrated at the laboratory of the Metrological Center, the Czech Republic (Pribram, Kamena).

Data interpretation

Data interpretation is based on the recommendations made by the respective Czech institutions. Here, mean values of avRn together with soil permeability (K) have been determined. The map of radon volume activity, the map of soil permeability and the map of radon risk in soil/ground have been compiled in line with the data reported in the table of radon risk classification (Barnet and Neznal 1994; Matolin et al., 2000; Neznal et al., 1996). Basing on the interpretation of aforementioned maps, risk is rated as low, medium and high.

Results analyses

Divided into 52 sites, a surface area of 13 km^2 in Fier was investigated. Six-hundred and twenty four applications for the determination of the volume activity of Radon "a_vRn" and soil permeability coefficient (K) have been made. Data elaboration was a means to address the compilation of the three following maps at the scale 1:25000: i) the Map of soil permeability (figure 3a), ii) Map **"**a_vRn" (figure 3 b) and, iii) the Map of radon risk, (figure 3c) (Dogjani, 2006-2007). Compiled in the map of radon risk, detailed information on radon risk is here reported. The Surfer program was applied for the compilation of the map of radon risk.

Volume activity of radon in soil

Depicted in the figure (1a) results report that: i) 8 sites have radon concentration lower than 10kBq/m^3, ii) 15 sites have radon concentration values varying between 10-19,9kBq/m^3, iii) 21 sites have radon concentration varying from 20-29,9Bq/m^3, and the reminder have the radon concentration over 30kBq/m^3. Statistically elaborated, the results report that the concentration levels are: minimum 17, 8 kBq/m^3; maximum 43, 16 kBq/m^3 and mean 20, 2 kBq/m^3.

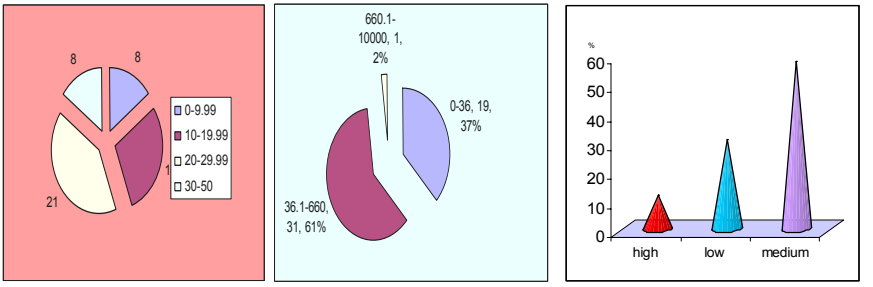

a) b) c)

Fig. 1: Distribution of Radon levels in kBq/m^3 (a); permeability in sec., (b) and Radon risk in soil (c).

Soil permeability

In the figure 1b, 1 site with a permeability of over 660 sec, 19 sites having permeability up to 36 seconds and the reminder with a permeability varying from 36 to 660 seconds are depicted.

Radon Risk

Figure 1c depicts 16 sites or 30.77 % of the area considered as low risk areas, 30 sites or 57.69% of the area considered as medium risk areas and the reminder considered as high risk area.

Figure 2(a) and (b) depict that radon concentration and soil permeability depend on geological features. The region is situated in the quaternary deposits of Holocene (Qh) having different physical and lithological properties.

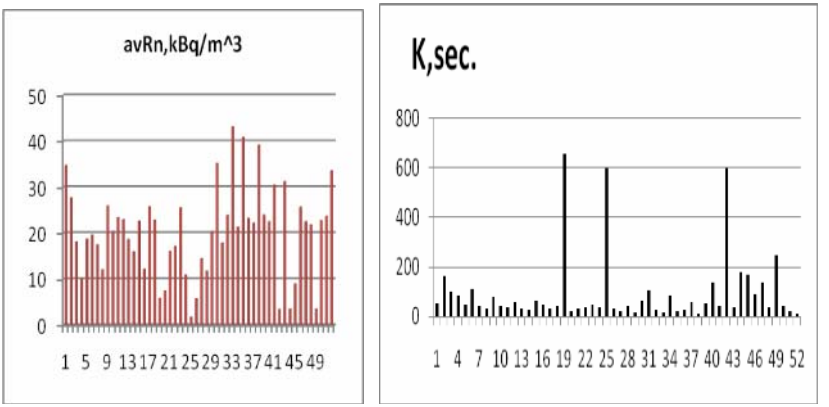

a) b)

Fig. 2: Distribution in the test site of Radon levels (a), and permeability in soil (b)

Measuring of indoor radon

In the present investigation, 17 indoor measurements within 24-72 hours have been made. Taking place once, in the spring only, measurements were made in the first floor, in an environment with a great number of people. In addition, these measurements were made in parallel with the measurement of radon concentration in soil. The sites were selected basing on the concentration of radon in soil. Results report that in 23% of the cases, the radon concentration goes up to 50 Bq/m^3, in 43% of the cases radon concentration varies from 51 to 100 Bq/m^3, in 23% of the cases radon concentration varies from 101 to 199Bq/m^3 . Finally, in 13% of the cases radon concentration is higher than 200 Bq/m^3. Moderate radon concentration is 94Bq/m^3. The present investigation helped in compiling the map of radon risk. Here, the Surfer program was involved.

Classification radon risk in soil gas

Compiled in the map, the figure 3 c depicts the radon risk in soil gas. Sixteen sites are considered as low radon risk areas, 30 sites are considered as medium risk areas and the reminder as high risk areas.

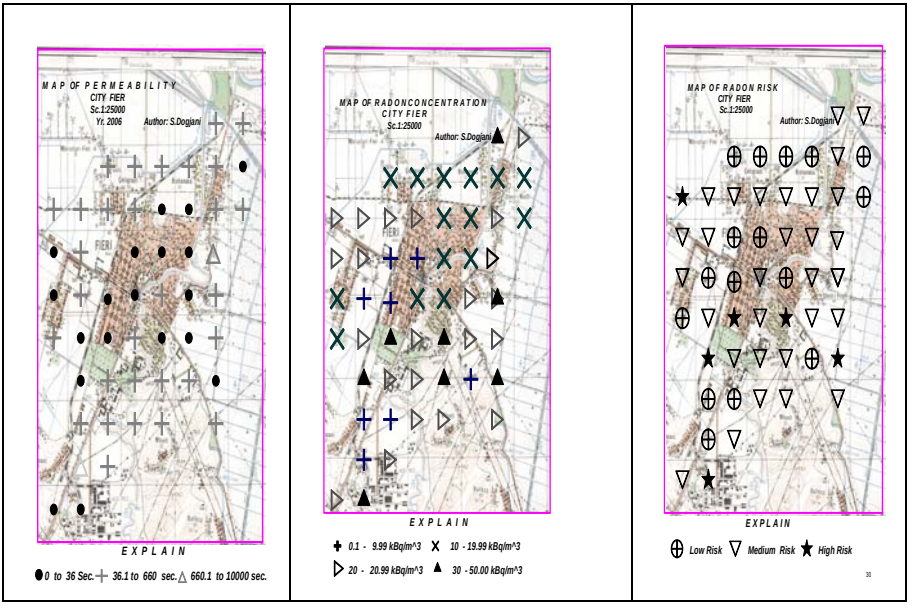

a) b) c)

Fig. 3: The map of permeability (a), radon soil concentration (b) and radon risk (c)

3. CONCLUSIONS

Fieri is considered as a high medium and low radon risk area due to geological features.

The quaternary deposits are lithologically complex. Consequently, the radon levels that vary from 17, 6 kBq/m^3 to 43, 16 kBq/m^3 . The mean values of radon risk is 20, 2 kBq/m^3.

Short-term testing measurements made for indoor radon concentration report that the mean value of indoor radon concentration is 94Bq/m^3. Fieri is characterized by medium radon concentration in soil and indoor.

ACKNOWLEDGMENTS

This investigation was carried out under the framework project "Monitoring investigation of radon concentration in soil, water, indoor air and drinking water" financed by the Ministry of Environment, Forestry and Water Administration (MEFAW).

REFERENCES:

Barnet I, Neznal M. 1994. Radon risk map of Prague. Radon investigations in the Czech Republic, Prague, V, 81-89.

Dogjani S. 2006-2007. Monitoring investigation of Radon concentration in soil, water, indoor air and drinking water. Archive Albania Geological Survey . 5-48.

Matolin M, Jane Z, Neznal M, Neznal M. 2000. Geometry of soil gas sampling, soil permeability and Radon activity concentration. Radon investigations in the Czech Republic, Prague, VIII, 27-29.

Neznal M, Neznal M, Smarda J. 1996. Radon Risk Classification of Foundation Soil. Published by Czech Geological Survey, Prague, VI, 25-35.

Plch J. 1996. Instruction equipment Luk-4, Prague.

United Nations Scientific Committee on the Effects of Atomic Radiation (UNSCEAR) 2000. V.I, Report, 4-7.

USEPA. 2012. A Citizen's Guide to Radon (2012), the guide to protecting yourself and your family from Radon. EPA 402/K-12/002, 11-12, May.

ASSESSMENT OF RADON LEVEL IN SOIL, INDOOR AND WATER IN ALBANIA

Safet DOGJANI
Institute of Geosciences, Energy, Water and Environment, Polytechnic University of Tirana, Albania
Salvatore BUSHATI
Academy of Sciences of Albania

ABSTRACT

Radon (chemical symbol Rn) is a naturally occurring radioactive odorless, colorless and tasteless gas found in soils, rock, and water throughout the world. In addition, it is very dangerous for the health, as when inhaling it or its decay products, sensitive lung tissues are stricken causing damage that can lead to lung cancer. Consequently, an accurate assessment of radon level would be of irreplaceable importance. The present paper provides information about the radon concentration in soils, indoor radon concentration indoor and radon concentration in water in Albania. Several indoor measurements at urban centers have been carried out for an accurate investigation. Results report three categories of radon risk in the country-low radon concentration risk, medium radon concentration risk and high radon concentration risk. In addition, the concentration radon indoor level varies between several becquerels per cubic meter to thousands of Bq/m^3. In addition, concentration levels go up to 508 kBq/m^3 at specific geological setting.
Key words: permeability, radon, soil, gas, red clay.

1. INTRODUCTION

The Institute of Geosciences, Energy, Water and Environment, Polytechnic University of Tirana, Albania (IGJEUM) has recently drafted an investigation plan with regard to the assessment of radon concentration level in Albania.

Radon is a colorless, odorless, radioactive gas. It is formed naturally from the decay of radioactive elements, such as uranium, which are found at different levels in soils and rock throughout the world. Radon gas in the soil and rock can move into the air, ground water and surface water. As radon itself decays, it produces new radioactive elements called radon daughters or decay products. Unlike the gaseous radon itself, radon daughters are solids

and stick to surfaces, such as dust particles in the air. If such contaminated dust is inhaled, these particles can stick to the airways of the lung and increase the risk of developing lung cancer. Radon decay products may attach to particulates and aerosols in the air we breathe (for example, cooking oil vapors). When they are inhaled, some of these particles are retained in the lungs.

World Health Organization (WHO) (2009) stated that Radon (Rn) is the second cause of lung cancer in the general population, after smoking. Current estimates of the proportion of lung cancers attributable to radon range from 3 to 14%, depending on the average radon concentration in the country concerned and the calculation methods. Most of the radon-induced lung cancer cases occur among smokers due to a strong combined effect of smoking and radon. Many ecological investigations about exposure to radon in the general population and leukemia either in children or in adults have been carried out. Some of the aforementioned investigations along with the most recent advanced study have found associations between indoor radon concentration and the risk of leukemia (Smith et al., 2007); at the geographic level (Laurier et al., 2001). An ecological study carried out in Norway showed an association between multiple sclerosis and indoor radon concentration (Bolviken et al., 2003). A main source of indoor radon concentration is the radon gas which comes from the soil under a house or building. Therefore, accurate measurements of the radon concentrations in the soil are very helpful in identifying doubtful areas and in minimizing some radon hazards. The interpretations of radon levels are based on the Czech National Standard (Barnet 2004).

There are many sources of indoor radon but, but the most important sources are: i) bedrock/soil, ii) construction materials and, iii) radon-contaminated drinking water used in bathroom showers and sprays, though this occurs only when the water comes from a private well. Radon comes from rock and soils, it can be found anywhere. Radon is emitted from the ground and enters a home through cracks in walls, basement floors, foundations and other openings (fig 1a). The three sources are closely related to geological setting, and make up 84% of general dose, taken by the man (fig.1b).

Theoretically, under stationary conditions and at different depths, U (Ra), density, coeficient of radon gas emanation and porosity expressed in the following equation are of great impact for the volumetric activity level of radon concentration in soil (AvRn).

$$avRn = a_{m}\, Ra^{226} \cdot \rho \cdot \frac{K_{em}}{P}$$

where: $a_{m}\, Ra^{226}$ - radium content 226 in soil, [Bq/kg] ;

ρ - soil density [kg/m^3] ;
Kem,- coeficient of Radon gas emanation,
P - value of soil porosity.

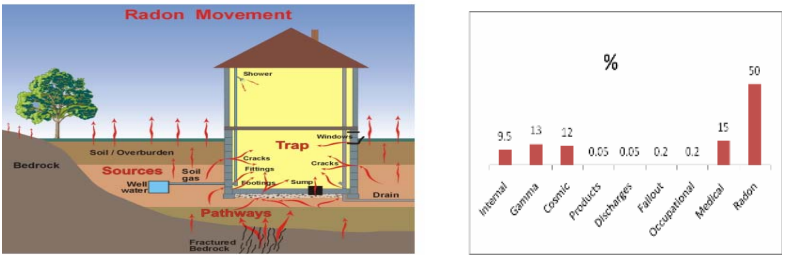

a b

Fig. 1: a) Radon movement and sources (directions of the entry of radon gas in building; b) Dose distribution components of radioactivity.

2. MATERIALS AND METHODS

Radon concentration in soils, water and indoor are in the present investigation measured for an accurate assessment of radon level in Albania**.**

Covering a surface area of 250-300m^2 as defined in (Matolin et al., 1998), in all the sites twelve to fifteen measurements of the activity volumetric of radon concentration in soils (*AvRn*) were carried out. The soil permeability (*K*) was measured as well.

Time required for the determination of *AvRn* was measured 6 minutes after sampling took place, or after the sample was extracted from the soil via *Janet Syringe* using Lucas camera of the Instrument Luk4 or Luk3p.

Air samples were collected 0.8m from the earth surface as defined by the Luka method (Matolin, 1994). The volumetric activity level of radon concentration in soils was measured using a 1.2m long cylindrical steel tube with the diameter 12 mm and metal pinnacles at its bottom (Matolin et al., 2000).

Gas permeability measurement of soils and rocks is one of the most important factors which determine the radon sources of any given site and, therefore one of the main parameters for final radon risk classification of building sites. Permeability measurement involved the *RADON – JOK* instrument based on Darcy's equation (Koorevaar et al., 1983).The air flow is expressed by the following equation:

$$Q = \frac{kF}{\mu} \Delta p$$

where: Q (m^3.s^{-1}) is the air flow through the probe.

F (m) is the shape factor of the probe, depending on site geometry.
K (m^2) is permeability of the soil.
μ (Pa.s) is dynamic viscosity of air (at10^o C $\mu=1.75.10^{-3}$ Pa.s).
Δp (pa) is pressure difference between surface and the active area of the probe.

Critical point of use of this equation is determination of the shape factor *F*. Solution has been presented by (Van der Graaf & Meijer, 1992). Resultant formula is as follows:

$$F = \frac{2\pi l}{ln\left(\frac{2l}{d}\sqrt{\frac{4D-1}{4D+1}}\right)}$$

where: l (m) is the length of active area of the probe head.
D (m) is the diameter of active area.
d (m) is the depth below the surface.

For the instrument *Radon - Jok*, the shape factor *F* is 0.149 m. The great advantage of *Radon - Jok* instrument is the possibility to perform measurements independently of any source of energy. The permeability measurements are achieved in all the locations where a soil gas radon measurement was carried out.

a b c d

Fig. 2. The introduction of Radon gas in the syringe (a); equipment Luk4 (b), equipment Luk3p (c) and radon Jok (d).

Indoor radon measurement involved the radon active detectors Fritra-2. Measuring time varied between 24 and 72 hours. Windows and doors remained closed while carrying out the short-term test.

a

b

Fig. 3: Passive detector (a); Equipment Fritra2 (b)

The measurement of radon in water involved the Aqua kit-alpha pump - Alpha guard (fig.4a and b). Alpha guard user involving the aqua kit set-up helps determine the radon directly in water. In a closed gas cycle, radon is expelled of the water sample by means of alpha pump. Radon enters the ionization chamber by natural diffusion through a filter that allows only radon to enter. Concentration in the system is determined and stored in its memory (1-resp.10-min cycle). Once rotating for 10 minutes, the operation mode of alpha pump switches off. Alpha Guard remains switched on for another 20min, e.g. for as long as radon measurement continues. The radon concentration expressed by the following equation:

$$C_{water} = C_{air} \text{ x } \left(\frac{V_{system} - V_{sample}}{V_{sample}} + K \right) - C_0$$

where:

C_{water} = Rn concentration in water sample, Bq/m^3, C_{air} = Rn concentration in the measuring set-up after expelling the Rn. C_o= Rn concentration in the measuring set–up before sampling. V_{system} = interior volume of the measurement set-up, ml. V_{sample}= volume of the water, ml. K= radon distribution coefficient (Clever, 1985).

a)

b)

Fig. 4: Alpha Pump with acessories (a) Equipment AlphaGuard (b).

The instruments in the present investigation used were periodically calibrated at the National Metrological Center, Kamena, the Czech Republic for accurate measuring purposes.

3. RESULTS

Radon concentration level in soil varies from 3 to 278kBq/m^3 . Radon indoor concentration level varies from 30 to 700Bq/m^3 and in some cases to 3600Bq/m^3. In water it varies from 5 to 70Bq/l. In addition, reddish terrigenous formations dating since Pleistocene-Holocene Era and flysch formations dating since Paleogene Age and Burdigalian formations are richer in radon than all the other formations. Muceku (2005; 2011) reported that Albania is rich in reddish terrigenous formation. In Albania, the indoor radon level goes up to 2500Bq/m^3. Dogjani (2007) reported that in several Albanian cities and towns there are several high-risk radon areas.

3.1. Phase 1: General knowledge on the levels of radon concentration in Albania (soil, air, water)

The radon risk classification of foundation soils is based on the soil gas radon concentration measurements and on the permeability of soils and rocks for gasses. The values obtained enable the determination of radon risk as low, medium and high. Concentration levels up to 278 kBq/m^3 are found at some specific geological settings.

Results on radon concentration in soil are as following: in 2.3% of the surface the radon gas concentration level goes up to 19.9kBq/m^3; in 10.9% of the surface the *AvRn* level varies from 20 to 29.9 kBq/m^3; in 10.5% of the surface the radon levels vary between 30 to 69.99 kBq/m^3. Finally, in 6.3 % of the surface the radon concentration level vary from 70 to 278 kBq/m^3.

Indoor air quality is recognized as a significant factor affecting the well-being of the population. Consequently, indoor air quality measurements were carried out in nurseries, kindergartens and residential homes. Results are as follows: in 55.4% of the cases radon concentration varies from 0-60 Bq/m^3; 17.4% of the cases it varies from 60 to 100 Bq/m^3; 9.8% of the cases it varies from 101-150 Bq/m^3; in 5% of the cases it varies from 151-200 Bq/m^3; in 7.4% of the cases it varies from 201 to 400 Bq/m^3. Finally, in 5% of the cases the average level measured in the range higher than 400 Bq/m^3 (fig. 5a and b).

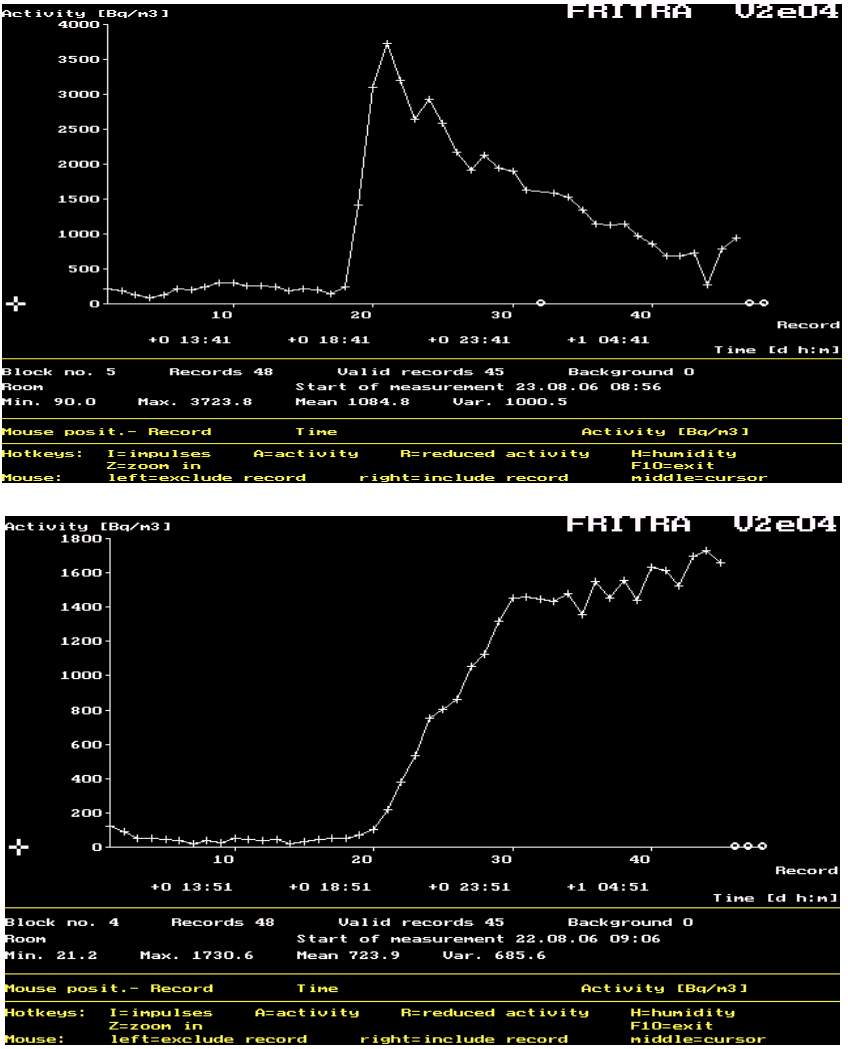

Fig. 5: a). Radon concentration up to 3723Bq/m^3 (average 1004Bq/m^3) ;b) Radon concentration up to1730 Bq/m^3 (average 724Bq/m^3)

Lack of clean water is very concerning for the health, development, economy, agriculture, productivity etc. Consequently, radon measurement is of irreplaceable importance for the life quality of the population. Results report that the radon concentration level in the water varies between 5 to 70Bq/l.

3.2. Phase 2: Establishment of a monitoring system in areas that are classified as areas with problems.

The first phase provides information about the geographical distribution of radon concentration in some of the Albanian urban areas. Here, higher risk areas are detected. Figure 6(a) and (b) provide detailed information about the radon concentration in Tirana (Dogjani et al., 2009).

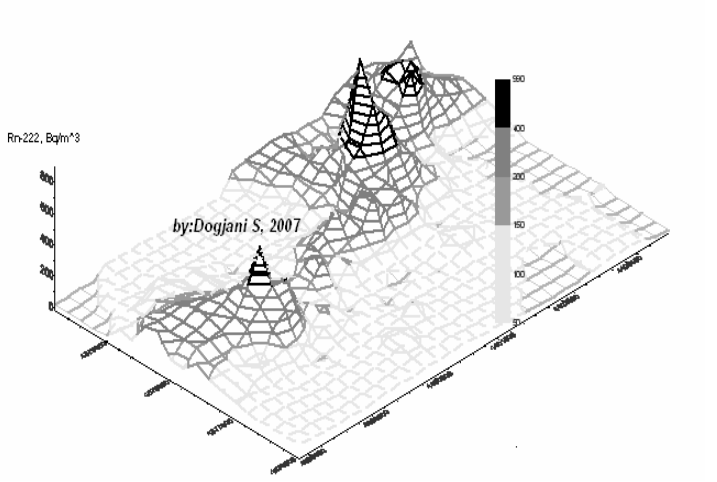

a

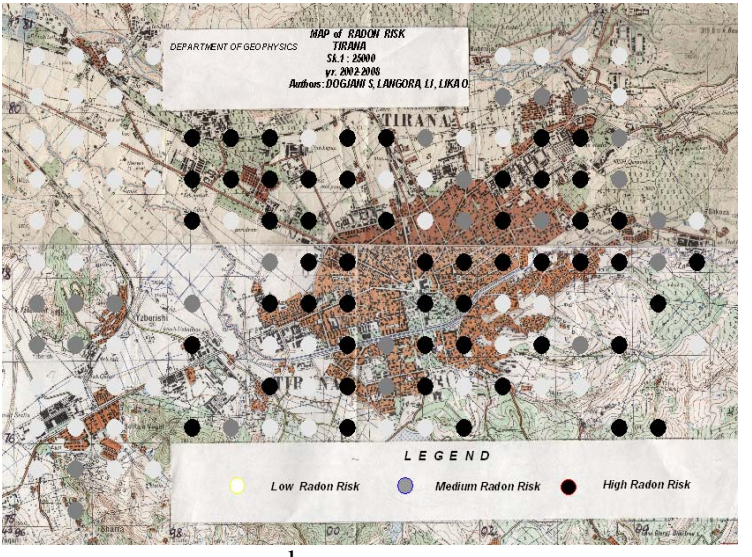

b

Fig. 6: a) Indoor Radon Map (draft), b) in soil Radon Map, Tirana city

Indoor radon measurements were carried out mainly in some working places to identify radon levels higher than 200Bq/m^3. In the second phase detectors were used mainly in winter. Currently, approximately 250 detectors have been used in different cities. Results report that there are some radon sectors in soil. The results obtained so far helped compile the map of radon concentration in soil, the map of ground permeability; the map of radon risk and the map of indoor radon concentration.

Currently, the map of indoor radon concentration levels in Albania, grid (10x10) km is under compilation process. Nevertheless, investigation must further.

3.3. Phase 3: Studies in unknown areas

The third phase relates to the investigation carried out in some small towns and centers of rural areas. This phase is just in the start point. Time, awareness and funds are here needful.

4. CONCLUSIONS AND RECOMMENDATIONS

The amount of radon emanating from the earth and concentrating inside homes varies considerably by region and locality, and is greatly affected by the residential structure as well as soil and atmospheric conditions. In Albania there is a good correlation between radon concentration in soils with the radon indoor concentration levels. Detailed investigation on radon distribution of any given area is a long-term process. Public awareness is fundamental. Consequently, measurements known as “hot items” with frequency of 2-3 times per year were carried out. Further measurements in some new working places have been made to provide additional information on radon concentration in the working places. Radon gas is not solely connected with geological features. High levels of radon could be encountered in low – medium radon risk areas too. Here, combing active measurement techniques with the passive methods for an accurate and long-term measuring process is necessary. With regards to radon-resistant construction, legislators may take into account to adopt codes that require builders to follow prescribed procedures, or that require builders to put in the system and ensure that radon levels are lowered to a given standard.

ACKNOWLEDGMENT

The authors owe a debt of a special gratitude to the Ministry of Environment of Albania, Agency for Research Technology and Innovation of

Albania (ARTI) and the World Bank for financially supporting the three following projects: i) Monitoring of radon concentration in indoor, in soil and in water in the Republic of Albania from 2002 to 2007 and from 2010 to 2011, ii) the Investigation of radon concentration levels in Areas with high risk and definition of levels in natural radionuclides lithological main types of Albania, (2010-2014) and, iii) the Set-up of the Laboratory of Radioactivity of Natural Order for the implementation studies in the field of "Risk Radon" in Albania, (UNILAB 2010-2011).

REFERENCES

Barnet I. 2004. Radon risk classification in the Czech Republic**.** Radon investigation in the Czech Republic. Czech Geological Survey Radon Corporation. Prague. **5,** 18-24.

Bolviken B, Celius EG, Nilsen R, Strand T.2003. Radon: a possible risk factor in multiple sclerosis. *Neuroepidemiology* .**22 (1),** 87-94.

Clever HL.1985. Krypton, Xenon, Radon gas solubobilities. *Solubility data series.* **2**. 463-468, Pergamon Press, Oxford.

Dogjani S. 2007. Monitoring the levels of radon gas concentration in soil and indoor environments. Archive Albanian Geological Service. (in Albanian).

Dogjani S, Langore Ll, Lika O, Paci R. 2009. Soil gas Radon, Indoor Radon and Gamma Dose Rate in Tirana city, Albania. The 5th Congress of Balkan Geophysical Society. 10-16 May Belgrade.

Koorevaar P, Meuelik G, Dirksen C. 1983. Elements of soil physics. Elsevier Science Publishers, Amsterdam, the Netherlands.

Laurier D, Valenty M, Tirmarche M.**2001**. Radon exposure and the risk of leukemia: A review of epidemiological studies. *Health Physics.* **81(3),** 272–288.

Matolin M, Kovalczyk R. 1998. *M*easurement of radon in soil air at references test sites in the Czech Republic. Radon Investigation in CR, Geological Survey, Prague, (7), 125-127.

Matolin M, Jane Z, Neznal M, Neznal. M. 2000. Geometry of soil gas sampling, soil permeability and radon activity concentration. Radon Investigation in Czech Republic. Geological Survey, Prague, (VIII), 27-29.

Muceku Y. **2011**. Land evaluation and site assessment-engineering geological mapping for Regional planning and urban development in Velipoja area. Albanian Journal of Natural and Technical Sciences. Publisher, Academy of Sciences of Albania. 101-114. ISSN: 2074-0867.

Muceku Y. **2005**. The influence of chemical-mineralogical composition on physical properties of cohesive soils of Tirana-Vora region. *AJNTS* -

Albanian Journal of Natural and Technical Sciences. Academy of Sciences of Albania.**18** (**2)**, 101-114. ISSN: 2074-0867.

Smith BJ, Zhang L, Field RW. 2007. Iowa radon leukemia study: A hierarchical population risk model. State. Med. **1026(25),** 4619–4642.

Van der Graaf ER, Meijer RJ. 1992. Calculation of shape factors of and pressure fields around an ellipsoidal permeability probe in some simple geometries, Rijksuniversiteit Groningen, the Netherlands.

World Health Organization (**WHO**) **(2009).** Radon and cancer.

DEVELOPMENT OF A SUCCESSFUL PROTOCOL FOR *IN VITRO* PROPAGATION OF *PRUNUS WEBBII* VIERH. USING DIFFERENT SEEDLING EXPLANTS

Valbona SOTA
Faculty of Natural Sciences, Department of Biotechnology, University of Tirana, Albania
Efigjeni KONGJIKA
Academy of Sciences, Section of Natural and Technical Sciences, Tirana, Albania

---

ABSTRACT

Wild almond (*Prunus webbii* Vierh.) is a woody species, which is difficult to propagate either generatively by seed or by vegetative methods (grafting or cuttings). Micropropagation or tissue culture is a means to address the production of disease-free, high quality planting material and the rapid production of many uniform plants. Multiplication of wild almond was carried out using zygotic embryos, cotyledons or shoots as primary explants to develop a successful propagation protocol. New plantlets were induced from explants cultured on basal MS medium in which PGRs combinations varied according to the explants. Results report that zygotic embryos can proliferate through direct or indirect organogenesis (depending on embryos isolation), cotyledons developed through somatic embryogenesis in BAP 0.5 mg l^{-1} concentration, meantime shoots developed via direct organogenesis. A great number of new plantlets identical to mother plants derived from embryos, cotyledons or shoots culture was obtained in the subculture stage. This protocol might be of great benefit for mass propagation and for genetic manipulation of wild almond.
***Keywords*:** wild almond, micropropagation, direct and indirect organogenesis, somatic embryogenesis, growth regulators

1. INTRODUCTION

Prunus webbii Vierh. trees are located in dry or semidry woodlands at altitudes up to 700 in Central Asia, Balkan Peninsula, South Italy etc. In Albania, this tree specie is located in Përmet, Mallakastër, Butrint, Konispol, Delvinë, Himarë, Vlorë, Tepelenë, Përmet, Leskovik, Skrapar etc. (Vangjeli *et al.,* 1995; Qosja *et al.,* 1992). This specie is considered endangered (EN) as defined in the IUCN criteria (Vangjeli *et al.,* 1995).

The wild almond can be used as rootstock for almond, nectarine and peach and for cultivated almond (Ladizinsky, 1999; Zohary and Hopf, 1993).

Hard resistance to drought conditions make wild almond trees is used in forestation of arid areas. In addition, it is ornamental tree specie (Heidari *et al.,* 2008). This species is characterized by high concentrations of ribonucleases, compounds that have antitumor and anti-bacteriological properties (Fang and Tzi Bun 2011). Wild almond trees are cyanogenic, because they contain compounds called cyanogenic glucosides which cause toxicity, but in small quantities stimulate respiration and improve digestion (Russell *et al.,* 1997).

The seeds have a stony endocarp and their germination is very difficult. This is of great concern for propagation of wild almond (Qosja *et al*., 1992; Vangjeli 2003). Micropropagation is a suitable method for obtaining a large quantity of genetically homogeneous and healthy plant material which can be used for planting (Kongjika *et al.*, 2002; Damiano *et al*., 2008; Kongjika *et al.,* 2010; Spahiu and Rama, 2012; Qendro *et al.*, 2013). The rapid *in vitro* multiplication of clonal plants is desirable to shorten crossing programs in fruit tree breeding (Daorden *et al.*, 2004).

The present paper aims to determine the optimal method for micropropagation in order to produce a great number of plants in a short period and identical to mother-plants.

2. MATERIAL AND METHODS

Plant material: collection and disinfection

Shoots, zygotic embryos (fully isolated embryos and embryos with part of cotyledons) and cotyledons were used as primary explants to establish the most appropriate protocol for *in vitro* cultivation. These explants were taken from wild almond trees of Fushë – Kruja.

Sterilization of zygotic embryos and cotyledons

Once left for 12- 24 hours in tap water in order to alleviate the embryos isolation, seeds sterilization is carried out. Double sterilization with $HgCl_2$ 0.01% for 20 min before and after removing seeds tegument followed immediately after. Thereafter the explants are rinsed out three times with sterilized H_2Od (Muriithi *et al*., 1993).

Sterilization shoots

Active shoots were cut in two - or three-node sections. The stem sections are washed carefully with water and are shaken for 5 min. in 70% ethanol, followed by 20 min. treatment with $HgCl_2$ 0.01% and two drops of Tween 20. Finally, stem sections are rinsed three times with sterile distilled water.

Media composition for in vitro cultivation

*Stage 1.*Organogenesis or embryogenesis induction

Fully isolated embryos and embryos with part of cotyledons*:* For organogenesis induction, both types of explants were inoculated in the following two nutrient media:

1. Basal nutrient medium MS (Murashige and Skoog, 1962) without phytohormones or PGRs and,
2. Basal MS medium supplemented with cytokinin, 6-benzylaminopurine (BAP) 1 mg l^{-1} and auxin, indole-3-butyric acid (IBA) 0.1 mg l^{-1}.

Cotyledons culture: Cotyledons were inoculated in basal MS medium to obtain preliminary data in somatic embryogenesis induction. The two combinations of PGRs concentrations tested are:

1. BAP 1 mg l^{-1-} and IBA 1 mg l^{-1} and,
2. BAP 0.5 mg l^{-1-} and IBA 1 mg l^{-1}.

Shoots culture: the basal MS medium supplemented with BAP 0.3 mg l^{-1}, IBA 0.1 mg l^{-1} and gibberellic acid (GA_3) 0.3 mg l^{-1} is used for shoots proliferation.

Stage 2. Subculture:

All plantlets regenerated from stage I were inoculated in basal MS medium supplemented with BAP 0.7 mg l^{-1}, naphthalene acetic acid (NAA) 0.01 mg l^{-1} and GA_3 0.1 mg l^{-1}.

Stage 3. Rooting

All the plantlets which didn't show spontaneous rooting were inoculated in modified MS basal medium which contained: ½ MS macroelements, MS microelements, MS vitamins and supplemented with NAA 0.1 mg l^{-1}.

All media were enriched with sucrose 3% and agar 0.7%. The pH of the media is adjusted to 5.6.

Stage 4. Plantlets acclimatization

Rooted plantlets were transferred after 3 – 4 weeks on rooting media to a mixture of soil, peat and perlite (2:1:1) (v/v), in 7 cm diameter plastic pots and placed in a controlled growth chamber at 20^{o}C. The plantlets were covered with plastic bags in order to maintain high humidity by removing them periodically for some minutes day after day. The bags were removed completely about four weeks after.

Chamber conditions for in vitro cultivation

The explants in every developmental stage were grown in the growth chamber at 25° ± 2°C, in a 16 h light/24 h regime with cool, white fluorescent light.

Statistical analysis

All experiments were repeated at least twice. Data collections in experiment were subjected to analyses of variance and evaluated using the statistical evaluation program JMP 7.0.

3. RESULTS AND DISCUSSION

Stage1. Organogenesis or embryogenesis induction

Embryo culture

Zygotic embryos are isolated from mature seeds under aseptic conditions using a stereo microscope. Two types of explants, the fully isolated zygotic embryos and embryos with part of cotyledons are tested to evaluate the role of cotyledons in embryo germination (Fig. 1a and b).

The explants were inoculated for organogenesis' induction in two types of nutrient media in order to evaluate the response in presence or absence of PGRs. The results are in Table 1 and Graphic 1 reported.

Table 1. Organogenic response during embryo culture of wild almond for both types of explants inoculated in two different nutrient media

Type of nutrient media	Fully isolated zygotic embryo		Embryos with part of cotyledons	
	Roots and leaves	Only leaves	Roots and leaves	Only leaves
Basal MS medium without PGRs	18 % ± 1,299 St dev 4,109	57,6 % ± 2,320 St dev 7,336	63,5 % ± 2,320 St dev 7,337	18,8 % ± 1,576 St dev 4,984
Basal MS medium with PGRs	0 % ± 0 St dev 0	54,1 % ± 2,433 St dev 7,694	29,9 % ± 1,642 St dev 5,195	55,5 % ± 2,409 St dev 7,619

The germination of zygotic embryos and roots development was observed after three days of cultivation. The leaves developed after 6 – 7 days. Due to

juvenile properties, the embryos possess a great regeneration potential which makes them optimal explants for *in vitro* micropropagation purposes.

Results report that these differences depend on explants type and their reaction in different induction media. The explants that showed better response are the embryos isolated with part of cotyledons for both media tested.

As it is reported, in proliferation of proembryos of *Eruca sativa* (Corsi, 1972), *Phaseolus coccineus* (Yeung and Sussex, 1979), and *Capsella bursa-pastoris* (Monnier, 1984) better results are observed when the embryo is isolated with a part of cotyledon. Furthermore, the presence of cotyledonal pieces during *in vitro* cultivation of avocado (*Persea americana* Mill.) doesn't reduce the germination percentage and the regenerated plantlets are morphologically identical to mother plants (Sánchez-Romero *et al*., 2007). Such explants are of great help for the seeds manipulation technique.

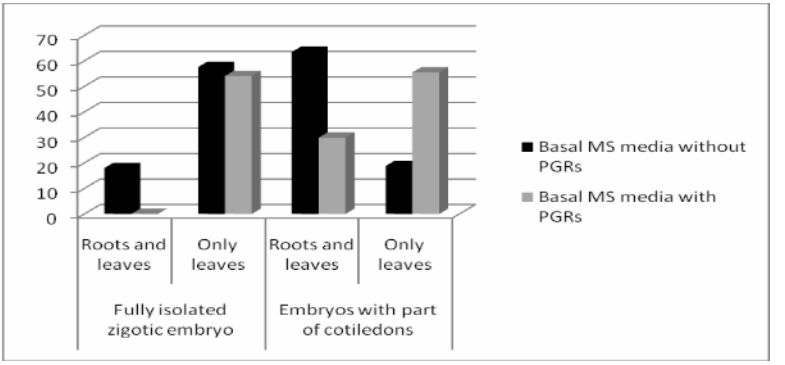

Graphic 1. Organogenic response during embryo culture of wild almond for both types of explants inoculated in two different nutrient media

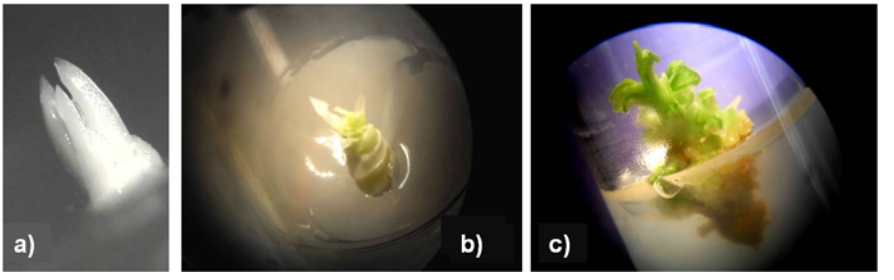

Fig. 1. Micropropagation of wild almond: **a)** Fully isolated zygotic embryo **b)** Embryos with part of cotyledons **c)** Shoots and roots regeneration after callusogenesis.

In the present investigation, callus formation for both explants especially in the contact zone with the nutrient media is typical. It resulted in a high percentage during cultivation in basal MS media with PGRs (Fig. 1c). In this case, the regeneration of new shoots occurs via direct and indirect organogenesis, because phytohormones or PGRs are present in the media. Their effect is added to the regulatory role that play the endogenous hormones, proteins and sugars deposited in the mature embryo. The role of PGRs in callus formation during embryo *in vitro* culture is considered an interesting process because in such way, in many plant species, is stimulated the formation of somatic embryos using zygotic embryos as initial explants (Maheshwari and Baldev 1961).

More effective resulted basal MS media without PGRs, especially when the isolated zygotic embryos are fully inoculated. Even for the other type of explants (zygotic embryos with part of cotyledons) organogenesis induction resulted in a high percentage in such media. In many cases, PGRs or phytohormones are not necessary when using mature zygotic embryos, as the embryo has a considerable size and is in an autotrophic phase. Raghavan and Srivastava (1982) stated that there is no specific need for additional amounts of PGRs in the nutrient media for a large broad of wild plants.

A minimal percentage of plantlets with roots and leaves and a very high percentage of those only with leaves for both of explants is typical of the basal MS media with PGRs. Maybe this is due to the high ratio cytokinin/auxin in the nutrient media. Murashige and Skoog, (1962) reported that a high ratio of auxin/cytokinin stimulates roots formation in tobacco callus, meanwhile a low ratio induces shoot formation. This hypothesis of organogenesis has been improved by (Torrey, 1966).

In many cases, cultivation of zygotic embryo is used to avoid successfully post zygotic incompatibility in many woody plants (Ramming, 1990).

Cotyledons culture

Wild almond cotyledons are cultivated to induce somatic embryogenesis from the proliferated callus. The later one is green in color (Fig. 2a). Basal media tested is different from BAP and IBA concentrations (1, 0.5 mg l^{-1}), meanwhile IBA concentration (1 mg l^{-1}) remained the same in both media. This difference is of great importance for the callus proliferation during this stage of culture (Table 2).

Table 2. BAP effect in callus proliferation during *in vitro* cultivation of cotyledons

	BAP (1 mg l^{-1})	BAP (0.5 mg l^{-1})
Callus proliferation (%)	**0 %**	**49 %**

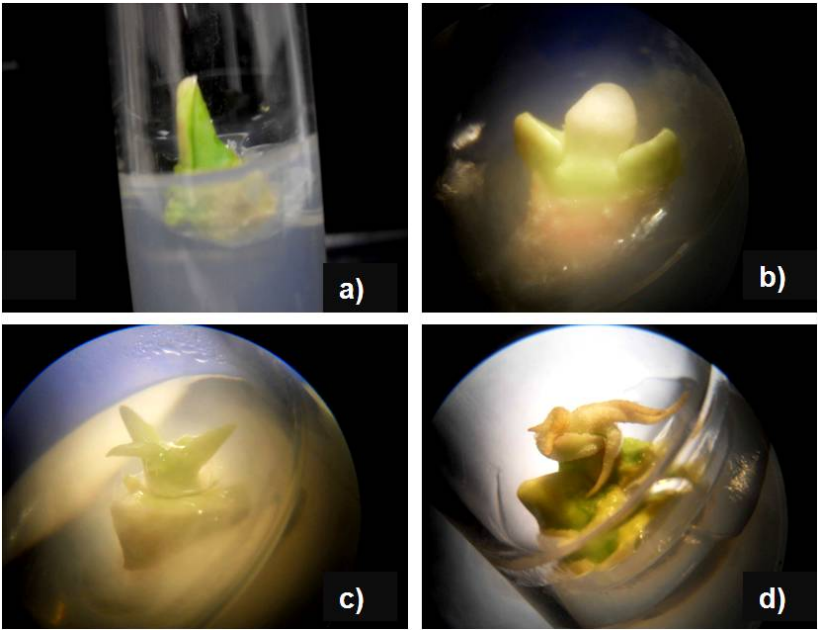

Fig. 2. Stages of cotyledons during *in vitro* cultivation **a)** compact callus with green color **b)** initial structures of somatic embryos **c)** shoots formation after callus differentiation **d)** bipolar structure (shoot and root apex) formed during somatic embryogenesis

It seems that a higher concentration of BAP cytokinin in basal medium inhibits callus induction in explants. The high ratio auxin/cytokinin stimulates somatic embryogenesis, roots and callus formation. Harvey and Grasham (1969) provide information about the efficiency of IAA, NAA and 2,4-D for callus induction in conifers. Regarding somatic embryogenesis of *Quercus castaneifolia* results report that these explants show embryogenic callus proliferation in nutrient media supplemented with BAP and IAA (0.5 and 1.0 mg l^{-1}), while in higher doses of this PGRs (BAP 1 mg l^{-1} and AIA 2 mg l^{-1}) callusogenesis induction is not observed (Ehsanpour and Zahedi, 2006). Embryogenic callus formation from cotyledons of *Juglans nigra* (Neuman *et al.,* 1993) and *Albizzia procera* (Datta, 1987) is also reported.

Shoots culture

Plant material is obtained by collecting the active explants between January and April, as buds start swelling from shoots in dormancy. Most often shoot tips and meristems are the explants of choice due to their genetic stability.

In the first days of cultivation, the explants did not show signs of proliferation. Organogenic response which is characterized by an increase in leaves number and shoots length was obtained 2-3 days later (Table 3, Graphic 2).

Table 3. Biometric parameters of plantlets during shoots proliferation and elongation

	20 days	**30 days**	**40 days**
Shoots length	1,05 ± 0,29	1,44 ± 0,32	1,89 ± 0,37
	St dev 0,93	St dev 1,02	St dev 1,17
Leaves number	2,20 ± 0,53	5,20± 0,55	7,10 ± 0,92
	St dev 1,68	St dev 1,75	St dev 2,92

Shoots did not show callusogenesis, but were developed via direct organogenesis. Results report that leaves number increases faster in comparison with shoots length. Here, lateral buds are not formed and the plantlets are fragile. The leaves are thin and poorly developed.

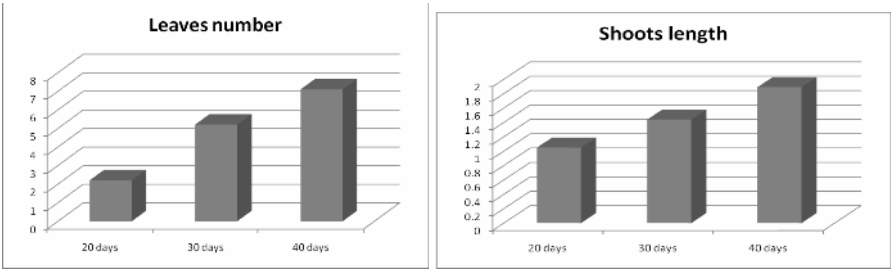

Graphic 2. Biometric parameters, observed during shoots proliferation and elongation

In the first stages of shoots proliferation and elongation, the impact of interaction of low doses of three types of PGRs in basal media (BAP, IBA and GA_3) is clear. Yildirim *et al.*, (2007) accentuated that only high doses of BAP (1 mg l^{-1}) are of positive impact for micropropagation of wild almond shoots.

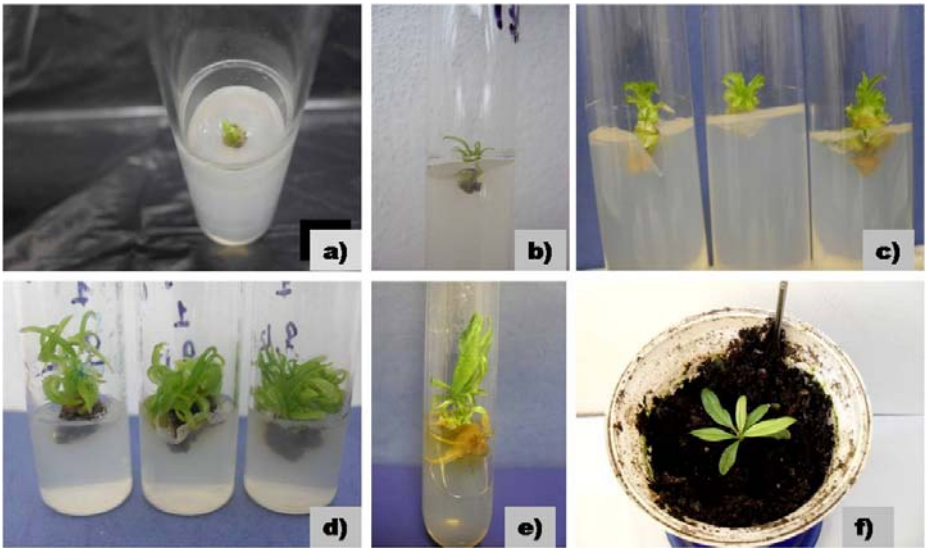

Fig. 3. Stages of wild almond shoots during *in vitro* cultivation: **a, b)** First stage of shoots proliferation; **c)** Plantlets with lateral shoots regenerated after stage I **d)** Hyper hydrated plants developed during subcultures **e)** Roots development after callus formation during cultivation in rooting media **f)** Acclimated plant of wild almond

Stage 2. Subculture

The regenerated plantlets from stage 1 were inoculated in subculture medium. Most of explants reacted normally giving a great number of leaves and lateral shoots (Fig. 1c). However, signs of hyper hydration were observed. Such plantlets do not survive and were eliminated (Fig. 1d).

Studies on wild almond propagation are of great interest and investigations to find a universal nutrient medium specific for this species further (Nas and Bolek 2009). As they supposed that the composition of such medium must imitate seed composition, a new specific medium using NAS nutrient medium as a basis was investigated (Nas and Read, 2004). The new tested medium is compared with several basal nutrient media such as MS, WPM, DKW using mature explants from different cultivars of wild almond and, NRM. MS and WPM are found suitable for subculture stage. These results are similar with those in the present paper reported.

Except new shoots formation, during subcultures, callus formation in shoot basis was observed and new shoots were developed from this callus. Micropropagation coefficient resulted very high and this is due to the presence of BAP cytokinin, whose function is apical dominance interruption and new shoots formation. Similar observations for the role of cytokinins in

micropropagation process are reported in (Muna *et al*., 1999; Pruski *et al.,* 2000; Saponari *et al.,* 1999).

Stage3. Rooting

Some regenerated plantlets from both explants tested showed spontaneous rooting during stage 1. Optimal rooting percentage was observed when embryos with part of cotyledons were inoculated in MS basal medium with PGRs (Table 1 and Graph. 2).

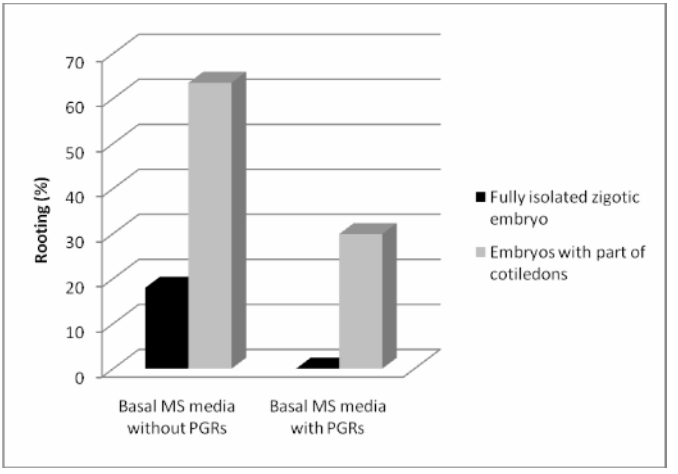

Graphic 2. Spontaneous rooting (%) in organogenesis induction medium for both types of explants

Many regenerated plants from stage 1 were not transferred to soil for acclimatization processes, but were inoculated in subculture medium to obtain a great number of plants. Once inoculated, the plantlets were transferred in rooting medium. Rooting response was observed more than 4 weeks later and rooting percentage resulted to be 41%. Here, callus formation in shoots basis in contact with the medium is typical (Fig. 1e).

Monter (1992) reported that auxin α-naphtaleneacetic acid (NAA) plays an important role in the in *vitro* rhizogenesis induction in *Malus* sp. These observations are similar to the results obtained from this study. Olate *et al.,* (2009) obtained high results in shoots rhizogenic response of *Juglans regia* L. using auxin IBA.

Stage 4. Plantlet acclimatization

This stage is very difficult for wild almond. The plantlets that showed spontaneous rooting during stage 1 were easily acclimated. For

micropropagation purposes, they were not acclimated but transferred in stage 2. The acclimatization was very difficult for the regenerated plantlets derived from stage 2 and 3. The number of acclimated plants was very low (Fig. 1f).

4. CONCLUSIONS

The following conclusions are drawn: i) in vitro embryo culture is of great impact for micropropagation of wild almond plants, ii) basal MS medium without PGRs resulted more effective for organogenesis induction, iii) plant regeneration resulted in a high percentage when using embryos with part of cotyledons as primary explants, iv) induction of somatic embryogenesis from cotyledons in vitro cultivation resulted efficient in BAP 0.5 mg l^{-1} concentration, v) a great number of new plantlets identical to mother plants derived from embryos, cotyledons or shoots culture was obtained during subculture stage the and, vi) spontaneous rooting resulted in a high percentage meanwhile the induced one was in a lower rate. Acclimatization was very difficult for micropropagated plantlets of wild almond.

REFERENCES

Corsi G. 1972. The suspensor of *Eruca sativa* Miller (Cruciferae) during embryogenesis in vitro. *Giornale Botanico Italiano.* 106:41–54.

Damiano C, Arias Padro MD, Frattarelli A. 2008. Propagation and establishment *in vitro* of myrtle (*Myrtus communis* L.), pomegranate (*Punica granatum* L.) and mulberry (*Morus alba* L.), *Propagation of Ornamental Plants.***8 (1),** 3-8.

Daorden ME, Marín JA, Arbeloa A. 2004. Stratification Temperature affects the *in vitro* Germination of Immature *Prunus* Embryos, *ISHS. Acta Horticultura.* **658**, vol. 2: 135-140.

Datta SK. 1987. Tissue culture propagation of forest trees –limitations and perspectives. In: PK Khosla and DK Khurana (Eds.) Agroforesty for Rural Needs. Vol., *Indian Society of Tree Scientists.***1**, 234-241.

Ehsanpour AA, Zahedi S. 2006. Induction of somatic embryogenesis from cotyledon of oak (*Quercus castaneifolia*). *Journal of Science UT.* **32(1)**, 47-50.

Fang EF, Tzi Bun N. 2011. Ribonucleases of different origins with a wide spectrum of medicinal applications. *Biochimica et Biophysica Acta.* 1815: 65-74**.**

Harvey AE, Grasham JL. 1969. Procedures and media for obtaining tissue cultures of 12 conifer species. *Canadian Journal of Botany.* **47**, 547-549.

Heidari M, Rahemi M, Daheshvar MH. **2008**. Effects of Mechanical, Chemical Scarification and Stratification on seed germination of *Prunus scoparia* (Spach.) and *Prunus webbii* (Spach.) Vierh. *American – Eurasian Journal of Agricultural & Environmental Sciences*, 3 (1): 114 – 117, 2008. ISSN 1818 – 6769.

Kongjika E, Mata V, Zekaj (Trojani) Zh, Abdullai K. 2010. *In vitro* organogenesis of Balkanic Gesneriad species (*Ramonda*), *Albanian Journal of Natural and Technical Sciences* (*AJNTS*). **27 (1),** XVI: 115-130.

Kongjika E, Zekaj Zh, Çaushi E, Stamo I. 2002, Plant Biotechnology – *In vitro* Culture, Akademia e Shkencave, (in Albanian). 97 – 105;

Ladizinsky G. 1999. On the origin of almond. *Genetic Resources and Crop Evolution.* **46**,143–147.

Maheshwari P, Baldev B. 1961. Artificial production of buds from the embryos of *Cuscuta reflexa*. *Nature,* **191**,197–198.

Monnier M. 1984. Survival of young immature *Capsella* embryos cultured *in vitro*. *Journal of Plant Physiology.* **115**,105–113.

Monter AV. 1992. Micropropagation des fruitiers. In: Rosell C.H., Villalobos A.V.M. Fondements théoriques et pratiques de la culture des tissus végétaux, FAO, 145-153.

Muna AS, Ahmad AK, Mahmoud K, Abdul Rahman K. 1999. *In vitro* propagation of a semi-dwarfing cherry rootstock. *Plant Cell, Tissue and Organ Culture*. **59**, 203–208.

Murashige T, Skoog F. 1962. A revised medium for rapid growth and bioassays with tobacco tissue cultures. *Physiology Plantarum*. **15**, 473-497.

Muriithi WT, Harry IS, Yeung EC, Thorpe TA. 1993. Plantlet regeneration in chir pine (*Pinus roxburghii* Sarg): morphogenesis and histology. *Forest Ecology and Management.* **57**, 141–160.

Nas M, Read PE. 2004. A hypothesis for the development of a defined tissue culture medium for higher plants and micro-propagation of hazelnuts. *Scientia Horticulturae.* **101**,189-200.

Nas MN, Bolek Y. 2009. Short Cut to Long Distance: Developing an Almond Micropropagation Medium, 5th International Symposium on Pistachios and Almonds – ISHS – Sanliurfa – Turkey, Oct.06-10, 2009, *Book of Abstracts*. 230.

Neuman MC, Preece JE, van Sambeek JW, Gaffney GR. 1993. Somatic embryogenesis and callus production from cotyledon explants of Eastern black walnut. *Plant Cell Tissue Organ Culture*.**32**, 9-18.

Olate MS, Sáez P, Ríos D. 2009. Rhizogenic induction in adult *Juglans regia* L. cv. Serr tissue induced by indole butyric acid and *Agrobacterium rhizogenes*. *Chilean Journal of Agricultural Research.* **69(2)**, 286-291.

Pruski KW, Lewis T, Astatkie T, Nowak J. 2000. Micropropagation of Chokecherry and Pincherry cultivars. *Plant Cell, Tissue and Organ Culture*. **63,** 93–100.

Qendro A, Zekaj (Trojani) Zh, Mano R, Sota V. 2013. Reaction of two subspecies of *Aster albanicus* Degen. to different media during in vitro cultivation. *Albanian Journal of Natural and Technical Sciences* (*AJNTS*). **34 (1),** XVIII,159-170.

Qosja Xh, Paparisto K, Demiri M, Vangjeli J, Balza E. 1992. Albanian Flora, Akademia e Shkencave të Republikës së Shqipërisë. Qendra e Kërkimeve Biologjike, Tiranë, (in Albanian), **4.**

Raghavan V, Srivastava PS. 1982. Embryo culture. In: Johri, B. M., ed. Experimental embryology of vascular plants. Berlin: Springer-Verlag. 195–230.

Ramming D.W. 1990. The use of embryo culture in fruit breeding. *HortScience*. **25**, 393-398.

Russell AB, Hardin JW, Grand L. 1997. Poisonous Plants of North Carolina. North Carolina State University.

Sánchez-Romero C, Perán-Quesada R, Márquez-Martín B, Barceló-Muñoz A, Pliego-Alfaro F. 2007. In vitro rescue of immature avocado (*Persea americana* Mill.) embryos. *Scienta Horticulturae.* **111**,365-370.

Saponari M, Bottalico G, Savino G. 1999. *In vitro* propagation of *Prunus mahaleb* and its sanitation from Prune dwarf virus. *Advances in Horticultural Science*.**13**,56–60.

Spahiu E, Rama P. 2012. Effect of salt concentration on *in vitro* micropropagation of GF-677 peach rootstock (peach x almond). *Albanian Journal of Natural and Technical Sciences* (*AJNTS*). **32 (1), XVIII**. 107-116.

Torrey J.G. 1966. The initation of organized development in plants. Adv. Morphog., 5: 39 – 91.

Vangjeli J. 2003. Field Guide of Albanian Flora, Akademia e Shkencave të Republikës së Shqipërisë. Instituti i kërkimeve Biologjike, Tiranë (in Albanian).

Vangjeli J, Ruci B, Mullaj A. 1995. Red Book. Threatened and Rare Plants Species of Albania. (in Albanian), Akademia e Shkencave të Republikës së Shqipërisë. Qendra e Kërkimeve Biologjike, Tiranë. 52.

Yeung EC, Sussex IM. 1979. Embryogeny of *Phaseolus coccineus*: the suspensor and the growth of the embryo-proper in vitro. *Zeitschrift fur Pflanzenphysiologie*. **91**:423–433.

Yildirim H, Tilkat E, Onay A, Ozen HÇ. 2007. *In Vitro* Embryo Culture of Apricot, *Prunus armeniaca* L. cv. Hacıhaliloglu. *International Journal of Science & Technology*. **2 (2)**, 99-104.

Zohary D, Hopf M. 1993. Domestication of plants in the old world. Clarendon Press, Oxford.

POSSIBLE CORRELATION BETWEEN THE DIVERSITY OF 16-23S RDNA-ITS OF *SYNECCHOCOCUS* POPULATIONS AND QUALITY OF WATERS AT DURRËS BAY

LAURA GJYLI
Faculty of Professional Studies, Department of Medicine,
University Aleksandër Moisiu, Durrës, Albania
ARIOLA BACU
Department of Biotechnology, Faculty of Natural Sciences,
University of Tirana, Albania

ABSTRACT

Genus *Synechococcus* gathers organisms of considerable genetic diversity, which are classified into groups based on their physiological diversity, on the presence of the accessory pigment phycoerythrine, and the diversity of the 16S-23S rDNA internal transcribed spacer (ITS) regions. Correlation between the physical and biological indicators at six sampling stations from the Durrës Bay, Albania, which represent hot spots of different sources of pollution, and the diversity of populations of *Synechococcus* based on the dimensions of ribosomal DNA- ITS, was explored. Chlorophyll a (*Chl a*), nitrogen (as NO_3^-), and phosphorus (as PO_4^{3-}) were measured monthly from April to October 2011 and from June to October 2012 to investigate the quality of waters. Four different ITS-a and three ITS-b regions were amplified. Results report that in Plepa Channel there was an extra ITS, informing on a new population not present at the other stations. In addition, there is a positive correlation between the total phosphorus and diversity of populations and a negative correlation between nitrogen and diversity of populations of *Synechococcus*.
Keywords: internal transcribed spacer (ITS) region, *Synecchococus spp*., nitrogen, phosporus, *Chl a*, trophic state.

1.INTRODUCTION

In marine ecosystems, environmental clines exist in temperature, light intensity, spectral composition, and nutrient availability that can affect the distribution, composition and diversity of organisms (Lavin *et al.*, 2008). *Prochlorococcus* and *Syneccococus*, the unicellular cyanobacteria, have ecotypes, which have identifiable geographic ranges. They co-occur in many oceanographic regions, but *Synechococcus* tolerates a broader temperature

range, has a broader latitudinal distribution and usually is limited to shallower depths (less than 100 m). The indicators system provides useful information about the state of coastal waters, which are ecosystems with high biodiversity and assessment of the dynamics of environmental changes (progressive or regressive) (Bacu *et al.*, 2011). Bacu *et al.* (2010) have already reported a direct relationship between phosphorus concentrations, chlorophyll *a* (algal biomass), and clarity of the waters because, phosphorus drives algal growth which then affects water clarity.

The ribosomal operon, which in prokaryotes is generally composed of 16S and 23S ribosomal RNA (rRNA) genes separated by an internal transcribed spacer (ITS) region, is part of the slowly evolving bacterial set of genes. Several reports have indicated that any organism's gene content closely reflects phylogeny, and that incremental diversification of the core genome reflects the diversification of the 'accessory' genome over time (Feil, 2004). The ITS contains antitermination box B - box A motifs, which prevent premature termination of transcription (Berg *et al.,* 1989), and also have a role in holding the secondary structure of the nascent rRNA for processing to mature rRNAs (Apirion and Miczak 1993). The spacer between the 16S and 23S rRNA genes can encode 0, 1, or 2 tRNA genes. Because the ITS exhibits a great deal of length and sequence variation, it has been used in many bacterial groups to delineate closely related strains (Barry *et al.,* 1991; Leblond-Bourget *et al.,* 1996; Christensen *et al.,* 1999). Whole-genome sequences suggest that low-B/A *Prochlorococcus* strains possess a single rRNA operon, while high-B/A *Prochlorococcus* and marine *Synechococcus* strains possess two identical rRNA operons (http://www.jgi.doe.gov/JGI_microbial/html/index.html).

Investigation of cyanobacterial species at the coastal lagoons and marine waters in Albania, was based on PCR amplification of species-specific ribosomal DNA regions (Bacu *et al*., 2012; 2013; Gjyli *et al.,* 2013 b). The present investigation aims at using rDNA-ITS dimensions as a phylogenetic tool to identify the diversity of populations of *Synechococcus spp.* at the Durrës Bay and finding any possible correlation between the main biological and physical indicators of the trophic state of the waters (nitrogen, phosphorous, *Chl a*) and the level of diversity of ITS at populations of the six sampling stations.

2. MATERIAL AND METHODS

Sampling Stations and Collection Processing

Figure 1 depicts the sampling stations located along the Durrës Bay (35 km long) (Pano et al., 2006). Samples were monthly collected —from April to October 2011 and from June to October 2012— in the following stations:

Golemi Beach (GB), Plepa Channel (PCh), Hekurudha Beach (HB), Ex-Fuel Quay in Marine Durrës Harbour (EFQ), Water Channel of Durrës District (WChDD) and Currila Beach (CB), at 1 meter depth from the water surface. Sea water (~ 4 l) was collected for phytoplankton DNA isolation (2 l), and for chlorophyll *a*, total phosphorous and nitrogen (2 l) investigation purposes. Samples were stored in the dark at 2-litre plastic containers until delivery at the labs.

Fig. 1. Locations of sampling stations at Durrës Bay (from right to left Golemi Beach (GB), Plepa Channel (PCh), Hekurudha Beach (HB), Ex-Fuel Quay in Marine Durrës Harbour (EFQ), Water Channel of Durrës District (WChDD) and Currila Beach (CB). (Google Earth, 2014).

Filtration of Water for isolation of total phytoplankton DNA, DNA extractions and quality assurance

The water samples for picophytoplankton DNA isolation were filtered through a 47 mm diameter 0.7 µm pore size, GF/F filter under gentle vacuum. The filter was stored at -20ºC in a 1 ml of STE (100 mM NaCl, 10mM Tris HCl, 1 mM EDTA (pH 8.0) until DNA extraction. With little modifications, the DNA extraction was based on (Fuhrman *et al.,* 1988; Pichard *et al.,* 1993; Paul 2008). Quality and quantity of DNA were measured using the UV/VIS spectrophotometer as recommended in (Sambrook *et al.,* 1989).

Measurement of Chl a, nitrogen (as NO_3^-), phosphorus (as PO_4^{3-})

APHA *et. al.,* (1998; 2005) recommendations were followed for the extraction of *chlorophyll a.* The fluorometric method was applied for the determination of the *Chl a* concentration in µg/l.

Nitrate and phosphate were measured spectrophotometrically using the PhotoLab 6600 UV-VIS, WTW GmbH.

Polymerase Chain Reaction (PCR) for the amplification of ITS regions of ribosomal DNA

The primers used to amplify cyanobacterial 16S-23S ITS rDNA region were ITS-af / ITS-ar dhe ITS-bf / ITS-br as recommended in (Lavin *et al.,* 2008). PCR was run in a 25 µl total volume, with Taq polymerase (2,5 U), 3 µl $MgCl_2$ (25 mM), 2,5 µl PCR buffer (1X), 0,5 µl dNTPs 10mM, and 25 pmol of each primer. Cycling conditions were 95°C for 5 min, followed by 28 cycles of 95°C for 1 min, 61°C for 1min, and 72°C for 2 min. Final step was a 10 min stretch at 72°C. DNA products were checked by a 1.5 % agarose gel under the UV.

3.RESULTS

The amplification of 16-23S ITS regions to assess genetic diversity in Synechococcus populations from the sampling stations of Durrës Bay

In the present paper, the investigation of the picophytoplanktonic diversity based on the variability of the 16-23rDNA-ITS is of primary importance. The amplification gave products for both the ITS-a and ITS-b (Lavin *et al.,* 2008) regions of the bacterial operon. ITS-a amplified had four dimensions, respectively 1000, 900, 800, and 300 bp. The ITS-b amplified had three dimensions, respectively 550 bp, 400 bp, and 250 bp (Figure 2).

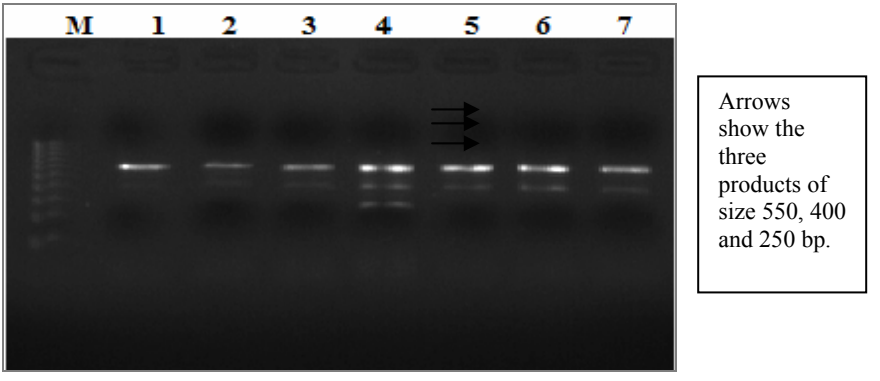

Fig.2. ITS-b PCR products of ribosomal DNA from picocyanobacteria *Synechoccocus.* From right to left : M = Marker 1kbp; 1 = GB (July, 2011); 2= WChDC (July, 2011); 3 = GB (September, 2011); 4 = PCh (September, 2011); 5 = EFQ (September, 2011); 6 = WChDC (July, 2012); 7 = GB (September, 2012).

Rocap *et al*., (2002) and Lavin *et al.,* (2008) provided information about the presence of different dimensions of ITS in marine and fresh waters. In the Durrës Bay, where sources of pollution such as fuels, heavy metals (Totoni and Mulla, 2009; Wilbur Smith Associates, 2003), waste spills, organic

compounds (Boçari *et al.*, 2006) and construction waste are of great impact for the growth of microbial populations, the genetic variability of the populations of *Synechococcus* might be interpreted in terms of the tendency for a better adaption to unfavorable environmental conditions. The ITS fragments, even a or b, were amplified at all stations, except for the smallest ITS-b fragment of 250 bp, which was found only at the PCh station (Fig. 2).

Quality of waters according nutrients N and P

Nitrate (NO_3^-)

Maximal values of nitrate (NO_3^-) (5.8mg/l and 2.1mg/l) were recorded respectively in May 2011 at the HB station and in August 2012 at the EFQ station, while minimal values (12.06 mg/l and 0.3 mg/l) were recorded in October, at the PCh station 2011 and September – October at the CB station, 2012 (Gjyli and Kolitari, 2011; Gjyli *et al.,* 2013a, b) (Table 1, Figure 3).

Nitrate levels were decreased in June, September and October 2011, leading to a depletion of nitrate load (Figure 5). Since nitrogen stimulates the growth of marine phytoplankton and is considered as a key nutrient to coastal eutrophication (Ryther and Dunstan, 1971), it is likely that nitrates have been absorbed by the algae. As in 2012 the NO_3^- concentration was 0.77 ± 8.9 (or1.8 times) lower than in 2011, i.e. records of nitrate level reduction, water quality has been improving over time (Gjyli *et al.,* 2013b).

Table 1. Maximum, minimum, mean, and total mean of NO_3^- concentrations measured in stations GB, PCh, HB, EFQ, WChDD, CB during sampling campaigns of 2011 and 2012.

		GB	PCh	HB	EFQ	WChDD	CB
2011	**Max.**	5.5	4.4	5.8	5.3	3.6	5.1
	Min.	0.08	0.06	0.11	0.09	0.15	0.08
	Mean	**1.89**	**1.48**	1.80	1.68	1.50	1.85
	Total Mean	1.70					
2012	**Max.**	1.6	1.5	1.5	2.1	1	1.8
	Min.	0.6	0.8	0.4	0.7	0.5	0.3
	Mean	0.90	1.12	0.88	**1.18**	**0.72**	0.78
	Total Mean	0.93					

Max. = maximum, Min. = minimum, Total Mean = total mean.

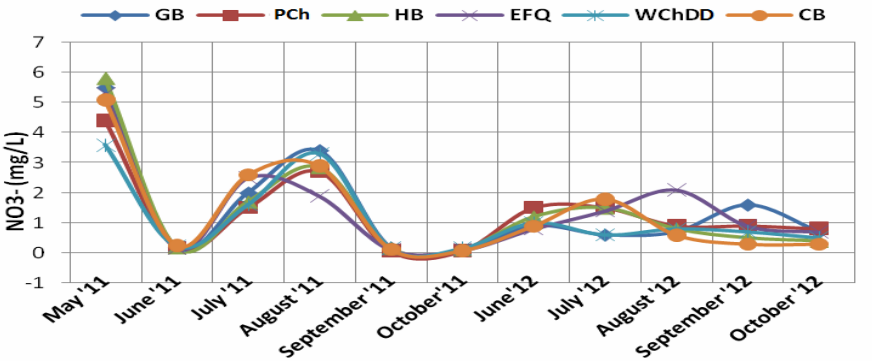

Fig. 3. Values of NO_3^- concentrations measured monthly.

Converted to NO_3-N as recommended by the ICES (International Council for the Exploration of the Sea; http://ocean.ices.dk/Tools/UnitConversion.aspx) (1µg NO_3^-/l = 0.225897 µg N/l), the total mean values of NO_3^- in 2011 and 2012 are respectively, 0.38 mg/l mg/l and 0.21 mg/l. Gjyli *et al.* (2013b) reported that the values are higher than allowance for surface waters under natural conditions (Chapman, 1996). In 2011, the highest levels of NO_3^- were found in the GB station. The lowest levels were found in the PCh station. In 2012, the highest levels of NO_3^- were found in the EFQ station. The lowest levels of NO_3^- were found in the WChDD station.

Fig.4. Channels of waste waters along coastal Durrës Bay, with constantly or temporarily discharge at night or early in the morning (Photo: Gjyli, 2013, from left to right 1 & 2 - WChDD; 3 &4- PCh; 5- GB; 6- channel near Durrës Archaeological Museum area).

Phosphates (PO_4^{3-})

Maximal values of phosphate (PO_4^{3-}) (0.6 mg/l and 0.41 mg/l) were recorded respectively in July 2011 at the WChDD station and CB station, and in June 2012 at PCh station, while minimal values (0.019 mg/l and 0.17 mg/l) were recorded in June for the PCh 2011, and October 2012 for the CB station (Gjyli and Kolitari, 2011; Gjyli *et al.,* 2013a, b) (Table 2, Figure 5). So, in May, June, and September (excluding PCh) and October 2011, the PO_4^{3-}

concentration levels were decreased, leading to phosphate depletion, probably due to the consumption of PO_4^{3-} from algae. In 2012 the concentration of PO_4^{3-} was 0.08 ± 0.14 (or 1.4 times) higher than in 2011, reporting an increase in phosphate level (Gjyli *et al.,* 2013b).

Table 2. Maximum, minimum, mean, standard deviation, variation coefficient and total mean of PO_4^{3-} concentrations measured in stations GB, PCh, HB, EFQ, WChDD, CB during the sampling campaigns of 2011 and 2012.

		GB	PCh	HB	EFQ	WChDD	CB
2011	**Max.**	0.4	0.5	0.5	0.5	0.6	0.6
	Min.	0.026	0.019	0.034	0.022	0.029	0.026
	Mean	**0.14**	**0.20**	0.17	0.17	0.19	0.16
	Total Mean	0.17					
2012	**Max.**	0.26	0.41	0.26	0.34	0.34	0.24
	Min.	0.19	0.21	0.18	0.2	0.22	0.17
	Mean	0.23	**0.28**	0.23	0.25	0.27	**0.22**
	Total Mean	0.25					

Legend: Max. = maximum, Min. = minimum, Total Mean = total mean.

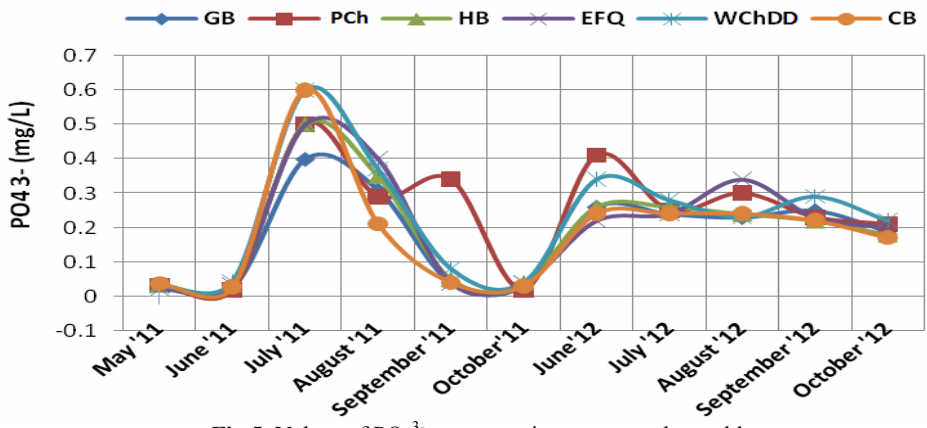

Fig 5. Values of PO_4^{3-} concentrations measured monthly.

Converted to (PO_4-P) as recommended by the ICES (International Council for the Exploration of the Sea; http://ocean.ices.dk/Tools/UnitConversion.aspx) (1µg PO_4^{3-}/l = 0.326138 µg P/l), the total mean values of PO_4^{3-} in 2011 and 2012 were 0.055 mg/l and 0.081 mg/l, respectively. Gjyli *et al.* (2013b) stated that the aforementioned values are higher than allowance recommended (PO_4-P) (0.005 - 0.020 mg/l) for surface waters under natural conditions (Chapman, 1996). In 2011, the

highest levels of PO_4^{3-} were found at the PCh station. The lowest levels of PO_4^{3-} were found at the GB station. In 2012, the highest levels of PO_4^{3-} were found at the PCh station. The lowest levels of PO_4^{3-} were found at the CB station.

Chlorophyll a (Chl a) content

Maximal values of total chlorophyll a (*Chl a*) (87.69 µg/l and 39.57 µg/l) were recorded in June, 2011 at the EFQ station and in September 2012 at the WChDD station, while minimal values (14.11 µg/l and 6.92 µg/l) were recorded in June 2011 at the PCh station and June 2012 at the CB station (Gjyli and Kolitari, 2011; Gjyli *et al.,* 2013a, b) (Table 3, Figure 6). As in 2012 the concentration of *Chl a* was 24.22 µg/l ± 0.91 (or 2.1 times) lower than in 2011, trophic state has been improved over time (Gjyli *et al.,* 2013b). Reported in Table 3, data on *Chl a* concentrations in 2011 and 2012 report that trophic state has been improved.

Table 3. Maximum, minimum, mean and total mean of *Chl a* concentrations measured in stations GB, PCh, HB, EFQ, WChDD, CB during the sampling campaigns of 2011 and 2012.

		GB	PCh	HB	EFQ	WChDD	CB
2011	**Max.**	70.66	70.31	70.32	87.69	71.9	55.3
	Min.	23.7	14.11	29.5	26.8	33.5	14.81
	Mean	47.22	41.14	49.72	**56.28**	53.11	**28.75**
	Total Mean	46.04					
2012	**Max.**	31.65	35.41	33.72	28.12	39.57	25.83
	Min.	11.79	12.37	8.45	10.38	13.43	6.92
	Mean	21.91	24.47	21.27	20.55	**26.44**	**16.26**
	Total Mean	21.82					

Legend: Max. = maximum, Min. = minimum, Total Mean = total mean.

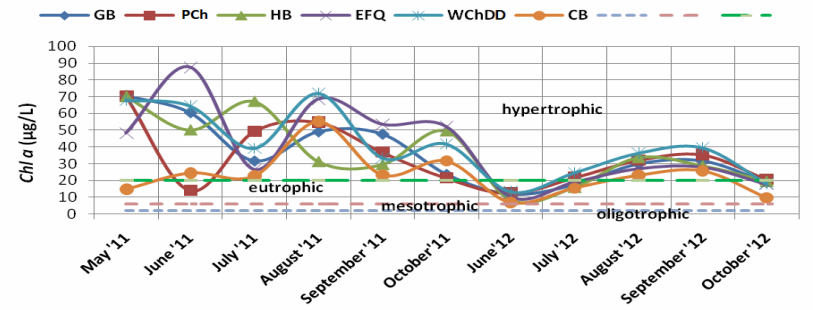

Fig. 6. Values of *Chl a* concentrations measured monthly (Multiparameter probe Idromar, APHA *et al*., 2005) and trophic state (Hakanson, 1983).

Here, using appropriate filters in (ChP) in summer of 2012 and restrictions imposed by the law to owners of buildings and businesses that discharge wastewater along the coast of Durrës Bay have been of great impact (Gjyli *et al.,* 2013b). Basing on Håkanson *et al*., (2007), coastal water systems of different trophic levels based on the content of *Chl a* (modified by OECD, 1982; Håkanson and Jansson 1983; Wallin *et al*., 1992), could be classified into four trophic classes: oligotrophic (Chl *a* <2 μg/l), mesotrophic (2-6 μg/l), eutrophic (6-20 μg/l), hypertrophic (> 20 μg/l). Eutrophic areas are areas of high primary production due to the excess of nutrients, and are subject to algal blooming, resulting in poor water quality. When the number of algae grows, there is also a risk for the production of biotoxins (from the harmful algal blooms HABs) (UNEP/MAP, 2012). All stations are categorized as hypertrophic, except PC that was in eutrophic state in 2012. Sewage remains the main source of water pollution, especially increased nutrient loads, which causes the blooming of algae. Thus, an accurate sewage treatment and waste disposal management should be of primary concern for local authorities and putting into operation of the processing plant wastewater in ShënVlash area, would significantly improve the trophic state of coastal waters. Hypereutrophic waters are rich in nutrients and are characterized by algae bloom and low transparency (EPA 2008). In 2011, the EFQ station was characterized by the highest level of *Chl a* and the CB station was characterized by the lowest level of *Chl a.* In 2012, the WChDD station had the highest level of *Chl* content, whereas the CB station was characterized by the lowest level of *Chl a* content.

The relationship between ITS region diversity and quality of waters

The ChP station is characterized by the highest variability of the population of *Synechococccus* according to the dimensions of the amplified ITS regions of their ribosomal DNA. Two ITS-b amplified (respectively 550 bp, and 400 bp) regions out of three are present at all stations, while the third category only at PCh samples (250 bp). In 2011, the PCh station had the lowest level of nitrate. Here, September and October mark the lowest concentration level 0.07 mg/l and 0.06 mg/l, respectively. Results report a negative correlation between nitrogen concentration and the diversity of populations of Synechococcus spp. However, in 2011, the PCh station had the highest level of phosphate, especially in September. September marked a high wastewater and sewage spill, coming from Golem area. Unfortunately, beach was still open. Furthermore, in autumn there is a lower tide of the sea which brings more fresh water than marine water in this station. In addition to the aforementioned reasons, extra phosphates loads are a means to address algal blooming in the PCh station. Results report a positive correlation between phosphorus and the diversity of the populations of *Synechococcus*. Being

hypertrophic does not discriminate the PCh station from the others. Regarding chlorophyll *a*– the third indicator–figure 6 does not depict any correlation between hypertrophic level based on *Chl a* content and the ITS diversity of picocyanobacteria.

4. DISCUSSIONS

Genetically different populations of picocyanobactieria of genus *Synechococcus* from six stations at the Durrës Bays have been monthly investigated basing on 16-23S ITS regions (according to the organizational scheme of the cyanobacterial operone of Rocap *et al.* (2002)). Four regions of ITSa and three of ITSb have been amplified. The ITSa fragments could not discriminate among the possibly different populations, because they were present at all stations of sampling. Three ITSb fragments were found, two biggest fragments at all stations, and the third one only at the PCh, respectively. Higher phosphate loads, lower nitrate loads at the PCh station, and low tide of the sea which brings more fresh water than marine water at this station are of great impact for the variability of the population of the different stations. The aforementioned results are in line with the results reported in (Sharpley *et al.,* 1984, 1995; Tiessen, 1995; Lavin *et al*., 2008, Rocap *et al*., 2002), which report the presence of different ITS regions at cyanobacterial rDNA operon, and emphasize that these organisms can grow in low concentrations of nitrogen because they can fix atmospheric nitrogen, even if nitrogen is a limiting factor for growth of algae, and that high concentration of phosphorous can increase density and diversity of cyanobacterial populations.

ACKNOWLEDGEMENTS

This study was supported partially by the project of the Department of Biotechnology of the Faculty of Natural Sciences, University of Tirana, Albania "Monitoring the quality of waters and trophic state at Kune-Vain Lagoon and Shkodra Lake". The authors owe a debt of a special gratitude to the prof. Efterpi Terpo at Laboratory of Molecular Biotechnology, Department of Biotechnology, Faculty of Natural Sciences, University of Tirana, Albania and Edmond Gorenca, ar the Hidrochemical Analysis in Aquaculture and Fishery Laboratory, Durrës, Agricultural University of Tirana, Albania for their precious assistance while carrying out laboratory of the samples.

REFERENCES:

American Public Health Association (APHA), **American Water Works Association (AWWA), Water Environment Federation (WEF). 2005.** Standard Methods for the Examination of Water and Wastewater, 21st ed. American Public Health Association, Washington D.C.

American Public Health Association (APHA), **American Water Works Association (AWWA), Water Pollution Control Federation (WPCF). 1998.** Standard Methods for the Examination of Water and Wastewater. 20th edn., Washington, D.C.

Apirion D. Miczak A. 1993. RNA processing in prokaryotic cells. *Bioassays*. **15**, 113–120.

Bacu A, Babani F, Gjyli L. 2010. Preliminary results on the presence of cyanobacteria Synechococcus in the Lagoon Waters of Northwestern Albania and Lake of Shkodra, Proceedings of BALWOIS, Ohrid, Republic of Macedonia, 25-29 May 2010.

Bacu A, Babani F, Malollari I. 2011. A comparative study on the efficiency of use of different physical and biological parameters for the evaluation of the level of trophy in the lagoon system of Kune-Vain, Albania. *Journal of Environmental Protection and Ecology*. **12 (1),** 45-53.

Bacu A, Babani F, Uku S, Malollari I. 2012. PCR based identification of the presence of Aureococcus and Synechoccocus in the waters of lagoon ecosystem of Kune-Vain, Albania. *Journal of Environmental Protection and Ecology*. **13 (2),** 651-660; ISSN 1311-5065.

Bacu. A, Babani F, Gjyli L. 2013. Does the trophy state of polluted areas have impact on the presence of picophytoplankton species? - Case study in marine coastal waters of Durrës Bay, Albania. *International Journal of Ecosystems & Ecology Science – IJEES*. Vol. **3/1**. ISSN 2224-4980.

Barry T, Colleran G, Glennon M, Dunican LR, Gannon F. 1991. The 16S/23S ribosomal spacer region as a target for DNA probes to identify eubacteria. *PCR Methods Application*. **1(1),** 51–56.

Berg KL, Squires C, Squires CL. 1989. Ribosomal RNA operon antitermination. Function of leader and spacer region box B-box A sequences and their conservation in diverse microorganisms. *Journal of Molecular Biology*. **209(3),** 345–358.

Boçari D, Tafaj L, Totoni R. 2006. Assesment of the pollution of Durrës Port from some organic compounds. *Albanian Journal of Natural and Technical Sciences* (*AJNTS*). **19-20 (1-2)**, XI, 247-253.

Chapman D. 1996. Water Quality Assessments - A Guide to the Use of Biota, Sediments and Water in Environmental Monitoring, Second Edition,

Published on behalf of UNESCO, WHO, and UNEP.Chapman and Hall, London.

Christensen H, Jorgensen K, Olsen JE. 1999. Differentiation of *Campylobacter coli* and *C. jejuni* by length and DNA sequence of the 16S-23S rRNA internal spacer region. *Microbiology* 145: 99–105.

EPA. 2008. Water Quality in Ireland 2004 – 2006. The quality of estuarine and coastal waters, Chapter four. 4-11. Environmental Protection Agen*cy*, Wexford, 2008.

Feil EJ. 2004. Small change: keeping pace with microevolution. *Nature Reviews Microbiology*. **2,** 483–495.

Fuhrman JA, Comeau DE, Hagstrom A, Chan AM. 1988. Extraction from natural planktonic microorganisms of DNA suitable for molecular biological studies. *Applied* and *Environmental Microbiology*. **54(12),** 1426–1429.

Gjyli L. Kolitari J. 2011. Variation of Phytoplankton Biomass as Chlorophyll a in coastal waters of Durrës. *Proceedings of International Conference Biotechnological Development,* 20-21 November 2011, Tirana, Albanian. *BSHN (UT)*, 2011, Special: 247-255. ISSN: 224-1779.

Gjyli L, Bacu A, Kolitari J, Gjyli S. 2013a. Primarily results of phytoplankton and variation to environmental factors in Durrës's Bay coastal waters (Albania). *Journal of Microbiology, Biotechnology and Food Sciences, (JMBFS*).**3 (2),** 132-136. ISSN: 1338-5178.

Gjyli L, Bacu A, Kolitari J, Gjyli S. 2013b. Dynamics of picophytoplankton and presence of cyanobacteria *Synechoccocus* in coastal waters of Durrës Bay (Albania). *Albanian Journal of Agriculture Sciences (AJAS)*.**12(4),** 585-592**.** ISSN: 2218-2020**.**

Håkanson L, Jansson M. 1983. Principles of lake Sedimentology. Springer, Berlin, 316.

Håkanson L, Bryhn AC, Brenckner T. 2007. Operational Effect Variables and Functional Ecosystem Classifications – a Review on Empirical Models for Aquatic Systems along a Salinity Gradient. *International Review of Hydrobiology*. **92(3),** 334.

http://www.jgi.doe.gov/JGI microbial/html/index.html

ICES. International Council for the Exploration of the Sea (ICES). Conseil International pour l'Exploration de la Mer (CIEM). http://ocean.ices.dk/Tools/UnitConversion.aspx

Lavin P, Gómez P, González B, Ulloa O. 2008. Diversity of marine picocyanobacteria *Prochloroccus* and *Synechococcus* assessed by terminal restriction fragment length polymorphisms of 16-23S rRNA internal transcribed spacer sequences. *Revista Chilena de Historia Natural*. 1988, 81: 515-53.

Leblond-Bourget N, Philippe H, Mangin I, Decaris B. 1996. 16S rRNA and 16S to 23S internal transcribed spacer sequence analyses reveal inter- and intraspecific *Bifidobacterium* phylogeny. *Int. J. Syst. Bacteriol.*46: 102–111.

OECD. 1982. Eutrophication of waters. *Monitoring, assessment and control.* OECD, Paris, 154.

Pano N, Frashëri A, Simeoni U, Frashëri N. 2006. Outlook on seawaters dynamics and geological setting factors for the Albanian Adriatic coastline developments. *Albanian Journal of Natural and Technical Sciences* (*AJNTS*), 2006 (1-2), XI (19-20), 152-166.

Paul J. 2008. Phytoplankton DNA extraction. Text Book, 2008.

Pichard SL, Fricher ME, Paul JH. 1993. Ribulose bisphosphate carboxylase gene expression in subtropical marine phytoplankton populations. *Marine Ecological Progress Series.* **101**, 55-65.

Rocap G, Distel DL, Waterbury JB, Chisholm SJ. 2002. Resolution of *Prochlorococcus* and *Synechococcus* ecotypes by using 16S-23S Ribosomal DNA Internal Transcribed Spacer Sequences. *Applied and Environmental Microbiology*. **68(3)**, 1180-1191.

Ryther JH, Dunstan WM. 1971. Nitrogen, phosphorus and eutrophication in the coastal marine environment. *Science*.**171**: 1008-1013.

Sambrook J, Fritsch FF, Maniatis T. 1989. Molecular Cloning. A Laboratory Manual, Cold Spring Harbor Laboratory Press. New York, 2nd. edn, ISBN-10: 0879693096; ISBN-13: 978-0879693091.

Sharpley AN, Hedley MJ, Sibbesen E, Hillbricht-Ilkowska A, House WA, Ryszkowski L. 1995. *Phosphorus transfers from terrestrial to aquatic ecosystems*; Chapter 11, In: Phosphorus in the Global Environment: transfers, cycles and management; Tiessen, H.(ed.); John Wiley and Sons, Chichester.

Sharpley AN, Jones CA, Grey C, Cole CV. 1984. A simplified soil and plant phosphorus model II: Prediction of labile, organic and sorbed phosphorus. *Soil Science Society of America Journal* **48**, **(4),** 805–809.

Tiessen H. (ed.). 1995. Phosphorus in the Global Environment: Transfers, Cycles and Management. Scientific Committee on Problems of the Environment (SCOPE) 54; John Wiley and Sons, Chichester.

Totoni (Lilo) R, Mulla E. 2009. Heavy metal pollution in Durrës Harbor and potential environmental impacts of dredging and dredged sediment disposal activities. *Albanian Journal of Natural and Technical Sciences* (*AJNTS*). **26 (2),** XV, 111-120.

United Nations Environment Program (UNEP)/The Mediterranean Action Plan (MAP). 2012. State of the Mediterranean Marine and Coastal Environment, UNEP/MAP – Barcelona Convention, Athens.

Wallin M, Håkanson L, Persson J. 1992. Load models for nutrients in coastal areas, especially from fish farms (*in Swedish with English summary*). Nordiska ministerrådet. **502**, 207 .

Wilbur Smith Associates. 2003. Vlerësimi i ndikimit në mjedis i gërmimit emergjent të Portit të Durrësit, (shqip dhe anglisht), TEC Infrastructure Consulants, pp: 108-119.

THE SURVEILLANCE OF THE FREQUENCY AND THE RESISTANCE OF *ACINETOBACTER BAUMANII* ISOLATED IN HOSPITAL'S BURN INTENSIVE CARE UNIT (BICU) BETWEEN JANUARY 2010 AND DECEMBER 2012

Vasilika MANO
Laboratory of Microbiology, Mother Theresa University Hospital Center, Tirana, Albania
Betim BYKU
Laboratory of Microbiology, University of Medicine, Tirana, Albania
Monika BELBA
Burns and Plastic Surgery Department, Mother Theresa, University Hospital Center, Tirana, Albania

ABSTRACT

The present paper aims to evaluate the changes in frequency and resistance of *Acinetobacter baumanii* to different antimicrobial agents. The bacterial strains here involved were isolated from January 2010 to December 2012 in the Hospital's Burn Intensive Care Unit (BICU). The strains were mainly isolated from the burn wounds and also blood catheters. The susceptibility testing involved the disc diffusion method (Kirbi-Bauer), the sensi-test gram-negative (Liofilchem) and partly Witek-2. The proportion of *Acinetobacter baumanii* isolated in the burn unit, increased from 23.6% in 2010 to 30.3% in 2011 and to 43.2% in 2012, becoming a very frequent isolate in all gram negatives in burn wounds. The resistant rates to imipenem increased from 20% in 2010 to 90.1% in 2011 and remained in that level throughout 2012. The surveillance of antimicrobial susceptibility testing showed a significant increase of multi-drug resistant strains of *Acinetobacter Baumanii*. Known the antimicrobial resistance of *Acinetobacter,* preventing infections from occurring and therapy of infections could be followed. Consequently, hospitalization rate would be decreased and faster recovery could be obtained.

***Keywords*:** *Acinetobacter baumanii*, carbapenems, multidrug resistant, susceptibility testing, Intensive Care Unit

1. INTRODUCTION

Acinetobacter is a gram-negative coccobacillus similar in Gram stain to *Haemophilus influenzae*. In culture media the colonies are grey, smaller than

enterobacteriacae. It is an opportunistic pathogen. It was considered until recently of low pathogenic potencial, but Acinetobacter baumanii is now considered as an important pathogen implicated in nosocomial infections (Kempf and Rolain 2012)**,** causing a wide spectrum of nosocomial infections such as pneumonia, bacteremia, surgical site infections, secondary meningitis, urinary tract infections mostly in patients with impaired host defenses (Basseti *et al*., 2008).

Multidrug resistant Acinetobacter is not a new or emerging phenomenon; it has always been an organism inherently resistant to multiple antibiotics (Cunha *et al*., 2013). Acinetobacter has an intrinsic resistane to the following antibiotics: Ampicillin, Amoxicillin-clavulanate, Ceftriaxone, Cefotaxime, Ertapenem, Trimethoprim, Fosfomycin (Abbott *et al*, 2013). Results report that *Acinetobacter* is susceptible to Fosfomycin *in vitro*. In recent years the increasing resistant rate of A. baumanii to a wide range of antibiotics is causing serious clinical problems leading to an increase in morbidity and mortality (Jung *et al*, 2010). Carbapenems were considered as antibiotics of last resorts in treating infections. Now carbapenem resistance limits treatment options in resistant strains as there are few new agents in treating infections. In European surveillance of 2009, *Acinetobacter spp* was implicated in ICU acquired infections where carbapenem-resistant isolates in *A.baumanii* appeared to be up to 80%, where the overall rate of imipenem-resistant strains were 47.1% (ECDC, 2011)

2. MATERIALS AND METHODS

The bacterial isolates collected from the patients hospitalized at Hospital's Burn Intensive Care Unit (BICU), Mother Teresa Hospital Center, Tirana, Albania have been investigated between January 2010 and December 2012. We studied a total of 381 isolates. More than 80% of *acinetobacter* isolated in our laboratory originated from the BICU. As they grow in aquatic tissues, *Acinetobacter* and *Pseudomonas* bacteria, find here optimal conditions for growth due to extravasal fluids in burn wounds. After 48 hours of hospitalization the wounds become colonized with *Acinetobacter* and *Pseudomonas*. Once *Acinetobacter* and *Pseudomonas* are colonized, infection occurs in considerable rates (up to 12%) (Belba *et al*., 2013).

We cultured the samples in blood-agar and MC conkey. Antibiotics such as cehalosporines (ceftazidime, cefuroxime, cefotaxime, ceftriaxone), aminoglucosides (amikacine, gentamicine, tobramicine, netilmicine), carbapenems (imipenem, meropenem, doripenem), fluoroquinolone (ciprofloxacine, levofloxacine, pefloxacine) and some compound agents only in 2012 (ampicillin/sulbactam, amoxicillin/clavulanate, piperacillin/tazobactam, Ticarcillin/clavulanic acid) monobactams

(aztreonam) were used for the susceptibility test. The test involved the Kirbi-Bauer disk-diffusion agar as defined in the CLSI standards, the sensi test gram-negative (Liofilchem) and partly with Vitek 2.

3. RESULTS

Pseudomonas aeruginosa in gram negative and *Staphylococcus aureus* in gram positive have been the predominant bacterial isolates up to 2010. Summer of 2010 marked an outbreak of *Acinetobacter baumanii* and patients were hospitalized at the BICU. One of the patient carried *acinetobacter* as he moved from Division of Infectious Diseases (DID) to BICU. Once the patient was admitted at the BICU, the other patients were contaminated. The environment was contaminated as well. Correlations were observed between temperature increase and rates of Acinetobacter infections (Richet 2012)**.** In a study of inpatients from American hospitals, *Acinetobacter spp* infections exhibited the greatest seasonal variations with a 52% increase in the summer as compared with the winter months (Eber *et al.,* 2011). In the present investigation, more than 50% of the cases of Acinetobacter were isolated in summer. In bacterial isolates of the second half of 2010 and especially during the hot season *Acinetobacter* was isolated in burn wounds and blood catheters as a dominant isolate where only 20% of the bacteria isolated were resistant to imipenem. Those isolates were almost sensible to chloramphenicol (5% resistant). It is clear that the enzyme chloramphenicol acetyl-transferase responsible for chloramphenicol resistance was not produced in that first isolates (Table 1).

Table 1. Resistance(R %) of *Acinetobacter* to some antibiotics used in 2010

Antibiotics	Resistance %
Imipenem	20
Carbenicillin	83
Netilmicin	38
Chloramphenicol	5
Trimethoprim-sulfamethoxasole	72

The resistance to these antimicrobials is higher compared with (Lahsoune *et al*., 2007) where the results were netilmicin 17.9%, imipenem 16.1%, tmp-sulfamethoxasol 75.8%, gentamicin 72.1%

In 2010 the isolation rate was: *Acinetobacter* 23.6%,(26 *acinetobacter* out of 110 isolates) *Pseudomonas* 36.8%, *Staphylococcus aureus* 31.1% , *enterobacteriacae* 8.5%. *(Escherichia coli, Proteus, Citrobacter freundi, Klebsiella).*In 2011, *Acinetobacter* comprised 30.3% of isolates and in 2012 ,

it comprised 43.2% of isolates. The rates of the other isolates are in figure1 depicted.

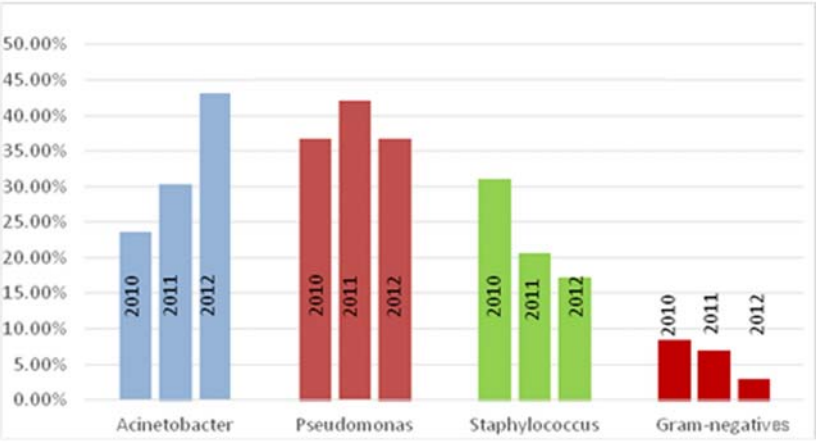

Fig. 1. Trend of pathogens in three years

As we see in the graphics *Pseudomonas aeruginosa* remains high in isolation throughout the investigation period. *Acinetobacter* has an increasing trend and staphylococcus *aureus* a decreasing one.

Table 3. Resistance of *Acinetobacter* to antibiotics(R %) between 2010 and 2012

			Antibiotics			
Bacterium	imipenem	gentamicine	ceftazidime	amikacine	cefotaxime	ciprofloxacin
Acinetobacter 2011	90.1	71	76.4	77.7	75	76.4
Acinetobacter 2012	92	78.1	96.3	91.9	92.1	81.2

Results report that the resistance for all the groups of antibiotics is increased. Imipenem has rapidly increased in resistance since 2010—from 20% in 2010 to 92% in 2012 (Figure2). The results of the present investigation are similar with the results reported in (Ting Xu et al, 2013) where the resistance to imipenem increased from 14.8% in 2008 to 90.8% in 2011. Meropenem resistance in 2012 was 37.5%, while doripenem resistance in 16 isolates tested in 2012 was 93.7%. The increase of the resistance to imipenem and doripenem occurs due to implication of carbapenemases in the mechanisms of resistance to Acinetobacter along with other mechanisms, as imipenem is used in considerable rates in treating burn patients.

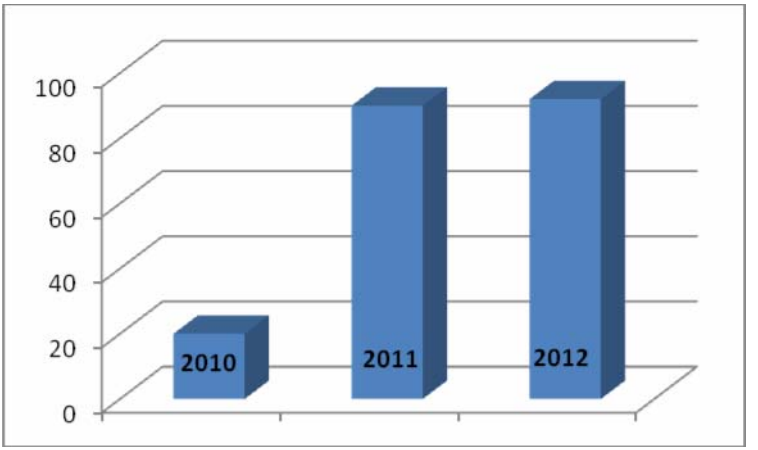

Fig. 2. Resistance of *Acetinobacter* to imipenem.

The resistance rates to other groups of antibiotics such as cephalosporines and aminoglucosides increased steadily over the years as compared to the rapid increase of resistance to imipenem.

The resistance to quinolones was different: the resistance to ciprofloxacin was high, up to 81.2% while the resistance to levofloxacin and pefloxacin was low, 18% and 16%, respectively. These two antibiotics were not commonly used in this hospital.

As for the compound agents we found that acinetobacter isolated in 2012 was susceptible to ampicillin/sulbactam; 30% resistant to piperacillin/tazobactam, resistant to amoxicillin/clavulanic acid, resistant to ticarcillin/clavulanic acid.

We found Acinetobacter to be susceptible to monobactams (Aztreonam) and Fosfomycin and also susceptible to Colistine.

4. DISCUSSION

Acinetobacter species posses an intrinsic resistance to antibiotics and also an ability to acquire genes encoding resistance determinants. Among the mechanisms of resistance, the production of β-lactamases and aminoglycoside –modifying enzymes are important (Bonomo *et al*, 2006) while carbapenemases have an important role too. Other mechanisms include efflux pumps, porin deficiency. In different studies we find that mobile genetic elements in Acinetobacter are acquired by contact with bacteria such as *Pseudomonas* (Gallego and Towner 2001). In our samples of burn wounds in more than 90% of the cases, Acinetobacter and Pseudomonas are co-isolated and they both are very resistant to most of antibiotics (posible transposons exchanges).

Treatment options for A. baumanii

According to our susceptibility testing, treatment with meropenem or piperacillin-tazobactam remains a good choice, while for the resistant strains ampicillin-sulbactam, aztreonam, colistine are good alternatives. Aminoglycoside agents as Tobramycin and quinolones as Levofloxacin and Pefloxacin show efficacy in our testing too.

REFERENCES

Abbot I, Gustavo M, Cerqueira GM, Bhuiyan S, Anton Y Peleg AY. 2013. Carbapenem resistance in *Acinetobacter baumanii*. *Expert Rewiew of Anti-infective Therapy* 11(4): 395-409.

Basseti M, Righi E, Esposito S, Petrosillo N, Nicolini L. 2008. Drug treatment for multidrug- resistant *Acinetobacter baumanii* infections. *Future Microbiology,* 3(6): 649-660.

Belba M.K, Petrela E.Y, Belba A.Gj.2013. Epidemiology of infections in a Burn Unit, Albania. *Burns* 39: 1456-1467.

Bonomo RA, Szabo D.2006. Mechanisms of multidrug resistance in *Acinetobacter* species and *Pseudomonas aeruginosa*. *Clinical Infectious Diseases*. 43 (suppl.2), S49-S56.

Cunha BA, Bronze MS, Levy CS, Talavera F, Brown RB. 2013. *Acinetobacter* Updated Jan 31, 2013.

Eber MR, Shardell M, Schweizer ML, Laxminarayan R, Perencevich EN. 2011. Seasonal and temperature associated increases in Gram-negative bacterial blood stream infections among hospitalized patients. PLoS ONE; 6: 25298.

European Center for Disease Prevention and Control. Annual Epidemiological Report. 2011. Reporting on 2009 surveillance data and 2010 epidemic intelligence data. ECDC. Stockholm, Sweden.

Gallego L, Towner KJ.2001. Carriage of class 1 integrons and antibiotic resistance in clinical isolates of *Acinetobacter baumanii* from northern Spain. *Journal of Medical Microbiol*ogy. 50: 71-77.

Jung JY , Park MS, Kim SE, Park BH, Son JY, Kim EY, Lim JE, Lee SK, Lee SH, Lee KJ, Kang YA, Kim SK, Chang J. 2010. Risk factors for multi-drug resistant *Acinetobacter baumanii* bacteremia in patients with colonization in the intensive care unit. *BMC Infectious Diseases* 2010; 10: 228.

Kempf M, Rolain JM. 2012. Emergence of resistance to carbapenems in *Acinetobacter baumanii* in Europe: clinical impact and therapeutic options. *International Journal of Antimicrobial Agents.* 39(2): 105-114.

Lahsoune M, Boutayeb H, Zerouali K, Belabbes H, El Mdagri N. 2007. Prevalence and in vitro antimicrobial susceptibility patterns of *Acinetobacter baumanii* strains in a Moroccan university hospital. DOI:10.1016/Medecine et Maladies Infectieuses .05.006.

Richet H. 2012. Seasonality in gram-negative and health-care associated infections. Clinical Microbiology and Infection, vol 18, 934-940. DOI:10.1111/j.1469-0691.2012.03954.x.

Xu T, Xia W, Rong G, Pan Sh, Huang P, Gu B. 2013. A 4-year surveillance of antimicrobial resistance patterns of *Acinetobacter baumanii* in a university-affiliated hospital in China. *Journal of Thoracic Diseases.* 2013;5(4): 506-512. Doi 10.3978/j issn. 2072-1439. 08. 36.

EVALUATION OF TEMPERATURE COEFFICIENT OF RESISTANCE OF ELECTROCONDUCTIVE TEXTILES

Ilda KAZANI, Genti GUXHO
Department of Textile and Fashion Polytechnic University of Tirana, Albania
Carla HERTLEER, Lieva VAN LANGENHOVE
Department of Textiles, Ghent University, Belgium
Gilbert DE MEY
Department of Electronics and Information Systems, Ghent University, Belgium

---

ABSTRACT

The emergence of smart textiles in recent years has revealed the need for electroconductive textiles. Characterised by flexibility and cost effectiveness, the potential of screen printing textiles with conductive ink is presented in this paper. The electroconductive properties of printed textiles are investigated as a means to address evaluation of the Temperature Coefficient of Resistance (TCR).
Key Words: smart textiles, temperature coefficient of resistance (TCR), electroconductive textiles

1. INTRODUCTION

Many research papers report on screen printing with conductive silver-based inks on different textile fabrics (Meoli, 2002; Karaguzel *et al.*, 2005; Merilampi *et al.*, 2009; Kim, 2010; Yang *et al*., 2010) as a means to address smart textiles. This technology provides excellent electroconductive properties for flexible and lightweight conductive textiles. Furthermore, the printed textiles are applicable in the area of textile antennas, feed lines or simple one-layer routing structures, electrodes and circuits (Merritt *et al*., 2005; Locher and Tröster, 2007).

In the area of electronics, the variation of electrical resistance with temperature of printed thick films is very important and must be taken into account by engineers in the design processes. This variation is known as the temperature coefficient of resistance (TCR) and is generally expressed in parts per million per degree Celsius (ppm/°C). In granular metal films one can

distinguish three structural regimes (Coutts, 1974; Wu and Liu, 1983): i) the dielectric regime, where the TCR is negative, ii) the transition regime, where the TCR is nearly zero and, iii) the metallic regime, where the TCR is positive.

A negative TCR corresponds to a decreasing resistance with increasing temperature. Conversely, a positive TCR expresses an increasing resistance due to a temperature increase. The ideal TCR equals zero. However, in some applications a positive TCR is required for safety reasons (like in most household electronics).

Moreover, the metallic particle size affects the electrical properties. The larger the particles the more negative the TCR is (Dziedzic and Golonka 1988; Boonstra and Mutsaers, 1980).

Jiang *et al*. (2010) revealed that the thickness of the film can greatly influence its electrical properties. As thickness increases, the TCR shifts from a negative value to a positive value.

As conductive screen-printed textiles are meant for use in the wearable electronics, investigation into the relation between resistance and temperature is unavoidable.

In the present research, the temperature coefficient of resistance expresses the effect of a changing temperature on the resistance of the screen-printed conductive layer on the textile fabric (Dziedzic and Golonka 1988; Kazani *et al*., 2011; Halder and Snyder 1984) and is calculated as follows:

$$TCR = \frac{R_{\square,max} - R_{\square,min}}{R_{\square,min}\,(T_{max} - T_{min})} \cdot 10^6$$

where $R_{\square,max}$ is the square resistance measured at T_{max} and $R_{\square,min}$ is the square resistance measured at T_{min}. In order to determine the influence of temperature on the Electroconductive properties, the square resistance of these electroconductive textiles is measured at different temperatures varying between a T_{min} of 23°C and a T_{max} of 60°C, in steps of about 10°C.

2. MATERIALS AND METHODS

2.1 Textile materials

Reported in Table 1, the selected woven fabrics involved in the present investigation are: viscose, polyamide, polyester, aramid, cotton/polyester 1, cotton/polyester 2 and polyester/viscose with different physical-mechanical properties.

Table 1 Properties of selected woven textiles

Woven textile materials	Yarn Density of fabric[1] Warp (threads/cm)	Weft (threads/cm)	The type of textile weave[2]	Thickness[3] (mm)	Basis weight[4] (g/m²)
Viscose	18	11	Plain 1/1	0.488	254
Polyamide	45	32	Twill 2/2	0.198	99
Polyester	46	25	Plain 1/1	0.38	163
Aramid	32	20	Plain 1/1	0.378	191
Cotton/Polyester 1	46	26	Twill 3/1	0.296	113
Cotton/Polyester 2	42	29	Twill 3/1	0.414	233
Polyester/Viscose	45	25	Twill 3/1	0.246	108

2.2 Conductive inks

Table 2 reports the properties of the commercially available silver-based ink from Acheson that was applied in this research.

Table 2 Properties of applied silver-based conductive ink

	Silver-based ink
Solid content (%)	73.5 – 76
Cure conditions (120°C)	15 minutes
Sheet resistance (Ω/□ at 25μm)	<0.025
Resin[5]	PES

2.3 Screen printing

Squares of 6 x 6 cm were screen printed on the substrates. A screen with a polyester mesh of monofilament 90 T, a sieve thickness of 110 μm and a sieve opening of 45% was used to achieve an even coverage of ink over the entire pattern.

2.4 Electrical characterization

[1]ISO 7211-2
[2]ISO 7211-1
[3]ISO 5084
[4]ISO 3801
[5]Determined by the authors

The electroconductive properties of the printed textiles were investigated by measuring their direct current (DC) resistance applying the Van Der Pauw method. The samples were prepared, as depicted in Figure 1, with four copper contacts at the edges A, B, C and D of the printed square. The woven fabric was oriented in such a way that AD and BC correspond with the warp direction and AB and DC with the weft direction. Figure 2 depicts the heating plate manufactured by Temptronic Corporation, model TPO315A-2 where the samples were placed for heating purposes (Kazani *et al.*, 2011). The heating plate was systematically heated up to 23°C, 30°C, 40°C, 50°C and 60°C. At each temperature, the resistance $R_{\square}$ was measured using the Van Der Pauw method: a current *I* was supplied at two contacts, e.g. C and D and the resulting voltage drop *V* was measured at the opposite contacts, e.g. A and B. Subsequently, the plate was cooled down and at 50°C, 40°C, 30°C and 23°C, *I* and *V* were recorded and $R_{\square}$ was calculated. At the intermediate temperatures, the plate was allowed to stabilize for about ten minutes upon reaching the desired temperature (Halder and Snyder 1984).

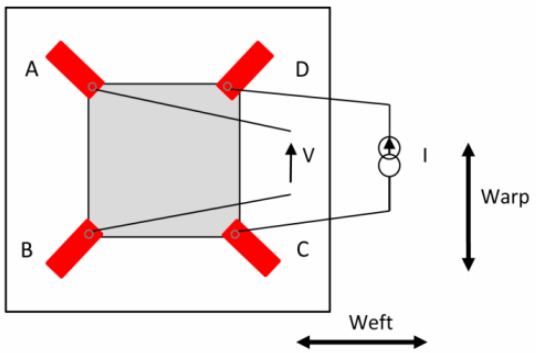

Fig. 1. The screen-printed sample prepared with four contacts according to the Van Der Pauw measurement configuration.

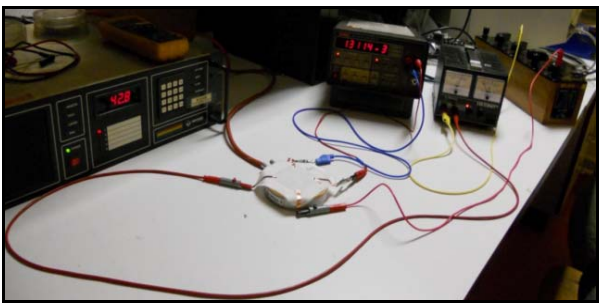

Fig. 2. Measurements of $R_{\square}$ when the sample is on the heating plate.

3. RESULTS AND DISSCUSSION

Table 3 reports the TCR values for the weft direction (C-D). Table 4 shows TCR values for the warp direction (A-D). In each table, two series of TCR values are given: TCR_1 expresses the resistance change when the temperature is increased and the TCR_2 when the temperature is decreased.

Table 3. Calculated values for $R_{\square}$ and TCR in C-D direction (***weft***)

	$R_{\square,min}$ *(Ω)*	$R_{\square,max}$ *(Ω)*	$R_{\square,min}$ *(Ω)*	TCR_1 (ppm/°C)	TCR_2 (ppm/°C)
Viscose	0.0162	0.0175	0.0149	**2169**	**4716**
Polyamide	0.0122	0.0156	0.0131	**7532**	**5158**
Polyester	0.0238	0.0259	0.0239	**2385**	**2262**
Aramid	0.0215	0.0236	0.0209	**2640**	**3492**
Cotton/Polyester 1	0.0599	0.0608	0.0582	**406**	**1207**
Cotton/Polyester 2	0.0272	0.0296	0.0271	**2385**	**2493**
Polyester/Viscose	0.0266	0.0235	0.0239	**-3150**	**-452**

Table 4. Calculated values for $R_{\square}$ and TCR in A-D direction (***warp***)

	$R_{\square,min}$ *(Ω)*	$R_{\square,max}$ *(Ω)*	$R_{\square,min}$ *(Ω)*	TCR_1 (ppm/°C)	TCR_2 (ppm/°C)
Viscose	0.0148	0.0161	0.0146	**2374**	**2777**
Polyamide	0.0122	0.0157	0.0129	**7754**	**5866**
Polyester	0.0240	0.0261	0.0239	**2365**	**2488**
Aramid	0.0202	0.0229	0.0208	**3613**	**2729**
Cotton/Polyester 1	0.0583	0.0596	0.0568	**603**	**1332**
Cotton/Polyester 2	0.0271	0.0295	0.0272	**2394**	**2285**
Polyester/Viscose	0.0258	0.0234	0.0257	**-2514**	**-2419**

Table 3 and 4 show that for all the materials, the TCR_1 and TCR_2 are different, i.e. the values are not the same when the temperature increases or decreases due to hysteresis shown in Graphs 1 to 7.

Furthermore, the TCR value in weft direction differs from the TCR in warp direction, showing anisotropy of the screen-printed samples (Kazani *et al.,* 2011).

The negative TCRs of the screen-printed Polyester/Viscose occur due to the thickness of the printed surface. Jiang *et al.* (2010) showed that as the film

thickness increased from 30 nm to 280 nm, the TCR of the samples shifted from a negative to a positive value.

One physical explanation can be that the electric conduction between two neighbouring particles is of the order of a few nanometers. For a larger gap, electrons can still be transferred from one particle to another by hopping between the so-called localised states (Figure 3).

For this physical explanation a theory can be given for screen-printed conductors on ceramic substrates used in electronics.

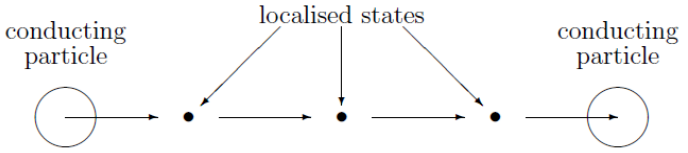

Fig. 3. Electron transfer from one particle to another when the gap is larger.

Basing on this theory, the resistance of such a material will be given by:

$$R(T) = R_0 \sqrt{\frac{T}{T_m}} \exp\left[2\left(\frac{T_m}{T}\right)^{\frac{1}{4}}\right]$$

where R_0 is a constant and T the absolute temperature expressed in Kelvin.

By solving the equation dR/dT =0 one can easily prove that R (T) has a minimum for $T=T_m$.

T_m is the temperature which is theoretically given by:

$$T_m = \frac{\alpha^3}{k\,N}$$

where α is the decay of the quantum wave function of an electron around a localised state,

k is the Boltzmann constant, 1.38066 x 10^{-23} J/K and N the density of localized states per unit volume and energy.

For $T>T_m$ the resistor will have a positive temperature coefficient and a negative one for $T<T_m$.

In the present analysis α can be considered as a constant. Localised states usually exist as interfaces between crystallites. As a consequence, the preparation of the materials can affect the size of the crystallites and hence the value N of localised states. Here, the only variable parameter is N. For high

values of N, T_m is small and the resistor has a positive temperature coefficient. For low values of N negative temperature coefficients can be expected. If N is reduced by 50 %, which means that the average distance between the localised states is increased by only $\sqrt[3]{2} = 1.259$ the value of T_m will double, e.g. from 200 K to 400 K, or the resistor will change from a negative TCR to a positive one.

The slope of the graph of resistance squared versus temperature determines the TCR. The figures below visualize the evolution of the square resistance with temperature for each textile substrate.

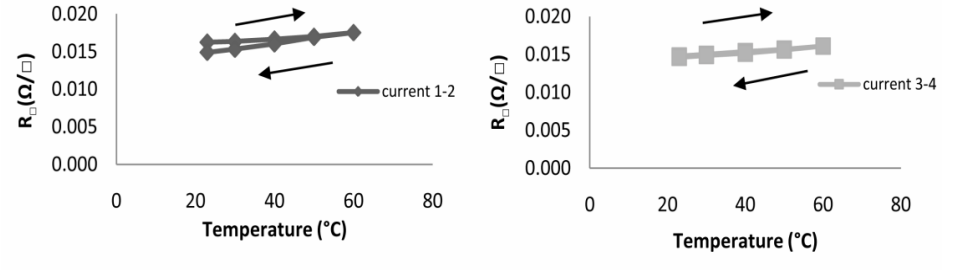

Graph. 1. Resistance plots of screen-printed samples of Viscose

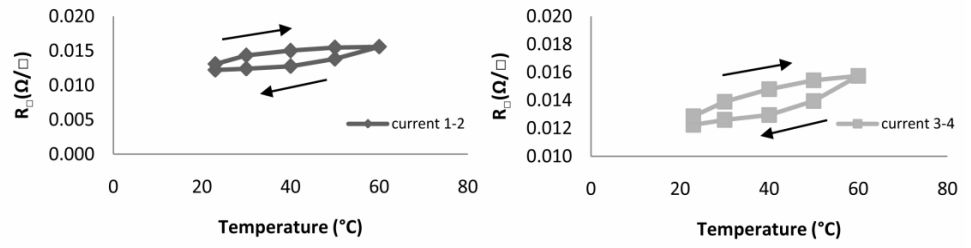

Graph 2. Resistance plots of screen-printed samples of Polyamide.

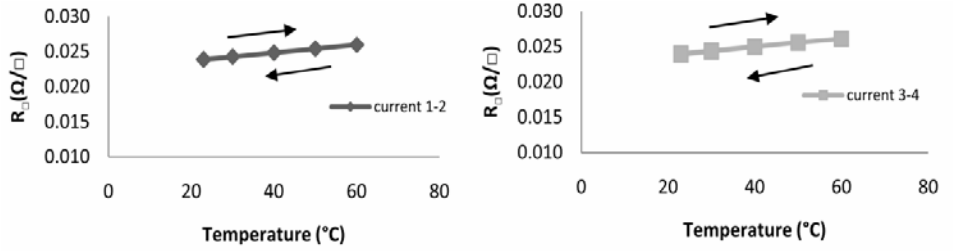

Graph 3. Resistance plots of screen-printed samples of Polyester

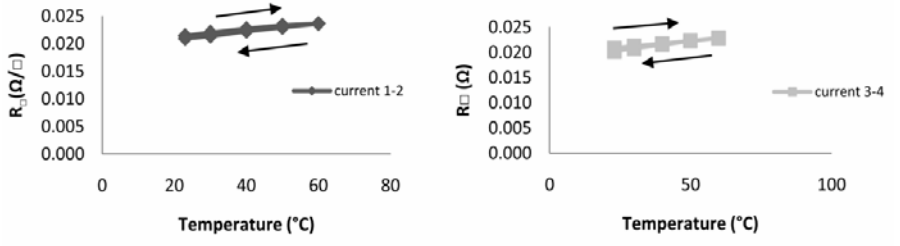

Graph. 4. Resistance plots of screen-printed samples of Aramid.

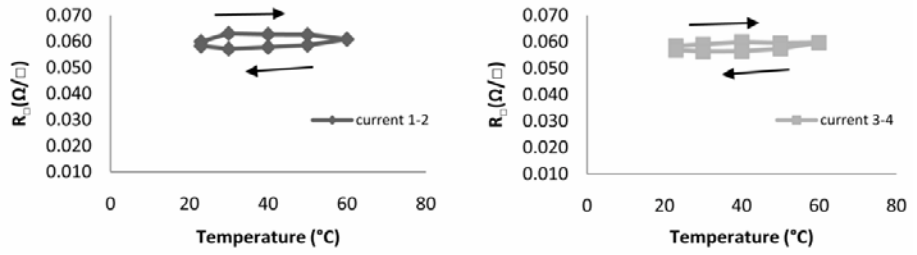

Graph. 5. Resistance plots of screen-printed samples of Cotton/Polyester 1.

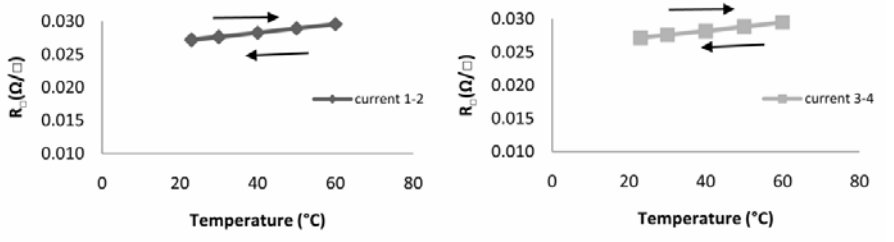

Graph. 6. Resistance plots of screen-printed samples of Cotton/Polyester 2.

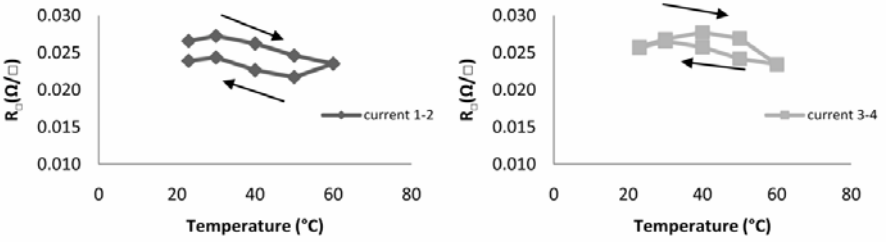

Graph. 7. Resistance plots of screen-printed samples of Polyester/Viscose.

The aforementioned graphs show that resistance of most of materials increases as the temperature increases. Alternatively, the conductance of most materials decreases as temperature increases. The reason the resistivity increases with increasing temperature may be the number of imperfections in the atomic lattice structure, that increases with temperature and this hampers electron movement. These imperfections include dislocations, vacancies, interstitial defects and impurity atoms.

In addition,Graphs from 1 to 7 along with the table 1 and 2 report that the TCR is positive for Viscose, Polyamide, Polyester, Aramid, Cotton/Polyester 1 and 2, varying from 406 to 7754 ppm/°C and TCR is negative for Polyester/Viscose TCR varying from -3150 to -452 ppm/°C.

The values of the TCRs for the screen-printed samples are high in sign but most of them are comparable with thick film materials (Dziedzic and Golonka, 1988; Halder and Snyder 1984; Czarczynska 1990; Morten, 1995; Scilingo *et al*., 2003; Prudenziati and Gualtieri 2008; Sibinski, 2010; Sloma 2010; Sloma, 1011) used in electronics.

Halder et al. (1984) screen-printed thick film resistors of ruthenium oxide (RuO_2) on alumina substrates to determine the tunnelling and hopping parameters means by the values of TCR. The thick films showed to have positive and negative values from -663 to 222 ppm/°C.

Dziedzic *et al.,* (1988) have examined the electrical properties of iridium oxide (IrO_2), ruthenium oxide (RuO_2) and bismuth ruthenium oxide ($Bi_2Ru_2O_7$) compounds screen-printed on alumina substrates as thick-film resistors. The TCR measured for IrO_2, RuO_2 was highly positive and increasing with longer firing time from 1550 to 2150 ppm/°C. It was negative for $Bi_2Ru_2O_7$ and with the prolongation of firing time became more negative—varying from -131 to -980 ppm/°C.

Czarczynska *et. al*., (1990) analyzed the electrical parameters of printed carbon/polyesterimide thick film resistors. The values of TCR varied from -100 to -1300 ppm/ºC.

Morten *et al*., (1995) have printed thick film of nickelate (NiCo) pastes on glazed alumina meant for sensor for linear displacement. The TCR measured for these sensors was approximately 2700 ppm/°C.

Being the only paper found where information on measurements of TCR and ageing of conductive textiles is provided, Scilingo *et al*. (2003) have analyzed the thermal and ageing properties of polypyrrole (PPy) coated fabrics used as sensitive glove able to detect the position and the motion of fingers. Here, TCR varied from $-0.018°C^{-1}$ or -18000 ppm/°C to a temperature range of 10 to 50°C. The value for this coated fabric is more high and negative than in our case, but the authors compare it with ceramic thermistors

that have a negative temperature coefficient ranging from -0.03°C^{-1} to -0.05°C^{-1}. They also mention that in applications related to the monitoring of kinematics of human body segments, temperature variations typically encountered do not significantly affect the acquired data.

Prudenziati et al. (2008) have studied the electrical properties of thermally sprayed nickel (Ni) and nickel-chromiumalloy (Ni20Cr) resistors. The TCR was measured in the temperature range of 20 to 500°C and the results were varying from 180 to 2830 ppm/°C.

Sibinski *et al.,* (2010) have presented flexible temperature sensors on separate yarns for textronic applications. As sensor core they used polyvinylidene fluoride fiber in a monofilament structure. Polymer conductive pastes based on carbon nanotubes were placed on the fibers to create sensor structures. The TCR, measured in the range of temperatures from 20 to 160°C in 20 second cycles, were from 1010 - 7500 ppm/K. Strong hysteresis for all the samples was noticed, which is similar to our case.

Sloma (2010) and Sloma *et al.,* (2011) screen-printed thick-films of carbon nanotubes (different percentage) for application of transparent electrodes and temperature sensors. A significant hysteresis was observed and the TCR values were negative and varying from -350 to -2100 ppm/°C (Halder and Snyder 1984) and from - 680 ppm/K at T=300 K to -0.162 K^{-1} at T=5 K (Sloma 2010).

4. CONCLUSIONS

Flexible and conductive smart textiles could be obtained from the combination of electroconductive inks and textiles. However, the resistance of these screen-printed textiles varies with the changing temperature, which is expressed in the temperature coefficient of ressitance (TCR).

The electrical properties of the conductive layer on the printed woven fabric samples were evaluated by measuring the square resistance after heating up to 60°C and cooling down to 23°C the samples. Anisotropic behaviour in the weft and warp direction of the fabrics was observed during the measurements.

From the TCR measurements positive and negative TCR values were obtained, comparable with TCR measurements in the field of electronics where they are commonly measured. Additionally, hysteresis was also observed for most of the samples in weft and warp directions.

REFERENCES

Boonstra AH, Mutsaers C.1980. The effect of particles size on the temperature coefficient of the resistance of the thick film resistors.*Thin solid films*. . **67.** 13-20.

CouttsTJ.1974. Electric conduction in thin metalic films. - [s.l.] : Elsevier.

Czarczynska H, Dziedzic A, Licznerski BW. 1990. Some properties of carbon black/polyestermide and electrode carbon/polyesterimide thick films. 14th Conference of the ISHM Poland. - Warsaw : [s.n.]. 35-38.

Dziedzic A, Golonka L. 1988. Electrical properties of conductive materials used in thick-film resistors. *Journal of materials science*. **23, (9),** 3151-3155.

Halder NC, Snyder RJ.1984. Measurement of the tunneling and hopping parameters in RuO2 thick films .*Electrocomponent science and technology*. **11**, 123-136.

Jiang H, Wang C, Zhang W, Si X, Li Y. 2010. Influences of Film Thickness on the Electrical Properties of TaNx Thin Films Deposited by Reactive DC Magnetron Sputtering .*Journal of materials science and technology*. **26 (7)**, 597-600.

Kazani I, De Mey G, Hertleer C, Banaszczy KJ, Schwarz A, Guxho G, Van Langenhove L. 2011. Van Der Pauw method for measuring resistivities of anisotropic layers printedon textile substrates. *Textile research journal*. 12 September. **81 (20),** 2117-2124.

Karagüzel B, Merritt CR, Tae-Ho K, Wilson J, Franzon P, Nagle HT, Grant E, Pourdeyhimi B. 2005. Using conductive inks and non-woven textiles for wearable computing. In: Proceedings of the 2005 Textile Institute World Conference, Session 1, Paper 15, Raleigh, NC, USA, March 23–25, 2005.

Kim Y, Kim H, Yoo HJ. 2010. Electrical charachterisation of screen – printed circuits on the fabric. *IEEE transaction on advanced packaging*. **33, (1),** 196-205.

Locher I, Tröster G. **2007.** Screen-printed textile transmission lines. *Textile research journal*. **77**(**11**), 837-842.

Merilampi S, Laine-Ma T, Ruuskanen P.2009. The characterization of electrically conductive silver ink patterns on flexible substrates. *Microelectronics Reliability*. **49 (7)** , 782-790.

Merritt CR, Karagüzel B, Kang T-H, Wilson JM, Franzon PD, Nagle HT, Poudeyhimi B, Grant E. 2005. .Electrical characterization of Transmission Lines on Nonwoven Textile substrates. *Material Research Society*. Vol.**870E**.

Meoli D. 2002. Interactive electronic textiles: technologies, applications, opportunities, and market potential. North Carolina State University, Raleigh. http://repository.lib.ncsu.edu/ir/bitstream/1840.16/1216/1/etd.pdf

Morten B, De Cicco G, Prodenziati M, Masoero A, Mihai G. 1995. Magnetoresistive thick film sensor for linear displacements. *Journal ofsensors and actuators: A-Physical.***46,** 261-265.

Prudenziati M. Gualtieri ML. 2008. Electrical Properties of Thermally Sprayed Ni- and Ni20Cr-Based Resistors. *Journal of thermal spray technology*. **17(3),** 385-394.

Scilingo EP, **Lorussi F, Mazzoldi A, De Rossi D. 2003.** Strain-sensing fabric for wereable kinaesthetic-like systems. *IEEE SENSORS JOURNAL.* **3.(4),**460-467.

Sibinski M. Jakubowska M, Sloma M. 2010. Flexible temperature sensors on fibres. *Sensors.* **10 (9),**7934-7946, 1424-8220.

Sloma M. 2010.Polymer composites with carbon nanotubes for printed electronics application. XII International PhD Workshop. http://mechatronika.polsl.pl/owd/pdf2010/437.pdf

Sloma M, Jakubowska M, Kolek A, Mleczko K, Ptak P, Stadler AW, Zawislak Z, Mlozniak A. 2011. Investigations on printed elastic resistors containing carbon nanotubes. *Journal of Materials Science: Materials in Electronics*. **22(9),** 1321-1329.

Wu Q-D, Liu X-Q.1983. Electric conduction in metallic Ag particles—Cs2O semiconductor thin films. *Journal of Vacuum Science and Technology* A. **1(2),** 371-37.

Yang YL, Chuang MC, Lou SL, Wang J. 2010. Thick-film textile-based amperometric sensors and biosensors. *Royal Society of Chemistry*. **135 (6),** 1230-1234.

EVALUATION OF EXTENSION SET OF DIFFERENT ALBANIAN LEATHERS

Majlinda HYLLI
Department of Textile and Fashion, Polytechnic University of Tirana, Albania

---

ABSTRACT

Its high extensibility, tensile strength and other desirable qualities make leather of considerable importance for different industrial sectors.
The present paper provides information about the determination and evaluation of extension set of different Albanian leather intended to use in car upholstery and home furnishing.
In the present investigation, the international standard ISO 17236:2002 was followed for the determination of extension set. An accurate evaluation of the extension would be of great importance for the industry.
Keywords: leather, extension set, parallel direction, perpendicular direction, upholstery, furnishing.

1. INTRODUCTION

Leather is a natural product and is made by converting animal hides and skins by means of a tannage, which consists of numerous mechanical and chemical operations.

Physical properties of the animal hides structure and mechanical and chemical process applied, make the leather of great interest for different sectors. The properties of leather depend on: i) the origin of the raw materials, ii) hide preparation process for chemical modification, iii) chemical modification process, iv) lubrication process of the leather and, iv) preparation process of the surfaces. It is the traditional art craft of leather technologist to control the parameters and variables of processing in order to make the leather with defined, desired or required properties (Covington 2009). For each application the leather of different physical and mechanical properties is obtained by means of variation in the processing technology (Milasiene 2003).

When hides are converted to leather all non essential parts of the original animal hide are removed, leaving only the surface "grain" and the middle

"corium" layers. The structure of leather consist of a three dimensional network of chemically crosslinked collagen fibres (Sturrock 2004).

Moreover, it is the remarkable structure of this corium made up of millions of microscopic fiber, twisted and interwoven by nature, that gives leather its highly tensile strength and other desirable qualities. The weave of collagen fibre bundles becomes more compact with age. The strength of the leathers is strongly associated with their apparent density wich in turn could be related to the compactness of fibre bundle weave in the skin (Wang and Attenburrow 1993).

It is found that on stretching the fibers, a constant extension value was reached after some time (Conabere and Hall 1946). Various chemical and mechanical processes that the leather undergoes are of great impact for the extensibility.

Extensibility and the tensile strength of leather depend not only on the quantity of the oil present in the leather but as well on how far the fatliquoring oil has penetrated into the thickness of the weave. These two mechanisms are considerable impact for the aforementioned tensile properties of the material. Fatliquoring is observed to increase the degree to which fibers pull out at break (Makhothe 1997).Tanning effect mainly depends on the extent of cross-linking between collagen molecules and thermodynamic stability of the cross-linking bonds (Mahdi 2009). Once the material has been stretched to a designated strain and not to failure and released from a stress-strain test, some of the total deformation is recovered as elastic deformation. Resiliency is very important to automotive upholstery makers because poor recovery from deformation creates bagginess in car seats made with upholstery leather (Liu 2007). Information about the evaluation of the mechanical properties provided by tensile testing is in the present paper reported. One important feature for leather intended to be used in car upholstery and furnishing is the determination of extension set. The minimum extension set of the leather is of irreplaceable importance for the car upholstery manufacturing.

2. MATERIALS AND METHODS

The International Standard EN ISO 17236:2002 was followed for the determination of extension set. A test piece is repeatedly extended at a specified rate until the forces reach a predetermined level and the permanent extension is calculated as a percentage of the original length.

2.1 Instruments

Depicted in figure 1, the tensile testing machine type YG026B was used for the determination of extension set. Tensile testing machine has a force

range appropriate for the specimen under test. In addition, the force could be accurately recorded in accordance with the international standard EN ISO 7500-1.

Jaws have the minimum length of 30 mm in the direction of the applied load, designed to apply constant clamping by mechanical or pneumatic means. The texture and design of the inside faces of the jaws shall be such that at the maximum load attained in the test piece does not slip at either jaw.

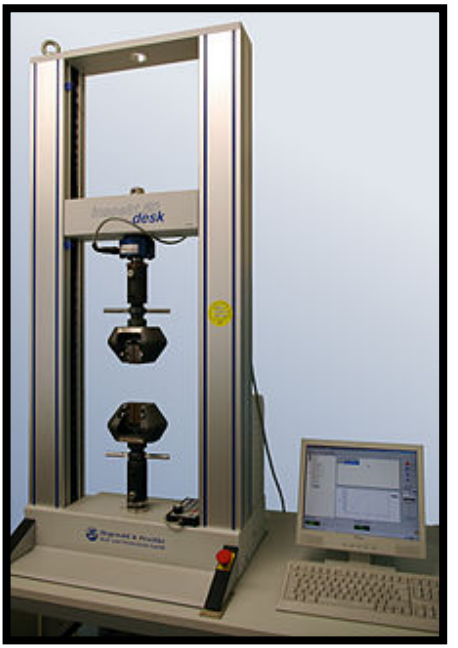

Fig. 1. Tensile testing machine (YG026B).

2.2 Sampling and preparation of samples

Different leathers of cows, goats and pigs are tested for the resistance and the percentage of the extension set. EN ISO 2418 for sampling and EN ISO 2419 for sample preparation and conditioning were unavoidably followed in the present investigation which is based on the standard method.

The table 1 reports the analysed samples. The labelled samples are hereafter referred by leather sample code L-1, L-2, L-3, L-4, L-5, L-6, L-7, L-8, L-9 and L-10.

Table 1. The leather samples analyzed

Index	Sample description
L-1	Black Cow lustred finished leather
L-2	Black Pig finished Leather 1
L-3	Black Cow finished leather 1
L-4	Black Cow finished leather 2
L-5	Black Goat finished Leather
L-6	Beige Cow finished leather
L-7	Black Pig finished Leather 2
L-8	Orange Cow finished leather
L-9	Red Cow finished leather
L-10	Cream Cow finished leather

Six test pieces were cut to the grain surface. Three test pieces were cut with the longer edge parallel to the backbone. The three other pieces were cut with the longer edge perpendicular to the backbone. The leather samples have been conditioned at standard atmosphere conditions (20 ± 2ºC and a relative humidity of 65 ± 5 %) for 24 hours.

Depicted in figure 2, once conditioned, the thickness of the leather samples was measured in accordance with EN ISO 2589. Results report that thickness of the leather is quite variable. Leather L-4 has the highest value (1.867 mm) and leather L-2 has the lowest value (0.646 mm).

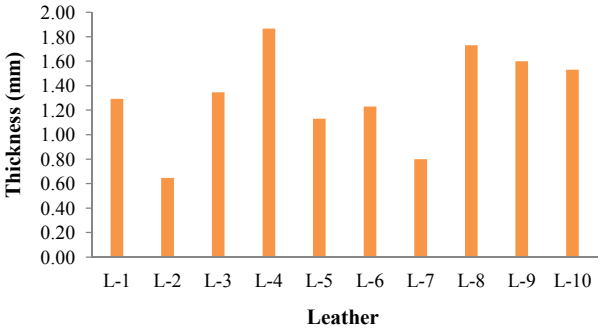

Fig. 2. The thickness of leather samples analyzed.

2.3 Method

A line of 35 ± 5 mm from each short edge of the test piece with the line parallel to the short edges was marked for each leather sample.

Once the line was marked, the distance L_0, between the two lines to the nearest 1 mm was measured.

The jaws of the tensile testing machine 200 mm were set apart. Once set apart, the test piece were clamped in the jaws such that the short edges of the test piece are parallel to the edges of the jaws, and about 25 mm of the test piece is clamped in each jaw.

Once the test piece is clamped with its grain and the surface lies in one plane, the tensile testing machine is run until a load of 20.0 N ± 0.5 N could be reached. Stop the crosshead and keep it stopped in that position for 10 ± 1s follows immediately after. Then we return the crosshead to its start position and repeat this in two steps so that the test piece is subjected to a total of 5 extension cycles.

The test piece from the tensile test machine was removed immediately after the final load cycle and the test piece is laid on a flat surface with the lines applied parallel to the short edges 60 ± 5 s. After this, the test piece is removed from the tensile tester and the distance, L_1, between the lines to the nearest 1 mm is measured.

The percentage extension set, Es shall be calculated using the formula:

$$Es = \frac{(L_1 - L_0)x100}{L_0} \qquad (1)$$

Where:

L_1- is the final distance between the marks, in millimetres measured after testing

L_0- the final distance between the marks, in millimetres measured before testing

3. RESULTS AND DISSCUSSION

Once thickness test is carried out, extension set could be evaluated. The results of the mean value for the distance L_0 and L_1 for six test pieces in two direction parallel and perpendicular with the backbone are in figure 3 depicted.

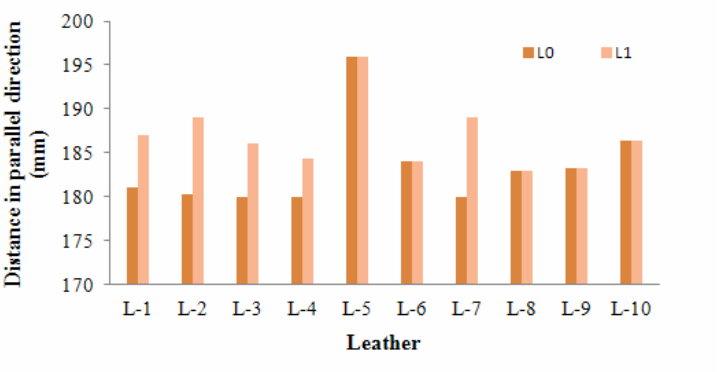

Fig. 3. Determination of L_0 and L_1 in parallel direction with the backbone.

The sample L-5 has the highest value of the distance before and after testing in parallel direction with L_0 (196mm) and L_1 (196mm). The sample L-4 has the lowest value in the same direction with L_0 (180 mm) and L_1 (184.3 mm).

The samples L-2 and L-7 (which belongs to pigs leather) have low values of L_0 (180.3 mm, 180 mm) and L_1 (189mm, 189mm) in parallel direction. Fibres orientation, the part where the leather is taken are of great impact for the values as here values of thicknesses and elasticity are low.

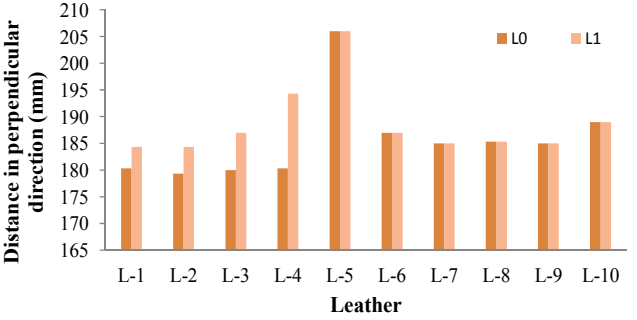

Fig.4. Determination of L_0 and L_1 in perpendicular direction with the backbone.

Figure 4 depicts the L-5 with the highest value of the distance before and after testing in perpendicular direction with L_0 (206mm) and L_1 (206mm) The samples L-2 have the lowest value in this direction of L_0 (179.3mm) and L_1(184.3mm).

Again, the variability depends strongly on thickness, orientation of fibres and extendibility of the leathers.

Samples from L-1 to L-10 (excluding L-2, L-5, L-7) have natural variation for each leather and different values of extension in both directions.

The aforementioned features depending on which part the leather is taken, orientation of the fibres and higher values of thickness comparing with the other types of leather. In adddition to the aforementioned factors, fatliquoring and elasticity of the leather are of great impact to the extension set .

The percentage extension set, E_s is calculated using the formula (1) and the percentage of the extension set values in both directions are in figure 5 depicted.

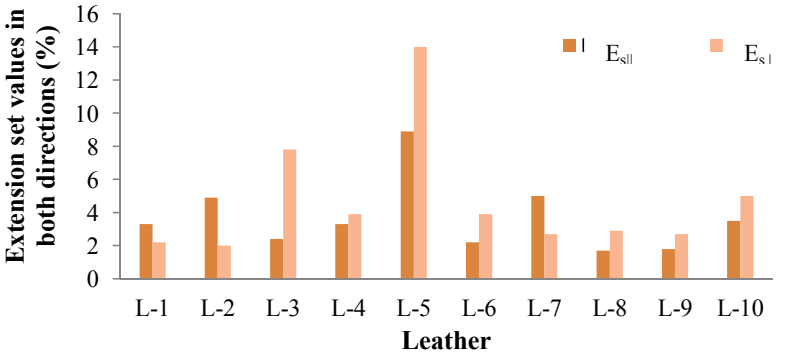

Fig. 5. The graphic of the extension set in parallel and perpendicular direction with the backbone.

Figure 5 depicts low values extension set in parallel direction and high values of extension in perpendicular direction for most of the tested leathers.

The L-5, has the highest values in both directions. The L-8 has the lowest value of Es in parallel direction (1.66 %) and L-2 has the lowest value of Es in perpendicular direction (2.04%). However, the extension at which leather fails does not depend on the degree to which the collagen cross-links are broken. Hence, when the leather is deformed by the application of the stress, the load is applied directly on the collagen fibre network. The failure of the leather may be result of the breakage of the fibre bundle, the slip of the fibre bundle or both.

The comparison of the extension of the leathers due to the applied stress varies from the leather to leather depending on various factors including the composition of the non-collagenous compound, elastic content and the fibre weave of the collagenous network (Arumugam 1994). Furthermore the orientation of fibres and fatliquoring are of great impact for the extensions values.

It is found that fatliquoring lubricates and opens up the fibre structure and thereby makes the weave more extensible (Makhothe, 1997). The increase in

the extensibility depends on the direction in which samples are cut and therefore the manner in which the fibres are orientated.

4. CONCLUSIONS

Different types of leather have diffrent extension set.

Results report that the values of extension from the same kind of leather are different in parallel and perpendicular direction. Generally, the low values of Es (%) are in the parallel direction.

The raw material used for upholstery predominantly comes from hides that have a low value of exension set. The extension of the leather depends on which part the leather covered, orientation of the fibres, fatliquoring and the elasticity of the leather.

Samples L-1, L-3, L-4, L-6, L-8, L-9 and L-10 — cow leathers— have higher values of thickness, the lowest values of extension and a good elasticity especially in parallel direction, comparing with the other types of leathers.

Albanian cows leathers in parallel direction are moderately extensible and suitable in the manufacturing of products that need to be able to withstand repeated loading.

REFERENCES

Arumugam V, Naresh MD, Sanjeevi R. 1994. Effect of strain rate on the fracture behavior of skin. *Journal Bioscience*. **19, (3),** 307-313. Available on line http://www.ias.ac.in/jarch/jbiosci/19/307-313.pdf.

Covington AD. 2009. Tanning chemistry. *The Science of Leather*. The Royal Society of Chemistry.

Conabere G. O, Hall R. H., 1946. "The physical properties of individual leather fibres", JSLTC, 30, 214.

European Standard EN I2007SO 2418:2002 Leather-chemical, physical and mechanical and fastness tests- Sampling location.

European Standard EN ISO 2419:2006 Leather-physical and mechanical tests- Sample preparation and conditioning.

European Standard EN ISO 2589:2006 Leather-physical and mechanical tests- Determination of thickness.

European Standard EN ISO 17236:2002 Leather – physical and mechanical tests – Determination of extension set.

Komanowsky M, Cooke PH, Damert WC, Kronick PL, McClintick MD. 1995. Stress relaxation behavior of leather. The ALCA Journal. *Indian Journal of Chemical Technology* . **90, (8)***,* 235.

Liu C-K, Latona NP, Cooke P. 2007. Milling effects on mechanical behaviours of leather. JALCA. **102 (6).** 191-197.

Mahdi H, Palmina K, Gurshi A, Covington D. 2009. Potential of vegetable tanning materials and basic aluminum sulphate in Sudanese leather industry. *Journal of Engineering Science and Technology*. **4, (1)** 20-31.

Makhothe K. 1997. The effect of different parameters on the rupture properties of leather in a tensile test. http://eprints.ru.ac.za/3082/1/MAKHOTHE-MSc-TR98-60.pdf.

Milašienė D, Jankauskaitė V, Arcišauskaitė R. 2003. Prediction of stress relaxation in laminated leather layers. *Journal of Materials Science (Medziagotyra)*. **9, (1)** 73-79.

Sturrock EJ, Boote C, Attenburrow GE, Meek KM. 2004. The effects of the biaxial stretching of leather on fibre orientation and tensile modulus. *Journal of Material Science.* **39 (7),** 2481-2486.

Wang Y-L, Attenburrow GE. 1993. Strength of Brazilian Goat Skin Leathers in Relation to Skin and Animal Characteristics. *Journal of the Society of Leather Technologists and Chemists*. **78 (2),** 55-60**.**

ENERGY INVESTIGATION OF THE FLAT PLATE SOLAR COLLECTOR DURING ITS DAILY OPERATION IN CLEAR DAYS OF SUMMER AND WINTER

Altin MARAJ, Andonaq LONDO
Department of Energy, Faculty of Mechanical Engineering,
Polytechnic University of Tirana
Coskun FIRAT
Energy Institute, Istanbul Technical University
Altin DORRI and Majlinda ALCANI
Department of Energy, Faculty of Mechanical Engineering,
Polytechnic University of Tirana

ABSTRACT

The daily operation and thermodynamic properties of the liquid flat are in the present paper investigated. The data were collected during a clear-day, in summer and winter. The first law thermodynamics was applied when evaluating the thermal efficiency of the liquid flat plate solar collector. Thermal efficiency of the liquid flat plate solar collectors during its daily operation in summer and winter was evaluated basing on the data obtained from the acquisition and storage system.
***Keywords*:** flat plate solar collector, global solar irradiance, clear days, thermal efficiency, daily efficiency.

1. INTRODUCTION

Utilization of solar energy differs from one country to another due to solar irradiation potential, application type, system type and solar collector type. However, using solar energy is of great benefit for the environment as it does not cause pollution and the economy due to costless services. Therefore, using solar water heating systems would be of great benefit.

The cumulative number of solar water heating systems installed in Albania was 11860 by the end of 2011. According to the installed area in the national level, glazed flat plate solar collectors constitute around 99.29% of the total of the installed systems, or $A_{FPC} = 90075$ m^2 (Mauthner and Weiss 2013). The main reason for this prevalence is because they are relatively cheaper than evacuated solar tube collectors.

Thermal performance of the exploited solar collector is very important for practical applications of solar water heating systems. The following paragraph provides information about investigations carried out from different authors:

Zambolin and Del Col (2010) followed the EN 12975-2 standard for the steady-state and quasi-dynamic efficiency tests. Ayompe and Duffy (2013) analyzed the thermal performance of a SWH system equipped with flat plate collectors in a temperate climate. Wolf *et al.,* (1981) carried out sensitivity studies to determine the effect of several parameters (fluid flow rate, plate absorptance, plate emmitance, insulation thickness, etc.) on the performance of a single-glazed solar collector. Mintsa de Ondo *et al*., (2013) evaluated numerically the influence of designing parameters and operating conditions on the performance of a polymer flat plate solar collector. Hamed *et al*., (2014) performed a numerical investigation of flat plate solar collectors to determine their optimal performance and design parameters. Hammad (1995) studied the performance of a flat plate solar collector cooled by a set of heat pipes. Rodriguez-Hidalgo et *al.,* (2012) carried out a study with a building experimental solar facility equipped with flat plate solar collectors. Hahne (1985) calculated the efficiency and the warming-up time of flat plate water collectors under steady-state and transient state conditions. Del Col *et al*., (2013) studied the performance of a prototype glazed flat plate solar collector with roll-bond absorber. Cristofari *et al*., (2002) studied the performance of a solar flat-plate thermal collector wholly manufactured in a copolymer material. Cristofari *et al*., (2003) used a thermal model of finite differences. Fischer et al., (2004) presented the improved approach to outdoor performance testing of solar thermal collectors under quasi-dynamic test conditions.

The present paper investigates the energy performance of a flat plate solar during the daily operation in clear days, in summer and winter. Here, the First Law of Thermodynamics is followed. In addition, the effect of the most important parameters on the instantaneous value of thermal efficiency of the selected flat plate solar collector is considered.

2. Description of the system

Figure 1 depicts the solar water heating system used in the present investigation. It is installed in the premises of the Department of Energy, Faculty of Mechanical Engineering, Polytechnic University of Tirana, Albania.

Fig. 1. External part of the exploited system.

Flat plate solar collectors in the present investigation used are of selective type and produced by Isofoton (Spain). They are designed to be integrated in the solar thermal applications in residential, service and industrial sector. Table 1 reports the main technical characteristics collector (Isofoton, 2010).

Table 1. Main technical characteristics of Isofoton flat plate solar collector

Characteristics	Values
Total length (m)	2.278
Total width (m)	1.075
Absorber area (m^2)	2.205
Transmittance of the cover (-)	0.91
Absorptance of the plate (-)	0.95±2%
Emittance of the plate (-)	0.05±2%
Zero loss efficiency (-)	0.773
Linear heat loss coefficient ($W/(m^2 \cdot K)$)	3.243
Nonlinear heat loss coefficient ($W/(m^2 \cdot K^2)$)	0.014

In the present paper, a solar water heating system with forced circulation is investigated. The main components of the solar water heating system utilized in this work and the sensor placement are in Fig. 2 depicted. The system is equipped with two selective solar flat plate collectors (No.1 in Fig.

2) connected in parallel. The collectors slope is 45° and the azimuthal angle is -10°.

A mixture of water and propylene glycol in 40% concentration is used as a heat transfer fluid. This mixture avoids problems related to freezing of the heat transfer fluid in low temperatures and those related to the corrosion of system components. The circulation of the heat transfer fluid is achieved by a solar pump, which turns on when the appointed temperature difference of 5°C is achieved. The temperature difference is monitored at the control system (No.2 in Fig. 2). Once returned from the solar collectors, the heat transfer fluid enters a hot water accumulator. Flowing in an internal spiral tube, it gives its heat to the sanitary water. The measurement of temperatures is achieved by using thermocouples S2, S3, and S4 (PT1000) (Fig. 2). The measurement of global solar irradiance on the tilted solar collector surface is realised using the sensor S1 (Fig. 2), which is a solar cell (CS10). The collected data during the daily operation are transferred from the control system to the data collecting system (Nr.3 in Fig. 2). Maraj *et al*., (2011) elaborated them using appropriate softwares (No. 4 in Fig. 2).

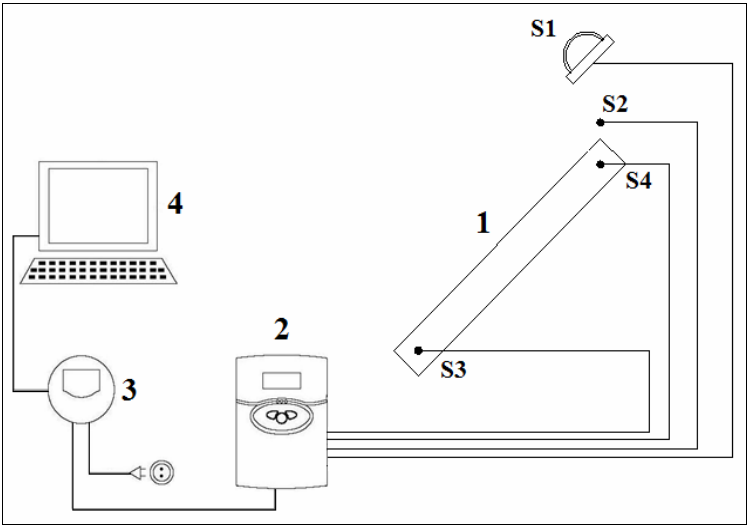

Fig. 2. Main components and utilized sensors of the solar water heating system

3. Mathematical model

The solar collector is the most important component of a solar water heating system. Its main function is to collect the solar irradiation, convert it into heat and further to transfer heat to the working fluid. The First Law of

Thermodynamics was followed for the investigation of the energy during the daily operation of the flat plate solar collector. Technical characteristics of the exploited flat plate solar collector are given above.

Collection efficiency is a measure of collector performance. It is defined as the ratio of the useful energy gain over some specified time period to the incident solar energy over the same period and is given as (Duffie and Beckman, 2013):

$$\eta = \frac{\int \dot{Q}_u \cdot dt}{A_c \cdot \int G_t \cdot dt} \quad (1)$$

where:

η - efficiency (%)

$\dot{Q}_u$ - useful energy gain (W)

A_c - collector area (m^2)

G_t - total solar irradiance (W/m^2)

t - time (s).

This way, the instantaneous efficiency of solar energy conversion to useful thermal energy is given as (Duffie and Beckman, 2013):

$$\eta_i = \frac{\dot{m} \cdot C_p \cdot (T_o - T_i)}{A_c \cdot G_t} \quad (2)$$

where:

η_i - instantaneous efficiency (%)

$\dot{m}$ - mass flow rate (kg/s)

C_p - fluid specific heat (kJ/(kg·K))

T_o - outlet temperature (K)

T_i - inlet temperature (K).

4. RESULTS AND DISCUSSIONS

A clear-days analysis for both winter and summer with regard to liquid flat plate solar collector during their daily operation is carried out. The investigation is based on the mathematical model and the data were obtained from sensors placed in different points of the system. The installed system on the roof of the Faculty of Mechanical Engineering, Polytechnic University of Tirana, Albania is equipped with two flat plate solar collectors connected in

parallel. To simplify the calculations, it is assumed having a unique collector with surface area of $A_c = 4.41$ m^2.

Global solar irradiance on the tilted solar collector surface, ambient temperature near the collector, mass flow rate of heat transfer fluid through the collector, and the temperature of heat transfer fluid at inlet and outlet of the collector are in the present investigation measured. These parameters are provided from the database built through the utilization of a data collecting system, which is installed in the premises of the Department of Energy, Polytechnic University of Tirana, Albania. From the recorded measurements available in the system database, the chosen days represent typical clear days for the summer and the winter season. This is related to the values of global solar irradiance for the selected days in these seasons.

In graph 1, the values of global solar irradiance on the tilted solar collector surface and ambient temperature near the collector are depicted. They refer to the selected days, June 15.2013 and December 27.2011.

The global solar irradiance on tilted collector surface continuing to increase after the sunrise (in a clear day) is in the graphs plotted. Near the midday, this quantity achieves its maximum value and later it diminishes gradually. In the selected day for the summer season (day s), the Sun rises at 05:10 h (standard time) and sets at 20:20 h. In the present investigation, the standard time is used. In the selected day for the winter season (day$w$), the Sun rises at 07:00 h and sets at 16:25 h. The maximum value of global solar irradiance on the tilted solar collector surface for the day (s) is $G_t^{max} = 963$ W/m^2 at 12:15 h. Its value for the day (w) is $G_t^{max} = 904$ W/m^2 at 11:15 h. Global daily solar radiation on tilted collector surface for the day (s) is $H_T^s = 6.085$ kWh/(m^2·day). Its value for the day (w) is $H_T^w = 4.739$ kWh/(m^2·day).

For the day (s) the minimum ambient temperature near the collector is $t_a^{min} = 17.2$ °C at 05:00 h. Its maximum value is $t_a^{max} = 34.9$ °C at 12:55 h. The average value for day (s) was $t_a^{ave} = 26.1$ °C. For day (w), we have the minimum $t_a^{min} = -2.4$ °C at 06:15 h, the maximum $t_a^{max} = 14$ °C at 12:25 h, and the average $t_a^{ave} = 3.9$ °C. The graphs clearly plot the effect of solar irradiance on ambient temperature.

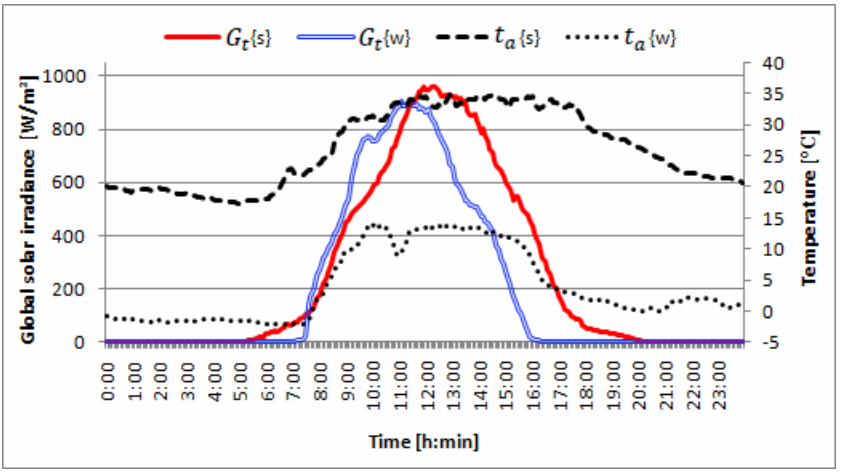

Graph 1. Global solar irradiance and ambient temperature for selected days.

The graph 2 plots the effect of mass flow rate through the flat plate solar collector tubes and the global solar irradiance on tilted collector surface on the thermal efficiency for the day $\{s\}$. Results report that the thermal efficiency of the flat solar collector undergoes several fluctuations of ±15 %. The time interval is $[08:20 \div 16:05]$, as accurate investigation of occurrences and proper analysis could run. Results report that the continuous increase of the global solar irradiance is followed by the increase of the mass flow rate of the heat transfer fluid. In addition, fluctuations of the mass flow rate fits with fluctuations of the thermal efficiency during the major part of the day. As the global solar irradiance achieves its highest values during the midday hours, the thermal efficiency diminishes because the related temperatures achieve their highest designed values. In addition, global solar irradiance is of greatest impact for the thermal efficiency of the flat plate solar collector because its magnitude is several times higher than the magnitude of the mass flow rate.

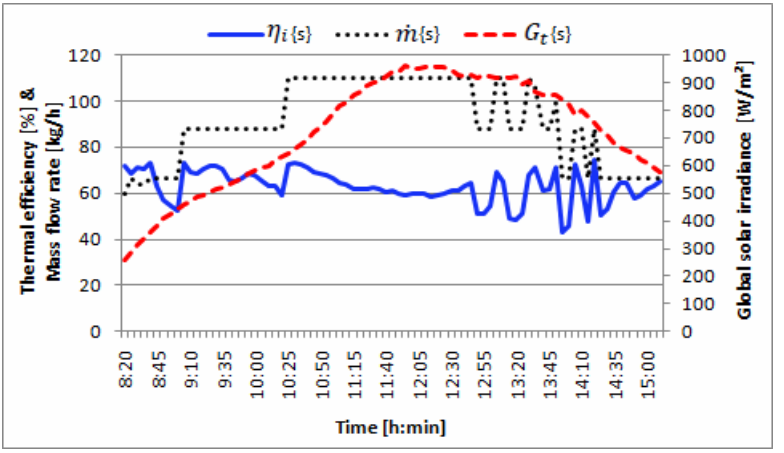

Graph 2. The effect of mass flow rate, global solar irradiance on thermal efficiency during the day $\{s\}$.

The graphic 3 plots the effect of the temperature difference of the heat transfer fluid between the outlet and the inlet of the flat plate solar collector $(\Delta t = t_e - t_i)$ during the selected time interval on the thermal efficiency for the day $\{s\}$. During this day, its minimum value is $\Delta t_s^{min} = 12.8$ °C at 08:25 h. Its maximum value is $\Delta t_s^{max} = 27.6$ °C at 14:40 h. Results report that the fluctuations of the temperature difference of the heat transfer fluid between the outlet and the inlet of the flat plate solar collector has a stronger impact on the thermal efficiency values only during the second part of the day, as here the global solar irradiance reduces showing its impact on the thermal efficiency evaluation.

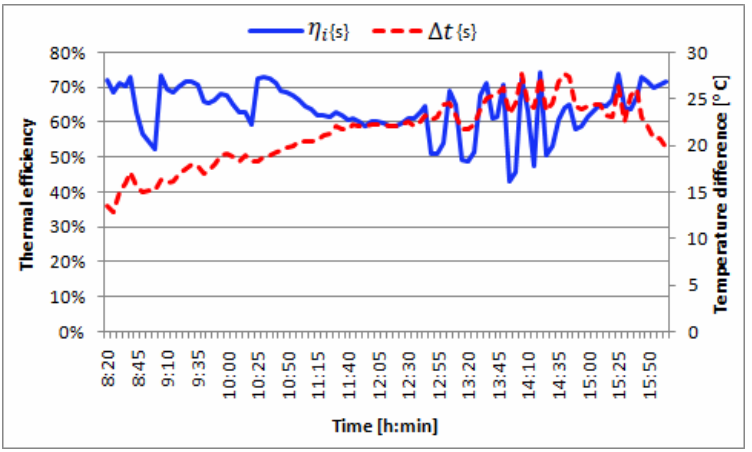

Graph 3. The effect of temperature difference of heat transfer fluid on thermal efficiency during the day $\{s\}$.

The graphic 4 plots the effect of mass flow rate through the flat plate solar collector tubes and the global solar irradiance on tilted collector surface on the thermal efficiency for the day {w}. It is noticed the heat transfer fluid starts to flow through the tubes of the flat solar collector at 08:40 h and ends at 15:35 h. During this time interval, thermal efficiency values of the flat solar collector undergoes several fluctuations of ±16 %. As the global solar irradiance increases in the midday {w}, the mass flow rate of the heat transfer fluid increases. In the other parts of the day where lower values of the global solar irradiance on tilted collector surface are present, increment of the mass flow rate of the heat transfer fluid is obtained because the temperature of the heat transfer fluid of the outlet of the flat plate solar collector differs from the temperature of the inlet of the flat plate solar collector.

The fluctuations of the mass flow rate show a modest impact on the fluctuations of thermal efficiency of the flat plate solar collector. Even for the day {w}, values of the global solar irradiance show the main influence on the values of thermal efficiency of the flat plate solar collector.

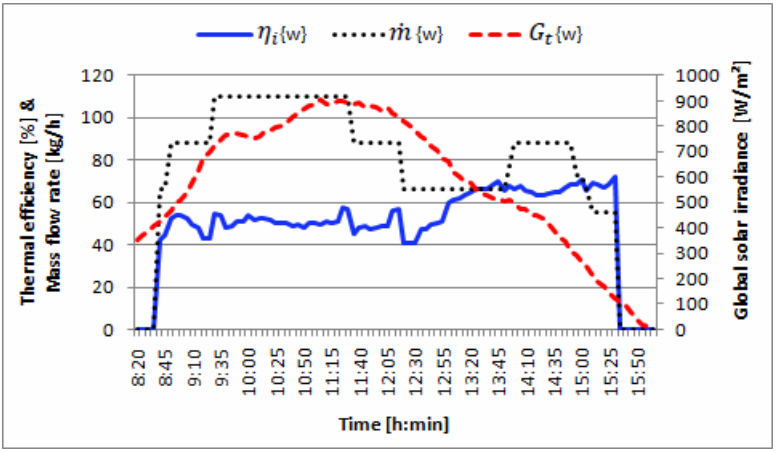

Graph 4. The effect of mass flow rate, global solar irradiance on thermal efficiency during the day {w}

The graphic 5 plots the impact of the temperature difference of the heat transfer fluid between the outlet and the inlet of the flat plate solar collector during the selected time interval on the thermal efficiency for the day {w}. During this day, its minimum value was $\Delta t_w^{min} = 6.8$ °C at 15:30 h. Its maximum value is $\Delta t_w^{max} = 25.6$ °C at 13:00 h. Results report that the fluctuations of the temperature difference of the heat transfer fluid between

the outlet and the inlet of the flat plate solar collector are of a stronger impact for the thermal efficiency values, only during the first part of the day as a result of highest values of the mass flow rate of the heat transfer fluid through the solar collector at this part of the day. The increment of thermal efficiency values during the second part of the day $\{w\}$ are mainly related with the continuous reduction of the global solar irradiance values and their weight in the expression (2).

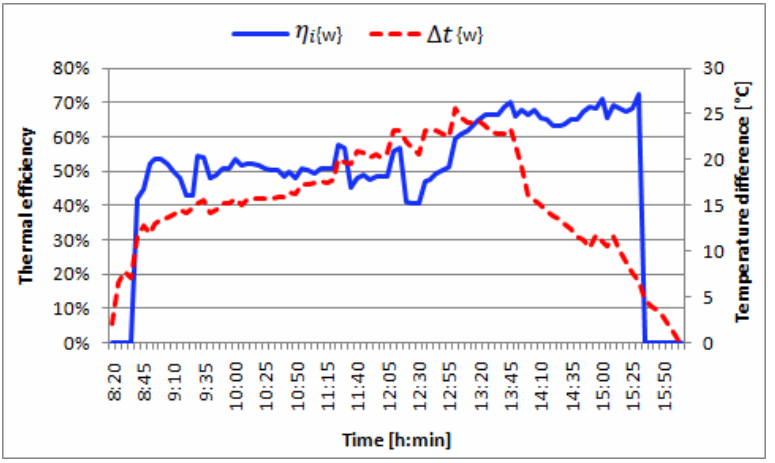

Graphic 5. The effect of temperature difference of heat transfer fluid on thermal efficiency during the day $\{w\}$

The graphic 6 plots the thermal efficiency curves of flat plate solar collector during their daily operation in typical selected days for the summer and the winter season. Values of the thermal efficiency undergo several fluctuations which are related with the summarized effect of global solar irradiance on tilted collector surface, ambient temperature near the collector, mass flow rate through the collector tubes, and temperature difference of the heat transfer fluid between the outlet and the inlet of the collector. Their influence is taken into consideration through expression (2).

For day $\{s\}$ it is noticed that the minimum value of the thermal efficiency of flat plate solar collector is $\eta_s^{min} = 0.432$ at 13:55 h. Its maximum value is $\eta_s^{max} = 0.744$ at 15:25 h. Here, the flat plate solar collector starts to generate heat 20-min earlier and continues 35 min later compared to the day $\{w\}$ because of the higher values and the longer duration of global solar irradiance during the summer season.

For day $\{w\}$ it is noticed that the minimum value of the thermal efficiency of flat plate solar collector was $\eta_w^{min} = 0.405$ at 12:30 h. While its

maximum values, was $\eta_w^{max} = 0.722$ at 15:30 h. The time period during which the flat plate solar collector generates heat is 55 -min shorter, compared to the day $\{s\}$.

For the selected typical clear day in the summer season, the day-long flat plate solar collector efficiency during the time interval $[08:20 \div 16:05]$ is $\eta_s = 0.636$. While, for the typical clear day in the winter season and during the operating interval it is $\eta_w = 0.558$. This difference in the day-long flat plate solar collector efficiency highlights the effect of global solar irradiance on tilted collector surface and ambient temperature near the collector.

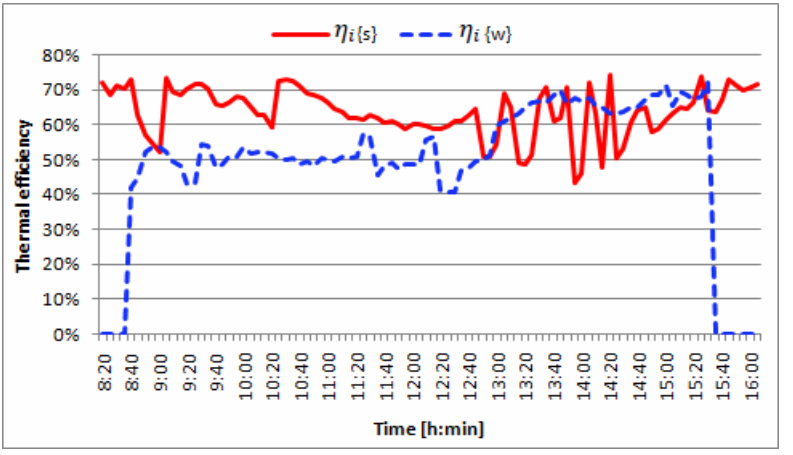

Graphic 6. Thermal efficiency curves for the selected typical days in the summer and in the winter season.

The global solar irradiance and the ambient temperature near the collector represent the main influence in the magnitude of thermal efficiency of flat plate solar collector. The temperature difference of heat transfer fluid between the outlet and the inlet of the flat plate solar collector and the mass flow rate represent a smaller influence because of their magnitude and fluctuations during the considered time interval.

5. CONCLUSIONS

A clear-days analysis for both winter and summer with regard to liquid flat plate solar collector during their daily operation is carried out. The impact the different parameters have on thermal efficiency of a flat plate liquid solar collector during its daily operation is here reported.

The results obtained for the global solar irradiance on the tilted solar collector surface highlight the solar radiation potential for hot water production in Tirana region. Global daily solar radiation on tilted collector surface for day $\{s\}$ (15 June) is $H_T^s = 6.085$ kWh/(m^2·day), while for day $\{w\}$ (27 December) is $H_T^w = 4.739$ kWh/(m^2·day).

Global solar irradiance on the tilted solar collector surface has the main impact on the magnitude of thermal efficiency of the flat plate solar collector during their daily operation.

The fluctuations of ambient temperature near the collector, temperature difference of heat transfer fluid between the outlet and the inlet of the flat plate solar collector, and the mass flow rate are of a smaller impact on the magnitude of thermal efficiency of flat plate solar collector.

For the selected typical clear summer $\{s\}$ and winter days $\{w\}$, the values of thermal efficiency during their daily operation are $\eta_s = 0.636$ and $\eta_w = 0.558$ respectively.

The reduction of ambient temperature near the collector in the winter season induces higher heat losses from the flat plate solar collector and the diminution of their day-long efficiency.

ACKNOWLEDGEMENTS

The solar water heating plant of the present investigation is installed at Department of Energy-Faculty of Mechanical Engineering, Polytechnic University of Tirana, Albania and is a gift of the Spanish Agency for International Development Cooperation (AECID). The authors gratefully acknowledge the financial support for this plant.

REFERENCES

Ayompe LM, Duffy A. 2013. Analysis of the thermal performance of a solar water heating system with flat plate collectors in a temperate climate. *Applied Thermal Engineering*. 58, (1-2), 447-454.

Cristofari C, Notton G, Poggi P, Louche A. 2002. Modelling and performance of a copolymer solar water heating collector. *Solar Energy*. 72, (2), 99-112.

Cristofari C, Notton G, Poggi P, Louche A. 2003. Influence of the flow rate and the tank stratification degree on the performances of a solar flat-plate collector, *International Journal of Thermal Sciences*. **42, (5),** 455-469.

Del Col D, Padova A, Bortolato M, Dai Pre M, Zambolin E. 2013. Thermal performance of flat plate solar collectors with sheet-and-tube and roll-bond absorbers. *Energy*. **Vol. 58, 258-269.**

Duffie JA, Beckman WA. 2013. Solar Engineering of Thermal Processes. 4-th ed., New Jersey: John Wiley & Sons.

Fischer S, Heidemann W, Müller-Steinhagen H, Perers B, Bergquist P, Hellström B. 2004. Collector test method under quasi-dynamic conditions according to the European Standard EN 12975-2, *Solar Energy*. **76, (1-3)**, 117-123.

Hahne E. 1985. Parameter effects on design and performance of flat plate solar collectors, *Solar Energy*. **34, (6),** 497-504.

Hamed M, Fellah A, Brahim AB. 2014. Parametric sensitivity studies on the performance of a flat plate solar collector in transient behavior, *Energy Conversion and Management*. **78**, 938-947.

Hammad M. 1995. Experimental study of the performance of a solar collector cooled by heat pipes, *Energy Conversion and Management*.**36, (3), 197-203.**

Maraj A, Londo A, Shtjefni A, Fundo A. 2011. Studimi energjitik i funksionimit tranzitor të kolektorëve të sheshtë diellor, në stinën e verës. *Bulletin of Technical Sciences***.** Polytechnic University of Tirana, (in press).

Mauthner F, Weiss W. 2013. *Solar Heat Worldwide. Markets and contribution to the energy supply 2011*. Graz: Steinhuber Infodesign. **62**. **http://www.aee-intec.at/0uploads/dateien932.pdf**

Mintsa de Ondo AC, Medale M, Abi C. 2013. Optimization of the design of a polymer flat plate solar collector. *Solar Energy***. 87, 64-75.**

Isofoton, 2010. *Operating and Maintenance Manual: Isotherm Plus Collector*. Available at: www.isofoton.com

Rodriguez-Hidalgo MC, Rodriguez-Aumente PA, Lecuona A, Nogueira J. 2012. Instantaneous performance of solar collectors for domestic hot water, heating and cooling applications, *Energy and Buildings*. **45**, 152-160.

Wolf D, Kudish AI, Sembira AN. 1981. Dynamic simulation and parametric sensitivity studies on a flat-plate solar collector. *Energy*. **6.** 333-349.

Zambolin E, De Col D. 2010. Experimental analysis of thermal performance of flat plate and evacuated tube solar collectors in stationary standard and daily conditions. *Solar Energy*. **84, (8)** 1382-1396.

CAN WE PREDICT CPAP FAILURE IN PRETERMS WITH RESPIRATORY DISTRESS SYNDROME?

Eda JAZEXHIU–POSTOLI
Service of Neonatology, University Hospital for Obstetrics and Gynecology, Koço Gliozheni, Tirana, Albania
Evda VEVEÇKA
Department of Pediatrics, University of Medicine, Tirana, Albania
Erinda RAPUSHI
Department of Pediatrics, University of Medicine, Tirana, Albania
Elizana PETRELA
Department of Statistics, University of Medicine, Tirana, Albania
Eduard TUSHE
Neonatal Department, University of Medicine, Tirana, Albania

ABSTRACT

Continuous positive airway pressure (CPAP) is a non-invasive treatment in preterm newborns with respiratory distress syndrome (RDS). However, some preterm infants fail with CPAP treatment.

In the present investigation, the Bubble and Biphasic NCPAP are used to evaluate the risk factors and neonatal outcomes associated with Nasal CPAP (NCPAP) failure in preterm newborns with RDS.

This is a prospective randomized study that involved 200 infants with gestational age (GA) 28-35 weeks, treated for RDS. They were assigned to Bubble NCPAP (n=100) and Biphasic NCPAP (Infant Flow) (n=100), using short bi-nasal prongs. Data about gender, way of delivery, gestational age, birth weight, Apgar score at 1^{st} and 5^{th} min., need for resuscitation, antenatal corticosteroids and Surfactant use were recorded. Need for ventilation (CPAP failure), incidence of air leaks, incidence of intraventricular hemorrhage (IVH) and persistent ductus arteriosus (PDA), FiO2 at admission, mortality rate were measured. The relation between CPAP failure and gestational age, way of delivery, need for resuscitation, corticosteroids and surfactant use; was in the present paper investigated. In addition, relation between pneumothorax, IVH, PDA, FiO_2 demand and CPAP failure was assessed.

Divided into two groups, the newborns had similar characteristics (gender, way of delivery, gestational age, birth weight, Apgar index, corticosteroids, Surfactant use); $p > 0.05$.

Results report that CPAP failure was 20/100 in Bubble vs 20/100 in IF CPAP; pneumothorax 4/100 vs 4/100; IVH 12/100 vs 11/100; PDA 19/100 vs 18/100; FiO_2 at admission 0.4 ± 0.1 vs 0.3 ± 0.1; mortality rate 8/100 vs 10/100 (p>0.05).
Using binary logistic regression analysis, CPAP failure resulted moderately related with lower gestational age [Od 1.26 CI 95%: 0.38-4.21] (p=0.07); CPAP failure was moderately related with the need for resuscitation after birth (p=0.056); no statistic relation was found with way of delivery, corticosteroids and Surfactant use. Infants with pneumothorax and IVH had significantly higher risk for CPAP failure [Od=3.35, CI95% :1.29-5.84] (p=0.002), [Od=6.8, CI95% : 2.06-7.96] (p=0.002); persistent ductus arteriosus moderately increased risk for CPAP failure [Od=2.89, CI95% :0.99-4.05] (p=0.61); every increase in FiO_2 was moderately related with CPAP failure [Od=2.42, CI95% :1.00-3.62] (p=0.057).
Factors that can predict CPAP treatment failure in preterm newborns with RDS are extreme prematurity, need for resuscitation, higher FiO_2 requirement, severe complications as pneumothorax and intraventricular hemorrhage.

1. INTRODUCTION

Respiratory distress syndrome (RDS) is an important cause of morbidity and mortality in preterm infants (Polin and Sahni, 2002; Goldsmith and Karotkin 1996; Kallapur and Ikegami 2000). Positive pressure ventilation and surfactant replacement are the standard treatments for infants with moderate and severe disease. However, ventilator-induced lung injury should be avoided to reduce the incidence of chronic lung disease. So, gentle ventilation strategies, among them Nasal CPAP, are in use to reduce CLD in preterm infants (Espagne and Hascoet 2002; Goldsmith and Karotkin 1996; Jonsson *et al*., 1997; Kamper *et al*., 1993). But in some of infants treated we face early CPAP failure (Bancalari *et al.,* 2003; Gittermann *et al*., 1997).

The present investigation aims at investigating the factors that can distinguish infants successfully treated from infants who fail in NCPAP. In addition, efforts to predict which infants can fail in CPAP have been made.

2. MATERIALS AND METHODS

We ran a prospective randomized study from January 2011 to March 2013, in the tertiary level neonatal intensive care unit (NICU) in Tirana, Albania. In the present study, infants between 28-35 weeks gestational age, inborn, affected by respiratory distress in the first 6 hours of life were considered and treated with NCPAP, two different techniques. Bubble continuous positive airway pressure (CPAP) is the conventional CPAP with continuous flow; it is inexpensive and easy to adapt for newborns. Biphasic NCPAP (Infant Flow CPAP) is an alternative of NCPAP which offers two

levels of CPAP to recruit unstable alveoli and prevent the alveolar collapse. It can reduce the variations in airway pressure. The constancy of continuous distending pressure in CPAP during the respiratory cycle is fundamental for restoring the functional residual capacity and for reducing the work of breathing.

We excluded from the study infants with severe congenital anomalies, infants that required intubation in the delivery room. We got written informed parental consent and the intervention was approved by the Hospital Ethics Committee. Respiratory distress was defined by clinical and radiological criteria and by the Silverman index of RDS severity. Steroids were administered to mother following the prenatal unit protocol.

After delivery all infants underwent similar interventions: transport from the delivery room to NICU in about 5 minutes in transport incubator with available oxygen supply, stabilization in NICU following the protocol, oxygen supply to maintain an oxygen saturation (SpO2) of 85 to 93% (following the protocol). The respective preterm newborns were numbered after birth and were randomized to Bubble NCPAP group (group A) or Biphasic NCPAP Infant Flow (group B). We adjusted these parameters: depth in water, fraction of inspired oxygen, lower CPAP level, upper CPAP level, mean airway pressure (MAP). We used short binasal prongs in both groups. If the newborn met the criteria of the NICU endotracheal porcine natural surfactant (Curosurf 100mg/kg) was administered with the INSURE method.

CPAP was discontinued when newborns with sufficient respiratory effort had Fi02< 0.30, PEEP < 3 cm H2O, Pa02>50mmHg and PaC02< 65mm Hg.

Infants were subdivided into “CPAP success” group where infants were successfully treated for at least 72 hours and a “CPAP failure” group where infants required intubation for respiratory failure within first 72 hours of life (FiO2 requirement > 0.6, pH < 7.2 and PaCO2 > 65mmHg). Gender, way of delivery, gestational age, birth weight, Apgar score at 1st and 5th minute, need for resuscitation, antenatal corticosteroids and Surfactant use are in the present paper investigated. In addition, need for ventilation (CPAP failure), incidence of air leaks, incidence of intraventricular hemorrhage (IVH) and persistent ductus arteriosus (PDA), FiO2 at admission, mortality rate have been recorded. Moreover, relation between CPAP failure and gestational age, way of delivery, need for resuscitation, corticosteroids and surfactant use were studied; and relation between pneumothorax, IVH, PDA, FiO_2 demand and CPAP failure was also assessed.

Data collection and statistic analysis

Categorical outcomes were presented in percentages and were tested using Chi-square test. Continuous variables were presented as mean ± standard deviation (SD).

Differences between continuous variables were analyzed with T Student's test. All data were analyzed using Statistic System SPSS 19.0. The level of significance was set to $p \leq 0.05$.

Prediction of early CPAP failure

Many of the variables used are not normally distributed, so we calculated median values and their corresponding 95% CI for each group. To evaluate possible associations between CPAP failure and variables we performed multivariate analyses using binary logistic regression. Non significant terms were removed sequentially from logistic models and the results recalculated at each removal. We analyzed the variables that are strongly associated with early CPAP failure (GA, BW, FiO_2 at admission) available at birth or immediately thereafter to construct models that can predict early CPAP failure; and variables that can predict later CPAP failure.

3. RESULTS

Two-hundred newborns are involved in the present study. They were randomized to group A (Bubble NCPAP) (n=100) and group B (Biphasic Infant Flow NCPAP) (n=100).

Table 1 reports that the newborns had similar clinical characteristics.

Table 1. Clinical characteristics

Clinical characteristics		Bubble (n=100)	Infant (n=100)		p value
Gender	M	65 (65%)	49 (49%)	Chi-square	
	F	35 (35%)	51 (51%)	0.147	0.61
Birth	vaginal	42 (42%)	41 (41 %)	Chi-square	0.567
	C.S.	58 (58%)	59 (59%)	0.121	
Gestational Age		32.06 ±1.91	32.13±1.95	t = - 0.241	0.810
Birth weight		1786.00 ± 439.22	1739.60 ± 484.52	t = 0.710	0.479
Apgar 1st		7.06±1.57	6.72±1.78	t = 1.435	0.153
Apgar 5 th		8.43±0.84	8.23±0.90	t = 1.624	0.106
Corticosteroids	Yes	57 (57%)	60 (60%)	Chi-square	0.387

	No	43 (43%)	40 (40%)	0.185	
Resuscitation	Yes	12 (12 %)	21 (21%)	Chi-square	0.063
	no	88 (88 %)	79 (79%)	2.94	
Surfactant	yes	36 (36%)	27 (27%)	Chi-square	0.112
	No	74 (74%)	73 (73%)	1.887	

With 40 (20%) patients requiring mechanical ventilation for respiratory failure (the CPAP- failure group), 160 (80%) were successfully treated with NCPAP (the CPAP-success group).

Table 2. Outcomes

	Bubble CPAP	**Infant Flow CPAP**	**Chi-square**	**P value**
CPAP failure (%)	20 (20%)	20 (20%)	1.23	0.86
Pneumothorax (%)	4 (4 %)	4 (4 %)	1.38	0.64
Persistent ductus arteriosus (%)	19 (19%)	18 (18%)	0.033	0.5
Intraventricular hemorrhage (%)	12 (12%)	11 (11%)	0.049	0.5
	0.4±0.1	0.3±0.1		0.658
FiO_2 on admission	8 (8%)	10 (10%)	0.244	0.403
Mortality (%)				

Table 3. Correlation between CPAP failure (yes vs no) and independent variables

Independent variables	**OD**	**CI 95%**		**P value**
Gestational age	1.26	0.38	4.21	0.07
Birth weight	1.16	0.74	1.83	0.498
Way of delivery (cesarean sect.)	1.04	0.39	2.78	0.926
Corticosteroids (no)	2.29	0.77	6.80	0.132
Resuscitation	3.05	0.10	1.03	0.056
Surfactant (no)	1.95	0.16	5.66	0.251
Persistent ductus arteriosus (yes)	2.89	0.99	4.05	0.061
Pneumothorax (yes)	3.35	1.29	5.84	0.002*
Intraventricular hemorrhage (yes)	6.80	2.06	7.96	0.002*
FiO_2 at admission	2.42	1.00	3.62	0.07

In multivariate analyses controlled for GA, BW and gender, none of these risk factors was associated with CPAP failure: cesarean section, maternal corticosteroids, birth weight, Surfactant use.

CPAP failure is moderately related with need for resuscitation after birth (p=0.056).

Median 1st minute Apgar scores were significantly lower in the CPAP-failure group than in CPAP-success group.

The median of FiO2 at admission differed between CPAP failure and CPAP success group: every increase in FiO_2 was moderately related with CPAP failure [Od=2.42, CI95%:1.00-3.62] (p=0.057).

Infants with pneumothorax and IVH had significantly higher risk for CPAP failure [Od=3.35, CI95% :1.29-5.84] (p=0.002), [Od=6.8, CI95% : 2.06-7.96] (p=0.002); persistent ductus arteriosus moderately increased risk for CPAP failure [Od=2.89, CI95% :0.99-4.05] (p=0.61).

Significantly higher rates of pneumothorax, IVH were associated with CPAP failure compared with CPAP success.

4. DISCUSSION

NCPAP treatment is associated with reduced need for intubation and a lower incidence of CLD (Bancalari *et al*., 2003). Infants who succeed on CPAP have lower mortality rates, IVH, ROP (Bancalari *et al.*, 2003**;** Espagne and Hascoet 2002; Gittermann *et al.*, 1997; *et al.*, 2000; Narendran *et al.*, 2003)**.** Although many retrospective studies attest to the effectiveness of different nasal CPAP in the management of RDS in preterm infants (Boo *et al.*, 2000; Blenow *et al.*, 1999; De Klerk and De Klerk 2001; Espagne and Hascoet 2002; Narendran and Donovan, 2003; Kero and Makinen 1979), no randomized prospective controlled trials compare their outcomes. NCPAP is the initial ventilator support for all spontaneously breathing preterm infants (Wung 1993; Lundstrom 1996). In the present study, 80 % of spontaneously breathing infants were treated successfully with nasal CPAP. Few studies have analyzed factors that might predict CPAP failure in preterm infants (Lindner and Wossbeck, 1999; Ammari and Suri 2005). In a study septicemia and pneumothorax during CPAP therapy were found to be significantly associated with CPAP failure in pretem infants (Boo and Zuraidah, 2000). In the present study, results report that the factors significantly related to CPAP failure were later complications such as pneumothorax and intraventricular hemorrhage. Complication rates were significantly worse for those failing CPAP than for infants who succeeded on CPAP. Although lower gestational age (GA) is moderately related with CPAP failure, difficulty in predicting this may be because our study group included GA 28-35 weeks (not 24-28 weeks,

where more significant results could be expected) (Blenow *et al.*, 1999; Merran AT (IFDAS study group) 2002; Verder *et al.*, 1999)**.** This may be true also for relation between birth weight and CPAP failure (Guerrini *et al.*, 2000; Joris *et al.*, 2000). Whether or not infants at risk for early CPAP failure are better of being treated initially with mechanical ventilation and surfactant is a question that only multicenter prospective, randomized controlled trials can predict. So it might be wrong to use CPAP in any infant with a reasonable chance of failure.

5. CONCLUSION

Factors that can predict CPAP treatment failure in our preterm newborns with RDS are extreme prematurity, need for intensive resuscitation after birth, higher FiO_2 requirement on admission in Neonatal Intensive Care Unit, severe complications as pneumothorax and intraventricular hemorrhage.

REFERENCES

Ammari A, Suri M, Milisavljevic V, Sahni R, Bateman D, Sanocka U, Ruzal-Shapiro C, Wung JT, Polin R. 2005.Variables associated with the early failure of Nasal CPAP in very low birth weight infants. *The Journal of Pediatrics*. September.

Bancalari E, Claure N, Sosenko IR. 2003. Bronchopulmonary dysplasia: changes in the pathogenesis and prevention of chronic lung disease of prematurity. *Seminars on Neonatology*. **8**: 63-71.

Boo Ny, Zuraidah Al, Lim Nl, Zulfiqar MA. 2000. Predictors of failure of nasal continuous positive airway pressure in treatment of preterm infants with respiratory distress syndrome. *Journal of Tropical Pediatrics.* **46:** 172-5

Blenow M, Jonsson B, Dahlstrom A, Sarman I, Bohlin K, Robertson B. 1999. Lung function in premature infants can be improved: surfactant therapy and CPAP reduce the need of respiratory support. *Lakartidningen.* **96:** 1571-6.

De Klerk AM, De Klerk RK. 2001.Nasal continuous positive airway pressure and outcomes of preterm infants. *Journal of Paediatrics and Children Health.* **37 (2),** 161-7.

Espagne S, Hascoët JM.2002. Non-invasive ventilation of premature infants. *Arch Pediatr.* **9 (10),** 1100-3.

Goldsmith JP, Karotkin EH. 1996. Assisted Ventilation of the Newborn. 3rd ed. WB Saunders.

Gittermann MK, Fusch C, Gittermann AR, Regazzoni BM, Moessinger AC. 1997.Early nasal continuous positive airway pressure

treatment reduces the need for intubation in very low birth weight infants. *European Journal of Pediatrics*. **156:** 384-8.

Guerrini P, Brusamento S, Rigon F.2000. Nasal CPAP in newborns with birth weight under 1500g. *Acta Biomedica Ateneo Parmense.* **71:** 447-52.

Joris N, Sudre P, Moessinger A.2000. Early application of CPAP in newborns with post-menstrual age below 34 weeks lowers intubation rate and shortens oxygen therapy without altering mortality and morbidity. *Schweiz Medicine Wochenschr.* **130:** 1887-93.

Jonsson B, Katz-Salamon M, Faxelius G, Broberger U, Lagercrantz H. 1997. Neonatal care of very-low-birth weight infants in special-care units and neonatal intensive-care units in Stockholm. Early nasal continuous positive airway pressure versus mechanical ventilation: gains and losses. *Acta Pediatrica Supplement.* **419.:**4-10.

Kallapur S, Ikegami M. 2000. The surfactants. *American Journal of Perinatology.* **17:** 335-43.

Kero PO, Makinen EO. 1979. Comparison between clinical and radiological classification of infants with the respiratory distress syndrome (RDS). *European Journal of Pediatrics.* **130:** 271-8.

Kamper J, Wulf K, Larsen C, Lindequist S.1993. Early treatment with nasal continuous positive airway pressure in very low-birth-weight infants. *Acta Paediatrica. 82:193-7.*

Lundstrom KE. 1996. Initial treatment of preterm infants: continuous positive airway pressure or ventilation? *European Journal of Pediatrics.* **155:** 525-9.

Lindner W, Vossbeck S, Hummler H, Pohlandt F.1999. Delivery room management of extremely low birth weight infants: spontaneous breathing or intubation? *Pediatrics.* **103:** 961-7

Merran AT (IFDAS study group). 2002. Early nasal continuous positive airway pressure with prophylactic surfactant for neonates at risk for RDS. The IFDAS multi-center randomized trial. *Pediatric Research* .**51**: 379A.

Narendran V, Donovan EF, Hoath SB, Akinbi HT, Steichen JJ, Jobe AH 2003. Early Bubble CPAP and outcomes in ELBW preterm infants. *Journal of Perinatology.* **23:** 195-9.

Polin RA, Sahni R.2002. Newer experience with CPAP. *Semin Neonatal.* **7:** 379-89.

Verder H, Albertsen P, Ebessen F, Greisen G, Robertson B, Bertelsen A 1999. Nasal continuous positive airway pressure and early surfactant therapy for respiratory distress syndrome in newborns of less than 30 weeks' gestation. *Pediatrics;* **103:** E 24.

Wung JT. **1993**. Respiratory management for low-birth-weight infants. *Critical Care Medicine.* **21:** 5364-5.

ADOPTIVE PUSHOVER ANALYSIS OF AN EXISTING STRUCTURE

Altin BIDAJ, Ervin PAÇI, Hektor CULLUFI and Irakli PREMTI
Polytechnic University of Tirana, Albania

ABSTRACT

The old national standards about the building constructions have been used in Albania for more than thirty years. If the EuroCode 8 (Design of structures for earthquake resistance) would be used even for the recently constructed buildings, they would either collapse or be heavily damaged.
The present paper provides information about the EN-Eurocode 8 for Design of Structures for Earthquake Resistance. European Code has an irreplaceable importance for both the construction industry and society as it aims at establishing skeleton of the future goals of the construction industry and saving lives.
Firstly, information about the conditions of the existing structure is in the present paper provided. Secondly, the paper reports the performed nonlinear analysis (adaptive pushover) and structural measures suitable for this type of structure.
In the end, the paper gives recommendations about the methodology of design and the most appropriate strategy of retrofitting these kinds of structures, in order to achieve the required level of performance and increase their level of security based on European Codes.
***Keywords*:** Seismic retrofitting, EuroCodes, existing structure

1. INTRODUCTION

Many private and public building have been constructed over years in Albania. Unfortunately, construction industry suffers from appropriate safety construction rules. The tools and techniques need to be adapted according to current seismic conditions. Following the European Code for seismic design and rehabilitation of buildings, it is important for the construction industry that the European Code to be fully consistent, user-friendly and seamlessly integrated and covers all types of civil engineering works, except nuclear power plants, off-shore structures and long-span (cable-stayed or suspension) bridges. It is already considered the basis of technical specifications for public works tenders or public procurements and the related engineering services.

In order to give the best solution fully consistent with the current trends in the area, there is reported a lot of information about construction based on Albanian code and retrofitting based on Eurocode.

Reported in (Manfredi et al., 2007), the control and retrofit process of the existing structures include: i) dimensions and geometric data information, reinforcement bars and detailing, material of the existing structure, ii) static analysis design for a new structure but with geometry and characteristics of existing material (simulation design), iii) check of structure deformations, etc. Comparison of provided reinforcement with required reinforcement. If reinforcement would not be sufficient, nonlinear analysis must be carried out and, iv) determination of the strategy of intervention, analysis and control the retrofitted structure.

The later part of the present paper provides **detailed information about the aforementioned stages.**

MATERIALS AND METHODS

Existing structure

Photo 1 shows the design of an existing building constructed in 2009. The building was divided in two separate structures. The first structure of the building is in the present paper investigated and will serve as offices premises. It has two above ground stories with irregular form in plan, with dimensions of 8m x 24.3m at maximal point.

Photo 1. View of the structure

The first structure is divided in 2 main axes in longitudinal direction (one main span) and 5 axes (4 spans) in transversal direction. Columns dimensions are 40 x 40cm and 40 cm diameter. The side beams and transversal beams are 40 x 60cm, while the beams for the port between axis “3”and “4” are 30x40cm and 25x60 cm. The slab height is 17 cm. Unfortunately, details on possible changes during the construction lack.

It has been noticed, observing the concrete elements, that the dimensions of the structural elements are the same as in the design. Non-destructive and some destructive tests were carried out to accurately investigate characteristics of the materials, and checking the height of the slab.

The Albanian Design Code “K T P 1985” was applied for the design of the building. The final design drawings and the real material characteristics provide sufficient information about the existing structure.

Concrete properties investigations

Currently, there are four methods applied for the evaluation of concrete properties. Based on their characteristics, their results are more or less reliable.

Italian Standarts UNI EN12504-1 for the tests on the concrete structures, Part 1: carrots, levy, examination and testing of compression and the UNI EN12504-2 for the tests on the concrete structures - non-destructive tests - determination of the sclerometric index have been followed during the two core tests (Photo2 and 3) 6 Schmid hammer tests, respectively.

Photo 2. Core drill hole 1.

Photo 3. View of core drill 1 concrete

For the core tests we have used the correction given by (Masi 2005; Manfredi *et al*., 2007).

$F_{c,i}=(C_{h/D} \times C_D \times C_s \times C_d)f_{core,i}$

where $C_{h/D}$ is a correction ratio for h/D (h-height and D- Diameter), where $C_{h/D} >2$ or $C_{h/D} <2$

C_D correction ratio for D different from 100mm

C_s correction ratio for steel presence influation

Cd correction ratio for core disturbance

From this expression we obtain the following characteristics:

Concrete properties from tests

Self weight	g=2455 kg/m^3
Cylinder concrete compressive strength	fck= 270 daN/cm^2
Cubic concrete compressive strength	Rck= 330 daN/cm^2

Design compressive, tensile strength

f_{cd}	=	180	daN/cm^2
f_{ctm}	=	28.5	daN/cm^2
$f_{ctk\ 0.05}$	=	19.4	daN/cm^2

Structure evaluation based on Eurocodes

Based on the Eurocode (EC8) and (ASCE 2000; ATC 1996*;* Pristley 2000*;* Pristley *et al.,* 2007), in general an additional limit state would be important for the structural evaluation of existing buildings. The new buildings are designed to fulfill the hierarchy of resistances and appropriate

ductility, and evaluated structures are designed according to these requirements (Paulay and Pristley 1992: Pristley 2000; Pristley *et al*., 2007).

The following requirements are of great importance for the determination of the state of damage of the structure (ASCE 2000; ATC 1996): i) limit state with limited damage (immediate occupancy) IO, ii) limit state with significant damage (from damage control- life safety) LS and, iii) limit state of structural stability (total or partial collapse) CP.

Pristley (2000) reported that the procedures followed for the evaluation of an existing structure are: i) identification of existing data, ii) determination of levels of recognition and selection of computer models, iii) determination of seismic loads in every limit stage, iv) modeling and analysis and, v) verification of elements

Information about the first two procedural steps is in the aforementioned paragraph provided. The later part of the paper provides information about the last three procedural steps.

Seismic action

Seismic identification zone

Albania is an active seismic country. The Albanian Construction Code was drafted based on the seismic data obtained from the earthquake intensity map and investigations on soil conditions. Based on the EC8, seismic hazard should be given only with the a_{gR} parameter on ground type "A" that corresponds to rock or rock like geological formations, including 5m weak formations (soil) at surface. The values of a_{gR}(maximum acceleration PGA) are obtained from the Probabilistic hazard map of Albania (Fig.1), recently recommended (not officially) by the Institute of Geosciences Water and Environment, Tirana, Albania . The return period of the reference event is T_R=475 years that corresponds to a life time of 50years (EC8).

The horizontal PGA in ground type A for Tirana District is PGA=0,30g .

Based on the values of PGA in rock and for the specific type of terrain is calculated the design spectrum for three limit states based on EC8 formulations and soil condition classifications. The design spectrum could be obtained by reducing the corresponding elastic spectrum with the appropriate structure behaviour factor "q" (Eurocode 8; Pristley 2000; Pristley *et al*., 2007). For the ultimate limit state of the local soil conditions (ground type C), the value of this factor is q=3.2. (Fig.2).

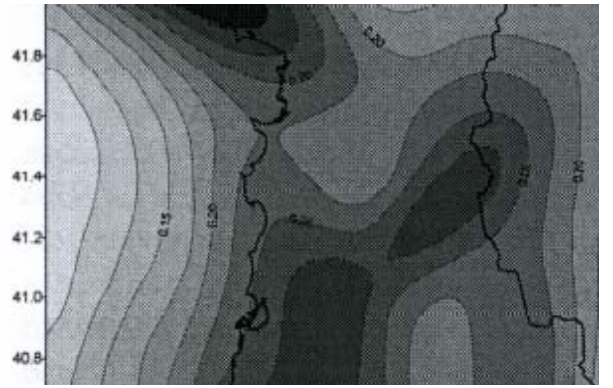

Fig.1. Peak ground acceleration Map of Albania

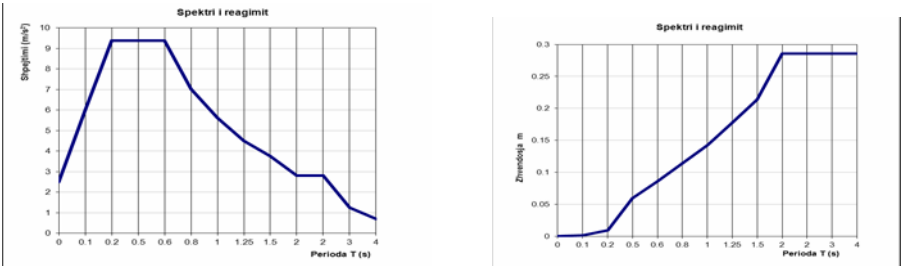

Fig.2. Graphical view of the elastic acceleration and displacement spectrum for soil type C.

Dynamic linear analysis

Structural modeorling and seismic characteristics have been determined similarly as for the new buildings—following the recommendations given by EuroCode 8 (CSI 2000). Spectral method involving concentrated masses in the centre of masses of each story was applied for the analyses and the determination of internal forces. The European Code EC1 (Actions on Structures, EN 1991-1-1, 2002) was followed for the combination of seismic loads and other actions above the building.

Model of the structure is the same as for a new building and the contribution of non-structural elements is neglected. The 3D model of the structure and graphical view of three first modes is in figure 3 and 4 depicted.

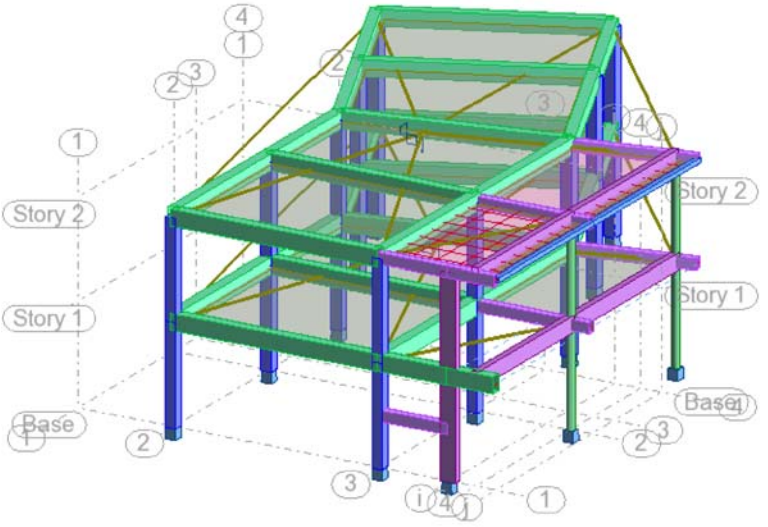

Fig 3. Graphical view of the linear model

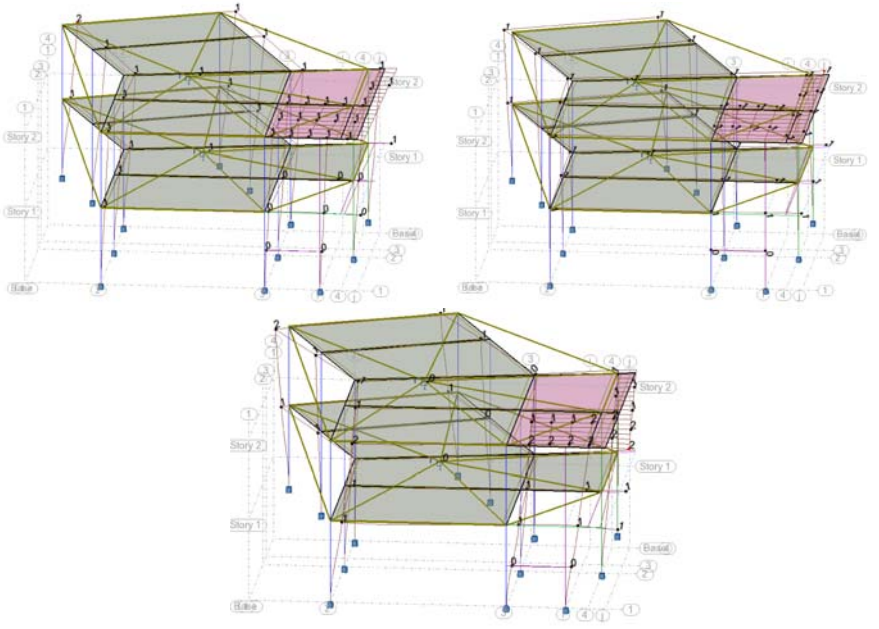

Fig.4. Graphical view of the three first modes.

Table 2. Modal results of the structure

Case/ Mode	Frequency (Hz)	Period (sec)	Rel.mas. UX (%)	Rel.mas. UY (%)	Cur.mas UX (%)	Cur.mas UY (%)	Total mass (kg)
4/1	1.67	0.60	11.09	72.01	11.09	72.01	704610.46
4/2	1.68	0.59	80.78	88.76	69.69	16.75	704610.46
4/3	2.04	0.49	90.96	92.47	10.18	3.71	704610.46
4/4	4.71	0.21	91.08	98.70	0.13	6.23	704610.46

The results of the Table1 report that the structure is irregular and torsion has a great impact on its seismic behavior (Beyer *et al*., 2008). Once the fragile or ductile behavior for each element is determined, the strength of all the elements is checked applying forces obtained from seismic combination. In addition, results report that the columns strength is assured (average safety coefficient is approximately around 1:03), while the beams meet the criteria of resistance in shear, but did not meet the criteria of flexural resistance. In order to take an accurate picture of the way the structure behaves, it is necessary to do the nonlinear analysis.

Static nonlinear analysis

Nonlinear static analysis is the simplest method for nonlinear analysis of structures involving normally concentrated plasticity models. Currently, distributed plasticity models are used as well.

Aspects emerging from the analysis of the structure are reported in the present paper.

The combination of results in both directions cannot be carried out, but each direction must be considered separately. For each direction there are taken into consideration two types of distribution of forces, one according to normalized first mode deformations and the second according to proportional mass of each floor (ASCE 200; ATC 1996).

The method cannot take into account the effects of progressive degradation of strength, the redistribution due to of the plastification and the change of modal characteristics. Also in torsionally eccentric structures, the first mode has important effective mass participation in both directions and may not be disconnected from other modal forms (Beyer et al., 2008; Manfredi *et al*., 2007), i.e., a first mode that effects only one direction to get real performance of the structure for each direction separately could not be evidenced.

In these cases must be used nonlinear dynamics analysis or adaptive nonlinear static analysis. Figure 5 and 6 depict the encountered problems.

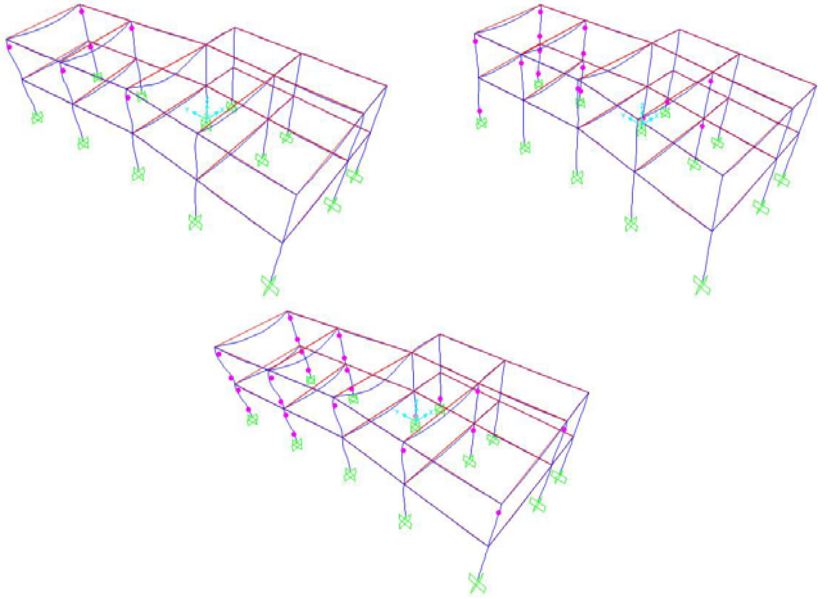

Fig. 5. Graphical view of the structure for three incremental following steps

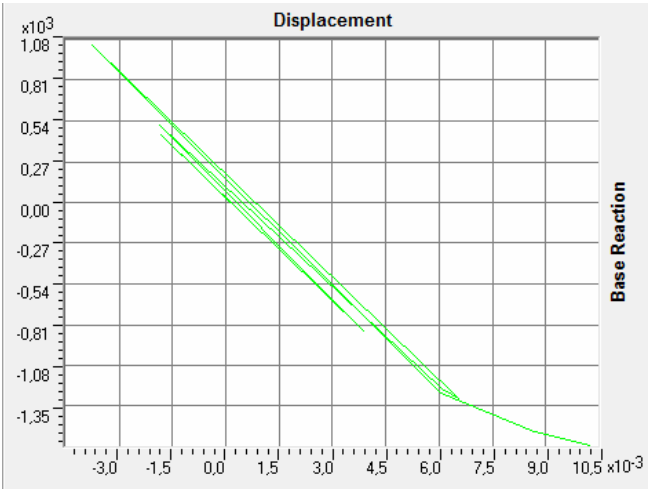

Fig. 6. Graphical view of the base force versus displacement for the structure (capacity curve)

Results report that the capacity curve, deformation base shear force relationship is not continuous in one direction and the performance point of the structure could not be obtained. In addition, the required maximum

displacement and the corresponding base shear force with any of the known methods cannot be determined (ATC 40, FEMA 356; ASCE 2000; ATC, 1996).

Consequently, neither the deformation capabilities (θ) nor the strength (M_{Rd},V_{Rd}) of the elements of the structure (Paulay and Pristley 1992) can be checked.

Adaptive static nonlinear analysis (Adaptive pushover) (Seismostruct version 6)

Here, the distribution of horizontal incremental loading is not constant but varies basing on modal forms and participation factors obtained from the analysis of its eigenvalues forms after each load step (Seismostruct version 6).

The analysis can consider the degradation (Softening) of structure elements strength, the change of eigenvalues forms after each load step and change the internal forces due to spectral amplification.

This type of analysis gives satisfactory results for torsionally eccentric structures and structures where the higher modes influence the seismic response.

The used methodology is quite similar to the classical nonlinear static analysis (PO). The figure 7-9 depict some results of deformation capacity the strength check of the most loaded frame B.

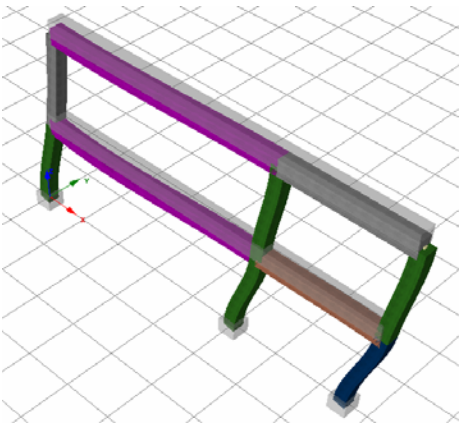

Fig. 7. Graphical view of performance criteria check for frame B of the structure ;

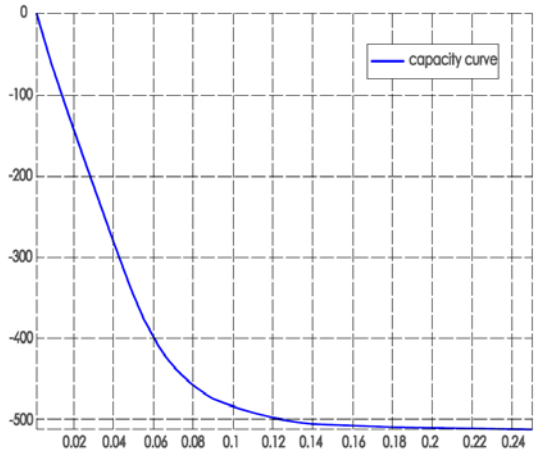

Fig. 8. Graphical view of capacity curve only for frame B of the structure

The curve of the relations in the function of displacement (incremental loading step) and the curve of the criterion of performance achieved for d_{max} report that the columns capacity to absorb the plastic deformation is greater than capacity of the beams. Consequently, the flexural capacity of the beams have been increased and the columns confined to achieve the performance determined, so that under the design earthquake the structure must achieve an acceptance criteria between Immediate Occupancy(IO) and Collapse Prevention(CP).

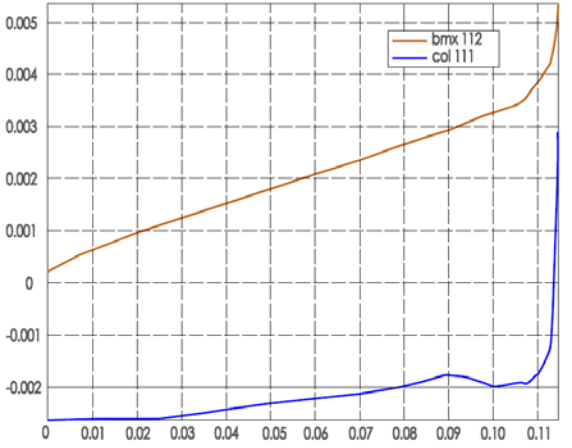

Fig. 9. Graphical view of θ-incremental deformation for the side column and the first story beam.

RESULTS

Depicted in the aforementioned figures, the flexural strength of the beams is more problematic. Four different approaches could be used for the rehabilitation of the structure: i) increasing the global capacity (strengthening) by the adding the cross braces or new structural walls, ii) reduction of the seismic demand by means of supplementary damping and/or use of base isolation systems, iii) increasing the local capacity of structural elements. This approach recognises the existing capacity of the structures and adopts a more cost-effective approach to selectively upgrade local capacity (deformation/ductility, strength or stiffness) of individual structural components and, iv) selective weakening retrofit. This is an intuitive approach to change the inelastic mechanism of the structure.

The third retrofit strategy approaches is in the present investigation applied due to the limited stiffness of the structure as it allows drifts to be carried out. Additional walls or braces are allowed due to architectural requirements. The use of seismic base isolation systems is quite expensive.

In our case, for this purpose we have used for the reinforcement of the beams longitudinal carbon fiber strips both in middle and supports and for columns confinement carbon fiber web.

Fiber design and placement of needed fibers is carried out following the Italian code CNR-DT 200/2004. Once the fiber design and placement of needed fibers is carried out, the structure with reinforced sections with distributed plasticity model could be checked out (Manfredi *et al.,* 2007).

Performance criteria with regard to flexure, shear strength, deformative capacity and the surface layer of column concrete are met when strengthening the elements the structures.

Figures 10 and 11 depict the results for the most loaded frame B.

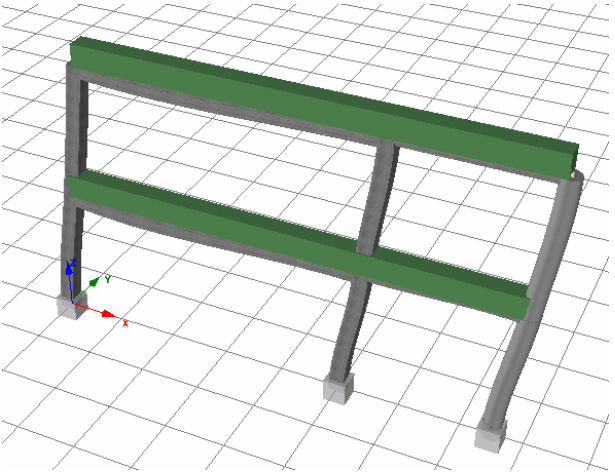

Fig. 10. Graphical view of performance criteria check for frame B of the structure after the increasing of capacity of structural elements.(no performance criteria is reached)

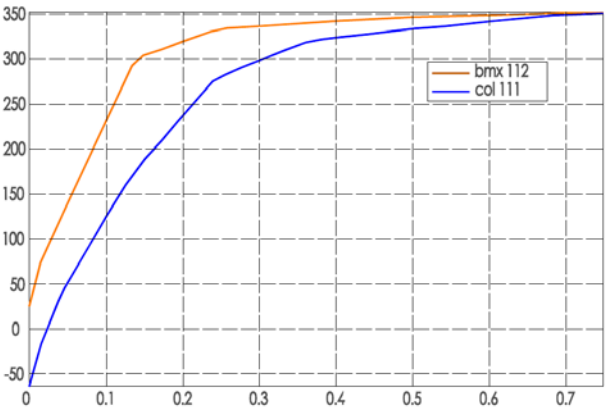

Fig. 11. Graphical view of M-incremental deformation step percentuality for the side column and the first story beam after the increasing of capacity of structural elements

DISCUSSIONS

The use of Adaptive pushover analysis is highly efficient and the results are consistent and close to the results from nonlinear dynamical analysis. Nevertheless, the use of this method remains limited to specialized software (Seismostruct version 6) and modeling requires plenty of time and care. If these analysis will not be implemented in ordinary commercial software the use of nonlinear dynamic analysis, although time-consuming will continue to

remain the most widespread method for the calculation of torsionally eccentric structures.

REFERENCES

American Society of Civil Engineers (ASCE). 2000. "FEMA356: Prestandard and commentary for the seismic rehabilitation of building,"Prestandard,Federal Emergency Management Agency(FEMA),Reston ,Virginia ,USA .

Applied Technology Council (ATC).1996. Seismic evaluation and retrofit of concrete buildings—volume 1 (ATC-40). Report No. SSC 96-01. Redwood City (CA).

Beyer K. Dazio A. Priestley, MJN. 2008. Seismic design of torsionally eccentric buildings with U-sped RC walls. IUSS Press, Pavia, Italy.

Computer and Structures, Inc. (CSI). 2000. SAP2000/NL-PUSH software, version 15, Berkeley (CA, USA).

European Committee For Standardization. EN 1998-1:2004 (E) Eurocode 8 (EC8). 2004. Design of structures for earthquake resistance.

Kushtet Teknike te Projektimit. K.T.P . Technical Conditions of Projecting. **1985**.

Manfredi G, Masi A, Pinho R, Verderame G, Vona M. 2007. Valutazione degli edifici esistenti in Cemento Armato. IUSS Press,Pavia, Italy.

Paulay T, Pristley MJN.1992. Seismic design of reinforced concrete and masonry buildings, John Wiley and Sons, Inc.

Pristley. MJN.2000. Performance – based seismic desing. Keynote address, Proceeding of the 12th Word Conference on Earthquake Engineering, Auckland, New Zealand.

Pristley MJN, Calvi GM, Kowalsky M.2007. Displacement-based seismic design of structures,IUSS Press,Pavia, Italy.

SeismoStruct version 6, Seismosoft Ltd., Via Boezio 10 27100 Pavia (PV) Italy**.**

ENVIRONMENTAL IMPLICATIONS OF SOME INDUSTRIAL SOLID WASTE AND AN ECONOMICALLY SOUND ALTERNATIVE FOR THEIR RECYCLING AND MANAGEMENT

Arjan KORPA
Department of Chemistry, Faculty of Natural Sciences, University of Tirana,Albania
Reinhard Trettin
Institute for Building and Materials Chemistry, University of Siegen, the Federal Republic of Germany

---

ABSTRACT

This paper highlights examples of waste utilization for energy recovery and environmental protection, expanding thus the alternatives for efficient solid waste management. It provides technical solutions to convert industrial waste by-products like slag (iron and steel slag) and fly ash found in the area into high value-added building materials and products. Many of these waste materials contain non-decaying elements and will remain in the environment for hundreds or perhaps thousands of years. Accumulation of massive amounts of such residues presents considerable environmental, aesthetic, economical and social problems. Meanwhile, re-evaluation of their use has taken place as significant energy has been invested in their generation and lost through disposal. Conversion of by-products into viable building and construction materials is probably the best way to recover this energy. Recycled materials can be a source of good quality, cost effective building materials that also benefit the environment. Conversion of by-products into building and construction materials is an appropriate solution as it helps conserve natural resources, while environmental damage caused by quarrying and pollution are reduced. The paper summarises the most advanced technologies and processing ways as well as own research results for converting fly ash and slag (iron and steel slags) by-products into high quality products that can be used in building sector.
Key words: *Clean environment, energy recovery, industrial solid waste management*

1 INTRODUCTION

Industrial waste is defined as waste generated by manufacturing or industrial processes. The major generators of industrial solid wastes are the by-products of thermal power plants producing coal ash, the integrated iron

and steel mills producing blast furnace slag and steel melting slag, non-ferrous industries like aluminium, zinc and copper producing red mud and tailings, sugar industries generating press mud, pulp and paper industries producing lime and fertilizer and allied industries producing gypsum. With the ever increasing quantities of industrial by-products and wastes solid waste management is gaining significant importance. In today's society, there are increasing requirements on recycling wastes and residues to the greatest possible extent. With the environmental awareness and scarcity of space for landfilling, wastes/by-products utilization has become an attractive alternative to disposal. The re-evaluation of "wastes" in which significant energy has been invested and lost through disposal via their conversion into sustainable construction materials and products is probably the best way to recover this energy (Goumans *et al*., 2001). The combination of interesting material properties and environmental acceptability makes these products suitable for application as building and construction materials. Among the waste by-products with major potentials for recycling are fly ash from thermal power plants and ferrous slags from metallurgical processes. This article is a literature survey on the main utilization of solid wastes like blast furnace slag, steel slag and fly ash generated in large quantities respectively from iron, steel industry and coal fired power plants, with emphasis on some recent innovations made by the authors. Specific innovations pertaining to utilization of these wastes that are highlighted in this paper include the production of fly ash bricks and the development of clinker free cements based on granulated blast furnace slag (GBFS).

1.1. Coal combustion by-products (CCBs)

Coal combustion by-products (CCBs) is a collective term referring to the residues produced during the combustion of coal regardless of ultimate utilization or disposal. It includes fly ash, bottom ash, boiler slag, and fluidised bed combustion ash and other solid fine particles (Asokan *et al*., 2005; http://www.ecoba.com). The CCBs represent incombustible materials left after combustion of coal in conventional and/or advanced clean-coal technology combustors.

1.1.1. Fly ash

The main product from the CCBs group is fly ash; it represents more than 75% of the generated CCBs. Fly ash is a heterogeneous mixture of inorganic particles, varying in shape, size, and chemical composition. Fly ash is predominantly composed of spherical glassy particles, which can be less than 1μm to more than 1mm in size. Major mineralogical component of fly ash is silica–aluminate glass containing Fe_2O_3, CaO, and MgO. Fly ashes are considered as pozzolans (substances containing silica and alumina) wherein

the silica reacts with calcium hydroxide $Ca(OH)_2$ released by hydration of calcium silicates to produce calcium silicate hydrate phases (Shi and Day 1993). It is when the silicate phases have an amorphous structure, rather than crystalline, that materials tend to be pozzolanic and contribute to the formation of hydration products when attacked by hydroxides. There are mainly two types of fly ash produced from coal combustion, type F or silicious and type C or calcareous fly ash. Type F is produced when anthracite, bituminous or sub-bituminous coal is burned and is low in lime typically less than 10% and contains more silica, alumina and iron oxide. Type C comes from lignite coal and contains more lime (15–30%) (Fisher *et al*., 1978). Fly ash has a hydrophilic surface and is extremely porous, with particle size the most important physical characteristic determining the reactivity. In general, smaller ash particles tend to be more reactive for two reasons. Firstly, smaller particles have larger specific areas making a large percentage of the particle available to attack by hydroxides. Secondly, and perhaps more significantly, smaller particles cool faster upon exiting the combustor, resulting in more disordered and, therefore, reactive structure. The surface area of fly ash ranges between 300 and 500m^2/kg. Generally, density of fly ash varies between 1.5 and 2.8 g/cm^3.

1.2. Ferrous slags

Various slags are produced as by-products in metallurgical processes or as residues in incineration processes. According to the origins and the characteristics, the main slags can be classified into three categories, namely ferrous slag, non-ferrous slag and incineration slag. Ferrous slag mainly includes iron slag (blast furnace slag), steel slag, alloy steel slag and ferroalloy slag. Blast furnace slag (BF slag) and steel slag make up the major part of ferrous slag.

1.2.1. Iron slag/blast furnace slag (BFS)

Blast furnace slag is defined as “the non-metallic product consisting essentially of calcium silicates and other bases that is developed in a molten condition simultaneously with iron in a blast furnace” (ASTM C989-99). In the production of iron, blast furnaces are loaded with iron ore, fluxing agents, and coke. When the iron ore, which is made up of iron oxides, silica, and alumina, comes together with the fluxing agents, molten slag and iron are produced. 220 – 370 kg slag per ton of iron may result (Proctor *et al*., 2000). Blast furnace slag is primarily made up of silica, alumina, calcium oxide, and magnesia (95%). Other elements like manganese, iron, sulfur, and trace amounts of other elements make up about other 5% of slag. The exact concentrations of elements vary slightly depending on where and how the slag is produced. BF slag can be cooled from its molten state in several ways to

form any of several types of BF slag products. Depending on the cooling method applied to blast furnace slag, the slag is divided into two types; air-cooled blast furnace slag and granulated with water to form Granulated Blast Furnace Slag (GBFS). The former is formed by gradual cooling in the air with occasional spray of water. The latter is formed by rapid cooling with continual spray of high-pressurized water, and possesses the characteristics of vitrified sand (Alexandre and Sebileau 1988). The latter has a variety of application areas, while the former can only be used as substitute of the crushed gravel for the road foundation material. Air-cooled slag has a rough finish and larger surface area when compared to aggregates of that volume which allows it to bind well with Portland cements as well as asphalt mixtures. Granulated blast furnace slag (GBFS) represents a wet sandy material. If dried and ground, it is called granulated blast furnace slag (GGBFS). Ground granulated blast furnace slag is a material that exhibits a distinct hydraulic reactivity only in the presence of suitable activators; it is considered latently hydraulic, unlike hydraulic materials, which exhibit hydraulic properties even when mixed with water alone (Pal *et al*., 2003).

1.2.2. Steel slag

Steel slag is produced from Basic Oxygen Furnace (BOF steel slag) and Electric Arc Furnace (EAF steel slag) in the steel making. It is the by-product of the steel producing process, containing fused mixtures of oxides and silicates. Its highly compressed structure results in a very dense and hard material. It is the coarse portion of the residues produced during the separation of the molten steel from impurities in steel making furnaces (Shi *et al*., 2004). Steel slag occurs to be in liquid melt of complex solution containing silicates and oxides, primarily calcium, iron, unslaked lime and magnesium and solidified upon cooling. Steel making process in electric arc furnaces generates up to 15% of slag per ton of steel. The structure of steel slag is based on two- and three-component compositions of the type CaO-SiO_2, CaO-FeO, CaO-SiO_2-MnO, CaO-Al_2O_3, CaO-FeO-SiO_2 and CaO-SiO_2-FeO-MgO (Lamut *et al*., 1992; Lamut and Gontarev 1994; Cioroi and Nistor 2007). The main mineral phases of BOF- and EAF-slags are metallic iron, dicalciumsilicate ($2CaO.SiO_2$), dicalciumferrite ($2CaO - Fe_2O_3$) and wustite (Motz *et al*., 2001). The CaO content varies between 42 and 55% and SiO_2 between 12 and 18%. But the mineral composition and mineral grain size are variable with chemical composition, cooling way and so on. For example, slow cooling of a typical BOF slag can produce larger phase grains than fast cooling (Fregeau-Wu *et al*., 1993). At higher basicities ($CaO/SiO_2+P_2O_5 >$ 2.5), tricalciumsilicate and lime (CaO) become dominant in steel slag (Huang and Wang, 2001). Other minerals reported in steel slag include periclase, manganosite, Fe and Mn-monticellite, Mn-cordierite, glass, and (Fe, Mn, Mg)

oxide solid solution (Radosavljevic *et al*., 1996). Materials added to the steel melt directly before the end of the reheating process are not fully embedded in the slag structure, so they can be found in the slag as "free"oxides (CaO, MgO). The content of free lime and free MgO is the most important component for the utilization of steel slags for civil engineering purposes with regard to their volume stability. In contact with water these mineral phases will react to hydroxides. Depending on the rate of free lime and/or free MgO this reaction causes a volume increase of the slag mostly combined with a disintegration of the slag pieces and a loss of strength. Therefore, the volume stability is a key criterion for using steel slags as a construction material. Steel slag can be air-cooled or water quenched. Most of steel slag production for granular materials use natural air-cooling process following magnetic separation, crushing and screening. The mineral composition of cooled steel slag varies and is related to the forming process and chemical composition. Fe in the steel slags is normally in the form of steel (7–10%), iron oxide and iron bearing minerals. Solid steel slag exhibits block, honeycomb shape and high porosity.

1.3. Industrial waste environmental concerns

There is growing concern about public health and degradation of groundwater quality from unregulated landfills. One of the major concerns with landfills of industrial solid waste is the leaching of heavy metals to surface and underground water source (Anderson *et al*., 1993; Sandhu *et al*., 1992). The release of metals or harmful elements from waste will cause environmental problems such as water and soil pollution. The effects of water pollution can be devastating to humans, animals, fish, and birds. Polluted water is unsuitable for drinking, recreation, agriculture, and industry. It diminishes the aesthetic quality of lakes and rivers. More seriously, contaminated water destroys aquatic life and reduces its reproductive ability. Eventually, it is a hazard to human health. Nobody can escape the effects of water pollution. A number of incidences have been reported in the past, where leachate had contaminated the groundwater (Kelly 1976; MacFarlane *et al*., 1983; Mor *et al*., 2006). According to the US Environmental Protection Agency (USEPA) the industrial solid waste is divided into hazardous and non-hazardous waste. Materials containing specific toxic chemical constituents which exceed regulated concentration levels are considered as hazardous waste (http://www.epa.gov/osw/nonhaz/index.htm). Hazardous waste/by-products contain heavy metals above regulated levels specified in various international standards. "Heavy metal" is a general collective term, which applies to the group of metals and metalloids with atomic density greater than 4000 kg/m^3, or 5 times more than water and they are natural components of the earth's crust (Garbarino *et al.*, 1995). Heavy metals are

extremely toxic for living beings and they are highly persistent pollutants. Once they get into the soil sub-surface or in groundwater, it becomes extremely difficult to handle them due to the complex speciation chemistry coming into play. Although some of them act as essential micro-nutrients for living beings, at higher concentrations they can lead to severe poisoning (Lenntech 2004). The most toxic forms of these metals in their ionic species are the most stable oxidation states e.g. Cd^{2+}, Pb^{2+}, Hg^{2+}, Ag^{+} and As^{3+} in which, they react with the body's bio-molecules to form extremely stable bio-toxic compounds which are difficult to dissociate (Duruibe *et al*., 2007). In the environment, the heavy metals are generally more persistent than organic contaminants such as pesticides or petroleum by-products. They can become mobile in soils depending on soil pH and their speciation. So a fraction of the total mass can leach to aquifer or can become bio-available to living organisms (Alloway 1990; Santona *et al*., 2006). Heavy metal poisoning can result from drinking-water contamination, intake via the food chain or high ambient air concentrations near emission sources (Lenntech 2004). The typical range of heavy elements (table 1) can vary within a wide range from trace to significant amounts well above the regulated concentrations specified by the international standards (table 2).

Table 1. The typical range of trace elements in coal fly ash and ferrous slag

Element	**Content in mg/kg**	**Element**	**Content in mg/kg**
Antimony	1-350	Lead	0.1-1000
Arsenic	1-110	Manganese	100-1555
Barium	0-4600	Mercury	0.01-7
Boron	5-900	Molybdenum	2-85
Cadmium	0-6	Nickel	100-700
Chloride	0-30000	Phosphorus	350-20000
Chromium	50-400	Selenium	2-200
Cobalt	1-170	Tin	900-2000
Copper	100-500	Vanadium	25-1500
Fluoride	0-18000	Zinc	120-1400

Table 2. Concentration limits for some heavy metals (Hashim *et al*., 2011)

Heavy metal	Speciation and chemistry	Concentration limits	References
Lead	Pb occurs in 0 and +2 oxidation states. Pb(II) is the more common and reactive form of Pb. Low solubility compounds are formed by complexation with inorganic (Cl^-,CO_3^{2-} ,SO_4^{2-} ,PO_4^{3-} and organic ligands (humic and fulvic acids, EDTA, amino acids). The primary processes influencing the fate of Pb in soil include adsorption, ion exchange, precipitation and complexation with sorbed organic matter	Surface agricultural soil: 7-20 ppm Soil levels: up to 300 ppm USEPA, Maximum Contaminant Level (MCL) in drinking water: 0.015 ppm	(Bodek et al., 1988; Evanko and Dzombak, 1997; Hammer and Hammer, 2004; Smith et al., 1995; WHO, 2000)
Chromium	Cr occurs in 0, +6 and +3 oxidation states. Cr (VI) is the dominant and toxic form of Cr at shallow aquifers. Major Cr(VI) species include chromate (CrO_4^{2-}) Þ and dichromate $Cr_2O_7^{2-}$ (especially Ba^{2+},Pb^{2+} and Ag^+). Cr (III) is the dominant form of Cr at low pH (<4). Cr (VI) can be reduced to Cr (III) by soil organic matter, S^{2-} and Fe^{2+} ions under anaerobic conditions. The leachability of Cr (VI) increases as soil pH increases	Normal groundwater concentration: < 0.001 ppm Lethal dose : 1-2g MCL of USEPA in drinking water: 0.1 ppm	(Lenntech, 2004; Smith et al., 1995)
Zinc	Zn occurs in 0 and +2 oxidation states. It forms complexes with a anions, amino acids and organic acids. At high pH, Zn is bio-available. Zn hydrolyzes at pH 7.0-7.5, forming $Zn(OH)_2$. It readily precipitates under reducing conditions and may co-precipitate with hydrous oxides of Fe or manganese	Natural concentration of Zn in soils: 30-150 ppm Concentration in plant: 10-150 ppm Plant toxicity: 400 ppm WHO limit in water: 5 ppm	(Evanko and Dzombak, 1997; Lenntech, 2004; Smith et al., 1995)
Cadmium	Cd occurs in 0 and +2 oxidation states. Hydroxide ($Cd(OH)_2$) and carbonate ($CdCO_3$) dominate at high pH whereas Cd^{2+} and aqueous sulphate species dominate at lower pH (<8). It precipitates in the presence of phosphate, arsenate, chromate, sulphide, etc. Shows mobility at pH range 4.5-5.5	Soil natural conc: >1 ppm Plant conc: 0.005-0.02 ppm Plant toxicity level: 5-30 ppm USEPA MCL in water: 0.005 ppm WHO: 0.01 ppm	(Matthews and Davis, 1984; Smith et al., 1995)

Arsenic	As occurs in -3, 0, +3, +5 oxidation states. In aerobic environments, As (V) is dominant, usually in the form of arsenate $(AsO_4)^{3-}$. It behaves as chelate and can co-precipitate with or adsorb into Fe oxyhydroxides under acidic conditions. Under reducing conditions, As(III) dominates, existing as arsenite $(AsO_3)^{3-}$ which is water soluble and can be adsorbed/co-precipitated with metal sulphides	MCL in drinking water- USEPA: 0.01 ppm	(Bodek et al., 1988; Smith et al., 1995)
Iron	Fe occurs in 0, +2, +3 and +6 oxidation states. Organometallic compounds contain oxidation states of +1, 0, -1 and -2. Fe (IV) is a common intermediate in many biochemical oxidation reactions. Many mixed valence compounds contain both Fe (II) and Fe (III) centers, e.g. magnetite and Prussian blue	Tolerable upper intake level (UL) - Dietary Reference Intake (DRI): For adults: 45 mg per day For minors: 40 mg per day	(Holleman et al., 1985; Medscape)
Mercury	Hg occurs in 0, +1 and +2 oxidation states. It may occur in alkylated form (methyl/ethyl mercury) depending upon the Eh and pH of the system. Hg^{2+} and Hg_2^{2+} are more stable under oxidizing conditions. Sorption to soils, sediments and humic materials is pH-dependent and increases with pH	Groundwater natural conc: <0.0002 ppm USEPA regulatory limit in drinking water: 0.002 ppm	(Bodek *et al*., 1988; Smith *et al*., 1995)
Copper	Cu occurs in 0, +1 and +2 oxidation states. The cupric ion (Cu^{2+}) is the most toxic species of Cu e.g. $Cu(OH)^{+}$ and $Cu_2(OH)^{2+}$. In aerobic alkaline systems, $CuCO_3$ is the dominant soluble species. In anaerobic environments CuS(s) will form in presence of sulphur. Cu forms strong solution complexes with humic acids	Soil natural conc: 2-100 ppm Normal range in plants: 5-30 ppm Plant toxicity level: 30-100 ppm USEPA MCL in water: 1.3 ppm	(Dzombak and Morel, 1990; LaGrega *et al*., 1994)

2. Main applications of fly ash and slags in construction industry

2.1. Fly ash main applications

Fly ash can be used either as a raw material in the production of the cement clinker, interground with the clinker, or blended with the finished cement. Fly ash can be utilized as a major component of blended cements (Korpa *et al*., 2012; Naik *et al*., 1995a; Naik *et al*., 1995b). It can be used as a replacement of sand up to 100% in manufacturing Controlled Low Strength Materials (CLSM), suitable for foundation support and backfilling of excavations, bridge abutments, buildings, retaining walls, utility trenches, etc.; for filling abandoned tunnels, sewers, and other underground facilities; and as embankments, grouts, etc (Naik *et al*., 1990; Naik and Singh 1997). Fly ash can be used in manufacturing of lightweight aggregates using sintered (fired) and unfired (cold bonded) processing methods reported that high volumes of Class C and Class F fly ashes can be used to produce high-quality concrete pavements with excellent performance (Courts 1991; Hay and Dumsten 1991; Ramme *et al*., 1995). Fly ash with and without silica fume can be used in manufacture of high-performance concrete (Korpa and Trettin 2004). High-performance concrete mixtures containing up to 30–40% fly ash can be proportioned to attain both high-strength and high-durability related properties. Naik *et al.*, (1995 a, b) have substantiated that concrete containing large amounts (more than 50%) of either class C or class F fly ash can be proportioned to meet strength and durability requirements for structural applications (Naik *et al*., 1995a; Naik *et al*., 1995b).

2.2. Slags main applications

2.2.1. GGBFS applications

Blast furnace slag has been used as a secondary cementing material for more than 100 years and there is a broad knowledge regarding its application. Most commonly it is used for the production of blended cements and slag cements. Currently, there is high interest in the application of this alternative material because the production of Portland cement clinker contributes about 5% to the global man-made CO_2 emissions. Despite the fact that the amount of available slag is limited, there is an increasing demand for slag cement to reduce the CO_2 emissions due to the production of cement and concrete (Lukasik *et al*., 2007). Recent reviews of the properties of blast furnace slag and its utilization for the production of blended cement were given by Taylor, Moranville - Regourd, Lang, and Glasser (Taylor 1997; Moranville-Regourd 1998; Lang 2002). Since BF slag contains little iron (Fe < 2%), recovery of metals from BF slag is not important.

2.2.2. Steel slag applications

The application of steel slags is closely related with their technical properties. Basically, the application can be divided into two parts. One is the direct application of steel slag in the iron and steel making process; the other includes recovery of metals from steel slag and then the application of the remaining steel slag outside the iron and steel making process. Recovery of metals and steel slag processing is needed prior to its application in the construction sector. Processing of steel slags for steel recovery is very important as it results in an angular, generally well-graded, material that is relatively free of metallics, and the recovered steel (2 to 4% of raw steel production) is a valuable scrap. Processed steel slag can be used in various applications, such as cement production, granular material in road base or sub-base courses and as aggregate in various concrete and asphalt mixes or pavement surfaces, (Tsakiridis *et al*., 2008; Shi 2004; Shen *et al*., 2009; Suer *et al*., 2009; Motz and Geisler 2001; Ahmedzade and Sengoz, 2009; Xue *et al*., 2006; Huang *et al*., 2007). The use of steel slag as an aggregate substitute to natural aggregates is considered a standard practice in many countries. The use of steel slag to replace natural aggregate in concrete is initially based on consideration of availability of natural resources and the good characteristics of steel slag. Steel slag possesses good physical properties which can be utilized in construction to enhance the characteristics of end products. Since it was discovered that the residue from the manufacture of steel could be crushed and processed into a product that looked like crushed rock, other testing was performed to determine the usefulness of this "waste" product. It was discovered that the highly angular, rough textured, vesicular, pitted surfaces provide the particle interlock, and if properly compacted, the high stability required for good serviceable pavements. Steel slags have superior skid and wear resistance compared to natural aggregates (Asi 2007). The principal problem associated with steel slag is volume expansion due to the hydration of free lime or magnesia that are common the components of steel slags. The calcium and magnesium oxides are not completely combined in steel slags, and there is general agreement in the literature that the hydration of unslaked lime (free CaO) and magnesium oxide (MgO) in contact with moisture is largely responsible for the expansive nature of most steel slags. The unslaked lime hydrates rapidly and can cause large volume changes in a few weeks. Magnesium oxide hydrates more slowly and contributes to the long-term expansion that may take several years to develop in the field, even when old steel slag dumps are being used. High levels of free lime or magnesia can adversely affect the performance of the materials made up of slag. Historically, the method of dealing with the free lime and magnesia has been to age the slag or accelerate the hydration reaction with water or washing

(Kneller *et al*., 1994). It is critical that these steel slags be checked for potential expansion, since even aging for long periods in large dumps does not guarantee the elimination of expansive behaviour (particularly if unprocessed so large lumps are involved).

3. Case-studies presentation/Own research results

3.1. Silicious fly ash bricks

Real-size bricks were produced from fly ash using a special set of mold and piston (figure 2). Pressed bricks were made using suitable siliceous (class F) fly ash as main constituent (at least 75% by mass), property modifying components and aerating agents. The fly ash was firstly sieved to a fineness which is close to the fineness of a Portland cement of strength class 42.5 N. The bricks were made by varying the proportions of fly ash, property modifying components, aerating agent and water. Two types of bricks; monolithic (without holes) and perforated bricks (with holes) were produced (figure 3). The molds were placed on a hydraulic pressing machine that applies the specified compaction pressure to shape the material into brick. After trying various water to binder ratios (blends of fly ash with the property modifying components), the most suitable water to binder ratio in terms of moldability, compaction and strength was chosen. The effect of compaction pressure on the fly ash compacts was previously studied by using various pressures at the optimum binder to water ratios. A fixed compaction pressure of 30 MPa was employed for the subsequent tests. Various combinations of fly ash and property modifying agents were tried and the most suitable specimens of this stage in terms of strength were further optimized by fine tuning their recipe. As suitable curing program in terms of strength gain rate, end strength, dimensions, appearance and production speed was found the initial curing for 24 hours in climate room (95% humidity and 25ºC) followed by water curing for up to six days at 20±1ºC. The brick specimens were subsequently visually inspected. Three specimens of fly ash bricks were tested for compressive strength after 7 days. The best bricks in terms of strength were further tested for their main properties including nominal value deviations, dry gross density, compressive strength, water absorption, initial suction rate and active soluble salts as required by the European standard for clay bricks (EN 771-1). For comparison, some regular commercial clay bricks were also tested. The properties of the fly ash bricks produced were tested based on the European standard for regular clay bricks.

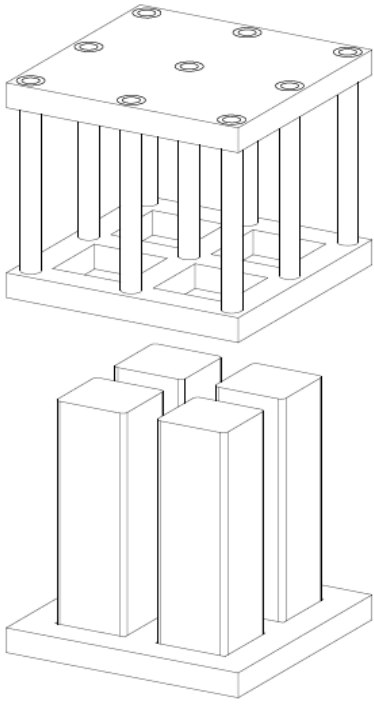

Fig. 1: Drawing of the special set of mold and piston employed for perforated brick production.

Fig. 2: Picture of a monolithic fly ash brick.

The compressive strengths of three specimens were tested in accordance with EN 772-1. For each tested specimen, the failure load was noted and recorded to estimate the uniaxial compressive strength.

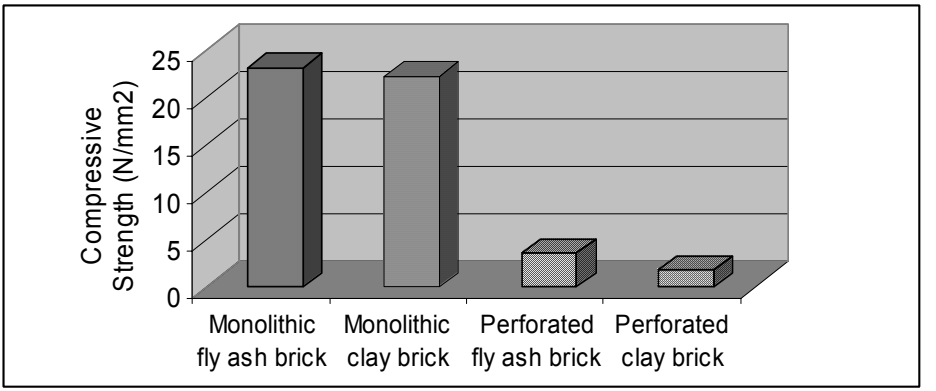

Fig.3. Compressive strengths of the four bricks types

.

In terms of compressive strength, the solid fly ash brick could develop compressive strength of more than 23 MPa (figure 4) after 7 days of curing, which exceeds that for clay or shale bricks (the average compressive strength of the clay brick tested was 20 MPa). The 7 days compressive strength of perforated fly ash brick is 3.6 MPa compared with 1.5 MPa which is the value recorded for the perforated regular clay brick (figure 4). The brick dimensions were measured with a caliber to establish compliance with the standard (EN 772-16). The recorded nominal value deviations along with the visual inspection of fly ash bricks indicate that fly ash bricks have more stable dimensions and are less prone to deformations than kilned clay bricks. They do not show any major shrinkage or expansion change apart from that related to that gained after the compaction pressure is released. The water absorption of both types of fly ash bricks was in all cases < 25%. Therefore the fly ash bricks meet the standard limit of water absorption for building clay bricks (< 25% after 90 minutes). The freezing and thawing resistance of both types of fly ash bricks was tested. For comparison, the regular commercial bricks were also tested. The tests were conducted according to ASTM standard C 67. This standard prescribes freezing and thawing cycles whereby each cycle consists of a 20 hours freezing at a temperature of –9ºC or lower and a 4 hours of thawing at 24±5.5ºC. Both types of fly ash bricks endured the 50 freezing and thawing cycles without significant damage. The strength of the bricks that successfully passed the 50 cycles was higher than 75% of the initial strength.

Further research is in progress to fully characterise the silicious fly ash bricks especially their durability aspects.

3.2. Clinker-free cements based on Granulated Blast Furnace Slag, (GBFS)

Five different granulated blast furnace slags (gbfs) were initially obtained for this research work, out of which only three gbfs products were selected and further employed for the development of the binders (clinker free cements). The selection was carried out based on theoretically assumed quality criteria by considering the gbfs chemical composition and degree of granulation. For simplicity the ggbfs will be referred to as "slag" hereafter. For commercial reasons the slag samples are labelled and will be referred to with their symbols without giving the plant names, as slag A, slag B, slag C, slag D, slag E. The results of the chemical composition of the slag samples assessed using the X-ray fluorescence method, are listed in table 3. In addition the requirements for ground granulated blast furnace slag (ggbfs) to be used as concrete addition and ggbfs to be used for the production of supersulphated cement are given. The SiO_2 content of the slags varies only slightly, the Slag A and Slag B are characterized by the highest CaO content (ca. 43%) and slag D by the lowest CaO content (ca. 29%). The later slag contains also the highest Al_2O_3 content that based on theoretical considerations is one of the various prerequisites for a positive response to sulphatic activation. The SO_3 content given in table 3 comprises the different forms of sulphur like sulphate and sulphide. From the difference between the sulphate and sulphide content calculated as SO_3, the sulphate content can be calculated which is maximally 0.3% SO_3. All employed slags fulfil the requirements (among them also the reactivity) to be used as concrete additive (EN 15167-1) and for the production of supersulphated cement (EN 15743). There is almost no difference between the own assessed chemical compositions and those provided by slag producers (slag plants), which shows that there is no considerable quality variation of the produced slag. Various activators were tested with all selected slags. We report here only the results and procedure of the binder development with the slag A. The setting time and compressive strength of respectively fresh and hardened pastes were assessed. The setting time of the binder depends on the mixing water quantity. In general, the setting time increases with the increase of the mixing water quantity. Therefore, initially the quantity of the mixing water and accordingly the water to binder ratio was kept constant at 0.38 (w/b = 0.38) for all pastes. As setting time reference was chosen the setting time of the paste prepared with Portland cement type CEM I 52.5 and having a water to cement (binder) ratio of 0.38 (w/c = 0.38). Its setting time was measured and resulted to be 270 minutes.

The results of setting time and compressive strength are listed in table 4. The setting time range for the binder to be used as cement should be in the range of 40 – 500 minutes in order to have any practical application interest, whereas the 2 days compressive strength should be at least 10 N/mm^2. Based on the results listed in table 4, the best activators (those giving pastes with properties of practical application interest) were chosen for further trials with slag A. The best activators were further employed at various contents with the purpose of assessing their influence on setting time and compressive strength properties of the resulting pastes.

Table 3. Chemical composition of the employed granulated blast furnace slags (gbfs) as well as the requirements of the standard (EN 15167-1) and standard (EN 15743)

Item	Unit	Slag A	Slag B	Slag C	Slag D	Slag E	EN 15167-1
SiO_2 "S"	[m.%]	34.9	36.2	31.4	33.6	33.0	
CaO "C"		42.5	43.0	38.8	29.1	40.0	
MgO "M"		6.1	6.4	11.5	15.8	6.2	≤ 18.0
Al_2O_3		7.1	6.0	8.4	12.1	11.0	
SO_3 *		2.0	2.0	4.1	3.2	3.0	≤ 2.5
TiO_2		0.47	0.17	1.8	2.2	1.0	
MnO		0.3	0.19	0.4	0.6	0.2	
K_2O		0.53	0.68	0.5	0.5	0.4	
Na_2O		0.51	0.56	0.5	0.4	0.3	
Fe_2O_3		0.52	0.15	0.4	0.2	0.3	
Sulphide		0.75	0.79	1.52	1.21	1.08	≤ 2.0
Others		5.0	4.0	0.0	2.0	3.0	
Sum		95.0	96.0	100.0	98.0	97.0	
Loss on ignition (LOI)		0.45	0.41	2.5	0.5	1.2	≤ 3.0
C + M + S		84.0	86.0	82.0	79.0	79.0	≥ 66.7
(C + M)/S	[-]	1.4	1.4	1.6	1.3	1.4	> 1.0

- Total sulphur content given as SO_3

In table 5 are listed the results of pastes prepared with the best activators of table 4 that were employed with various contents along with the effects of this variation on setting times and compressive strengths. The water to binder ratio was also varied in order to understand the influence of the water quantity on the properties of interest. The paste with 3.1% A_{10} was double prepared and tested in order to see the repeatability of the results. The difference in terms of setting time (20 minutes) was relatively small and within known limits as with common cements pastes. There is however a remarkable influence of the activator content on the setting time and compressive strength. This shows on one hand that relatively small variations of the

activator content brings about considerable alteration of the binder properties and on the other hand it shows that the optimization of the binder properties can be carried by only small variations of the activator content. With slag A and the activator A_{10}, at its optimal content, pastes for the 90 and 180 days compressive strengths were produced (table 3). With the purpose of comparing the setting time of the paste prepared with activator A_{10} and of the paste prepared with Portland cement (reference paste) according to EN 197-1, another series of pastes were prepared by varying the water to binder ratio until the standard consistence is achieved. In table 6 are listed the results of the slag series and of the reference paste. For comparison purpose in table 6 are shown also the needle penetration depth and setting time (175 minutes) of a reference paste prepared with Portland cement type CEM I 52.5 R at standard consistence. In the same table are listed also the results showing the influence of varying the water content of the pastes prepared with activator A_{10}. For the same needle penetration depth (standard consistence) the required water to binder ratio of the paste with A_{10} was only 0.246 (w/b = 0.246). The setting time of this paste was 117 minutes. Based on this result and on the 2, 7 and 28 days strength results (pastes with activator A_{10} in table 5) it can be stated that this combination of slag A – activator A_{10} – water behaves very similarly to a paste prepared with Portland cement.

Table 4. Pastes with slag A and various activators showing properties of practical application interest (w/b = 0.38); a "x" means the paste shows properties of practical application range.

Activator	Dosage	Activator showing practical application interest		**Chosen for further trials**
	[m.% vs. s*]	**Setting time (between 80 - 500 minutes)**	**2-days-compressive strength (>10 N/mm^2)**	
A_1	7.74		x	
A_1	3.87		x	
A_4	5.42	x	x	x
A_7	7.56	x	x	x
A_8	6	x	x	x
A_{10}	4.42	x	x	x
S_1	6		x	
A_2	8			
A_2	12	x		
A_3	6		x	
A_3	3		x	
S_5	6		x	
A_{11}	3.96		x	

* s means slag

Table 5. Test results for pastes prepared with best activators and slag A

Activator	*Dosage*	*w/s**	*Setting time*	*Compressive strength*					
				2	*7*	*28*	*90*	*180*	
	[m.% vs. s*]	**[-]**	**[min]**	**[N/mm^2]**					
A_3	10.0	0.38	110	42.5	55.0				
A_3	8.5	0.38	255	36.0	51.0				
A_3	8.0	0.38	341	35.0	45.0				
A_4	3.5	0.36	110	15.5	23.5				
A_4	2.8	0.35	130	12.0	27.0				
A_7	3.0	0.36	2036	12.5	31.5				
A_7	6.0	0.36	170	40.5	64.5				
A_7	5.8	0.37	241	34.5	58.5				
A_7	5.0	0.36	907	33.0	60.5				
A_7	5.7	0.37	130	34.0	64.5				
A_8	3.0	0.36	410	23.5	37.5				
A_8	4.5	0.35	190	38.0	54.0				
A_8	4.3	0.37	231	32.5	44.0				
A_8	4.2	0.36	690	13.0	29.5				
A_8	4.4	0.36	230	36.0	49.7	58.5			
A_9	6.3	0.36	120	54.0	61.5				
A_9	5.7	0.345	130	56.0	59.5				
A_9	5.0	0.33	150	48.5	55.5				
A_9	3.6	0.32	300	39.0	53.5				
A_9	3.8	0.32	300	40.5	44.0				
A_{10}	3.5	0.35	270	28.0	37.0				
A_{10}	3.0	0.34	310	27.0	38.5				
A_{10}	3.2	0.33	255	31.5	43.0				
A_{10}	3.1	0.32	270	33.0	48.0	49.5	68.0	73.5^a	70.5^w

* s – means slag, **a -** the specimen was cured in air (> 90 % r.h. and 20 °C),
w - the specimen was cured in water (20 °C)

Table 6. Setting time for the paste prepared with slag A – A_{10} as well as the same property of the reference paste with Portland cement type CEM I 52.5 R with a w/c ratio of 0.306; the setting time of the paste showing a penetration depth of 7 - 8 mm corresponds to the standard consistence of (6 ± 2 mm) according to EN 196-3

Activator	***Dosage [m.% vs. s*]***	***w/s****	***w/b*****	***Penetration depth [mm]***	***Setting time [min]***
A_{10}	3.1	0.235	0.228	Not applicable	Instantly
		0.285	0.276	0	176
		0.265	0.257		151
		0.255	0.247		132
		0.246	0.239	7	117
For comparison the reference paste					
CEM I 52.5 R		0.306	-	8	175

* s - means slag** b - means binder (slag + activator)

3.3. Concrete with steel slag aggregates (SSA)

Steel slag aggregates (SSA) were produced from samples of water cooled steel slag. The samples were allowed to stand in stockpiles for 6 months and exposed to weather so that the hydration process between lime and magnesia with water takes place. The aged samples were crushed and screened to produce the specified graded sizes. The average expansion of all fractions that was tested based on the standard ASTM 4792 was 0.017% at 7 days which is much lower than the limit value. In table 7 is summarized the leachate results of SSA along with TCLP regulatory limits. It is very clear from the results presented in table 7 that the average values of metals under consideration do not violate the limits set in TCLP regulation levels.

Table 7. Summary of leacheate results of SSA

Heavy metals (TCLP Extract)	**Method**	**Result obtained (mg/litre)**	**TCLP limits (mg/litre)**
Barium (Ba)	USEPA 1311/6010 C	0.905	100
Cadmium (Cd)	USEPA 1311/6010 C	<0.005	1.0
Chromium (Cr)	USEPA 1311/6010 C	<0.005	5.0
Lead (Pb)	USEPA 1311/6010 C	<0.005	5.0
Manganese (Mn)	USEPA 1311/6010 C	0.038	n.r
Nickel (Ni)	USEPA 1311/6010 C	<0.005	n.r
Silver (Ag)	USEPA 1311/6010 C	<0.005	5.0
Zinc (Zn)	USEPA 1311/6010 C	<0.005	n.r
Arsenic (As)	USEPA 1311/Hydride/6010 C	<0.002 µg/litre	5.0
Mercury (Hg)	USEPA 1311/Hydride/6010 C	<0.01 µg/litre	0.2

n.r – not required

Therefore, the use of SSA is safe and should not induce any contamination even in areas where ground water table is shallow. Some of the physico-mechanical properties of the SSA aggregates (the results represent average values of all fractions) that were assessed based on relevant international standards are shown in table 8.

Table 8. Some physico-mechanical properties of SSA (average values of all fractions)

Property of SSA	**Measured value**	**Standard value**
Flackiness index	6%	<30%
Elongation index	24%	<35%
Aggregate crushing value	18%	n.r
Aggregate impact value	13%	<32%
Los Angeles abrasion value	17%	<40%
10% fines value	180 kN	>150 kN
Clay lumps and friable particles	0.1%	<2%
Percentage of material finer than 75 micron	1.0%	<2%
Apparent particle density (specific gravity)	3340 (kg/m^3)	>2800
Bulk density (compacted)	1640 (kg/m^3)	>1600
Shell content	nil	<3%
Water absorption	1.4%	<1.5%

For producing the concrete mix with SSA, part of the largest size (10-20mm) of natural aggregate was replaced with SSA and mixed with gabbro (5-10mm) in order to compensate for the larger specific gravity of the SSA. The mix design of reference concrete and of the concrete mix that contains SSA is shown in table 9.

Table 9. Mix design for reference concrete and concrete that contains SSA

Raw material	**Ref. concrete mix**	**Concrete mix with SSA**
	kg/m^3	
Cement (OPC)	400.0	400.0
Water	156.0	156.0
Natural aggregate (10-20mm) SSA (10-20mm)	719.6 -	- 412.4
Natural aggregate (5-10mm) SSA (5-10mm)	480.4 -	- 274.3
Gabbro (5-10mm)	-	599.5
Washed sand	762.3	762.3
Superplasticizer	5.3	6.57

A higher amount of superplasticizer was required for the concrete with SSA in order to achieve the same slump for both concrete mixes. The results show that replacing about 50 to 75% of steel slag aggregates by volume for natural aggregates will not do any harm to concrete and also it will not have any adverse effects on the strength (table 10). The cement-aggregate interface seemed to be very dense without cracks or other discontinuities. As opposed to the microscopic pores of porous natural aggregates the macroscopic cavities of SSA improve the properties of concrete.

Table 10. Properties of reference concrete and of concrete that contains SSA

Property of concrete	**Ref. concrete mix**	**Concrete mix with SSA**
Slump (mm)	180	180
Temperature (□C)	22.7	22.7
Unit weight (kg/m^3)	2507	2507
Air content (%)	5.0	5.0
Compressive strength (MPa)		
7 days	50.3	47.3
28 days	58.8	55.0
56 days	63.0	60.4
Average density (kg/m^3)	2470	2515

4. CONCLUSIONS

The paper takes a critical look into the environmental implications of waste produced by power and ferrous metallurgical industries. A careful literature survey has been carried and the most advanced ways and methodologies of some industrial waste by-products utilization in building sector are briefly summarized. A few innovative ways to turn the industrial waste into high value-added building products, derived by own research, are highlighted. The specific innovations pertain to the production of silicious fly ash bricks, development of clinker free cements based on granulated blast furnace slag (GBFS) and production of concrete with water cooled steel slag aggregates. The developed products have properties that are practically similar to traditional ones. These methodologies and ways of waste recycling are on the cutting edges of energy recovery, sustainable development and environmental protection. Gainful utilization of the metallurgical wastes, reduction in CO_2 gas, environmental, cost and energy savings are the salient features of these methodologies. The incorporation of waste materials into high valuable building products rather than their disposal appears to be the economical solution that contributes to the protection of the environment. The heavy metals contained in the waste by-products can be chemically bonded to

be structural part of the building material. Hence the building materials that contain the waste by-products represent significantly lower leaching abilities and there is no significant influence of hazardous elements on the surrounding waters and soil due to leaching.

REFERENCES

Ahmedzade P, Sengoz B. 2009. Evaluation of steel slag coarse aggregate in hot mix asphalt concrete. *Journal of Hazardous Materials.***165 (1),** 300–305.

Alexandre J, Sebileau JL. 1988. *Le laitier de haut-fourneau*, éditions CTPL.

Alloway BJ. 1990. Soil Processes and the behavior of metals. (In: Alloway, B.J. (Ed.) Heavy Metals in Soils). New York, Blackie, J Wiley and Sons, Inc., 7-28.

Anderson MA, Bertsch PM, Zelazny LW. 1993. Multi component transport through soil subjected to coal pile runoff under steady saturated flow. In: Keefer R. F. , Sajwan K., editors. Trace element in coal and coal combustion residues. Advances in trace substances research. Florida: Lewis Publishers, CRC Press, pp. 137–162.

Asokan P, Saxena M, Asolekar SR. 2005. Coal combustion residues - environmental implications and recycling potentials. *Resources*, *Conservation* and *Recycling.* **43 (2),** 239–62.

Asi IM. 2007. Evaluating skid resistance of different asphalt concrete mixes. *Building and Environment.* **42(1)**, 325–329.

Cioroi M, Nistor L. 2007. Recycling possibilities of metallurgical slag, *The Annals of "Dunarea De Jos"* .University of Galati. Fascicle *IX. Metallurgy and Materials Science* .(**1**), 78-82.

Courts GD. 1991. The aggregate of the future is here today. In: Proceedings of the Ninth International Ash Use Symposium, ACAA. 121-1–121-10.

Duruibe JO, **Ogwuegbu MO**, **Egwurugwu JN. 2007.** Heavy metal pollution and human biotoxic effects. *International Journal of Physical Sciences.* **2 (5),** 112-118.

Fregeau-Wu E, Pignolet-Brandom S, Iwasaki I. 1993. *Liberation analysis of slow-cooled steelmaking slags: implications for phosphorus removal.* Proceedings of the 1st International Conference on Processing Materials for Properties, Sponsored by: TMS; MMIJ Publ by Minerals, Metals & Materials Soc (TMS), 153–156.

Gerald L. Fisher GL, Bruce AP, David S, John MO, Arthur HB, Richard CR, McFarland AR. 1978. Physical and Morphological Studies of

Size-Classified Coal Fly Ash. *Environmental Science and Technology*. **12**, (4), 447-451.

Garbarino JR, Heidi CH, David AR, Ronald CA, Terry IB, Howard ET. 1995. Contaminants in the Mississippi river. U. S. Geological Survey Circular, Virginia, U.S.A. 1133. http://pubs.usgs.gov/circ/circ1133/heavy-metals.html.

Glasser FP. 1991. Chemical, mineralogical, and microstructural changes occurring in hydrated slag-cement blends. in: J. Skalny, S. Mindess (Eds.). *Materials Science of Concrete II.* American Ceramic Society, Westerville (Ohio). **2**, 41–81.

Goumans JJJM, Van Der Sloot HA, Aalbers ThG. 1991. *Waste materials in construction. Studies in environmental science.* Elsevier Science Publishers B.V. Amsterdam, the Netherlands.

Hashim MA, Mukhopadhyay S, Sahu JN, Sengupta B. 2011. Remediation technologies for heavy metal contaminated groundwater. *Journal of Environmental Management.* **92**,(10), 2355-2388. http://www.researchgate.net/publication/51252917_Remediation_technologies_for_heavy_metal_contaminated_groundwater

Hay PD, Dunstan ER. 1991. Lightweight aggregate production and use in Florida. In: Proceedings of the Ninth International Ash Use Symposium. 1, 22-1–22-10.

Huang X, Wang F. 2001. An overview of steel slag processing and utilization. *Journal of. Manganese Ore of China.* **3**, 2001.

Huang Y, Bird RN, Heidrich O. 2007. A review of the use of recycled solid waste materials in asphalt pavements, *Resources of Conservation Recycling*. **52**, 58–73.

http://www.ecoba.com

http://www.epa.gov/epawaste/index.htm

Kelly E. 1976. Groundwater pollution near a landfill. *Journal of Environmental Engineering*. **102**, 1189–1199.

Kneller WA, Gupta J, Borkowski ML, Dollimore D. 1994. Determination of original free lime content of weathered iron and steel slags by thermogravimetric analysis, *Transportation research record 1434*, National Research Council, Washington, DC.

Korpa A, Trettin R. 2004. *The use of synthetic colloidal silica dispersions for making high performance and ultra-high performance systems (HPC/UHPC)*. International Symposium on Ultra High Performance Concrete, September 13-15, Kassel, Germany, 155-164.

Korpa A, Xhaxhiu K, Mele A, Seiti B, Spahiu E. 2012. *High volume fly ash cement an economical approach for reducing the pollution impact of the thermal power plant by-products in the Ohrid area.* International Conference

on Water, Climate and Environment. BALWOIS 2012 – 28 May to 2 June 2012 - Ohrid, Republic of Macedonia.

Lamut J, Gontarev V, Koch K. 1992. *Composition change during the slag phaseation both in the blast furnace and EAF slag.* 4th International Conference on Molten Slag and Fluxes, Sendai, Japan, 481-486.

Lamut J, Gontarev V. 1994. *The phase composition of slag in the steel making.* International Scientific Conference on the Occasion of the 35th Anniversary of the Department of the Ferrous and Foundry Metallurgy, Metallurgical Faculty, Technical University, Košice, 560-567.

Lang E. 2002. *Blast furnace cements, in: Bensted J., Barnes P. (Eds.), Structure and Performance of Cements*, Spon Press, London. 310–325.

Lenntech 2004. *Water treatment*. Lenntech, Rotterdamseweg, Netherlands (Lenn-tech water treatment and air purification).

Lukasik J, Damtoft JS, Herfort D, Sorrentino D, Gartner EM. 2007. *Sustainable development and climate change initiatives,* in: Proceedings of the 12th International Congress on the Chemistry of Cement, 8.-13.7.2007, Montreal, MPL-1.

MacFarlane DS, Cherry JA, Gillham RW, Sudicky EA. 1983. Migration of contaminants in groundwater at a landfill: A case study. 1. Groundwater flow and plume delineation. *Journal of Hydrology*. **63**, 1-29.

Mor S, Ravindra K, Dahiya RP, Chandra A. 2006. Leachate characterization and assessment of groundwater pollution near municipal solid waste landfill site. *Environmental Monitoring and Assessment*. **118**, 435–456.

Moranville-Regourd M. 1998. *Cements made from blast furnace slag, in: Hewlett P. C. (Ed.), Lea's Chemistry of Cement and Concrete,* Arnold, London, pp. 633–674.

Motz H, Geiseler J. 2001. Products of steel slags an opportunity to save natural resources, *Waste Manage.* **21**, 285–293.

Naik TR, Ramme BW, Kolbeck HJ. 1990. Filling abandoned underground facilities with CLSM fly ash slurry. *ACI Concrete International* .**12 (7),** 1–7.

Naik TR, Singh SS, Belonger SJ. 1995a. Development of manufacturing technology for low-cost, high performance, blended cements in Wisconsin. Experimental investigation CBU-1995-06. UWM Center for by-products utilization, University of Wisconsin – Milwaukee.. 47.

Naik TR, Singh SS, Hossain MM. 1995b. Properties of high performance concrete incorporating large amounts of high - lime fly ash. *International Journal of Construction and Building Materials.* **9 (4),** 195–204.

Naik TR, Singh SS. 1997. Permeability of flowable slurry materials containing foundry sand and fly ash. *ASCE Journal of Geotechnical and Geoenvironmental Engineering.* **123, (5),** 446–452.

Pal SC. Mukherjee A, Pathak SR. 2003. Investigation of hydraulic activity of ground granulated blast furnace slag in concrete. *Cement and concrete research*. **33 (10)**, 1481-1486.

Proctor DM, Fehling KA, Shay EC, Witteborn JL, Green JJ, Avent C, Bigham RD, Connolly M, Lee B, Shepker TO, Zak MA. 2000. Physical and Chemical Characteristics of Blast Furnace, Basic Oxygen Furnace, and Electric Arc Furnace Steel Industry Slags. *Environmental Science and Technology*. **34(8)**, 1576-1582.

Radosavljevic S, Milic D, Gavrilovski M. 1996. Mineral processing of a converter slag and its use in iron ore sintering. *Magnetic and electrical separation.* **7 (4),** 201–211.

Ramme BW, Nechvatal T, Naik TR, Kolbeck HJ. 1995. By-product lightweight aggregates from fly ash. In: A paper presented and pre-print published at the 1995 fall convention of ACI; 22.

Sandhu SS, Mills GL, Sajwan KS. 1992. Leachability of Ni, Cd, Cr, and As from coal ash impoundments of different ages on the Savnath river site. In: Keefer RF, Sajwan K, editors. Trace Element in Coal and Coal Combustion Residues. Advances in Trace Substances Research. Lewis Publishers, CRC Press. 165–182.

Santona L, Castaldi P, Melis P. 2006. Evaluation of the interaction mechanisms between red muds and heavy metals. *Journal of Hazardous Materials.* **136 (2)**, 324-329**.**

Shen W, Zhou M, Ma W, Hu J, Cai Z. 2009. Investigation on the application steel slag-fly ash-phosphogypsum solidified material as road base material. *Journal of Hazardous Materials.* **164 (1**), 99–104.

Shi C, Day RL. .1993. Chemical activation of blended cements made with lime and natural pozzolans. *Cement and Concrete Research*. **23**, **(6),** 1389-1396.

Shi C. 2004. Steel slag—its production, processing, characteristics, and cementitious properties. *Journal of Materials in Civil Engineering* . **16 (3),** 230-236.

Suer P, Lindqvist JE, Arm M, Frogner-Kockum P. 2009. Reproducing ten years of road ageing-accelerated carbonation and leaching of EAF steel slag. *Science of the Total Environment*. **407**, 511–518.

Taylor HFW. 1997. Cement Chemistry.Thomas-Telford, London.

ASTM C989-99, The American Society for Testing and Materials.

Tsakiridis PE, Papadimitriou GD, Tsivilis S, Koroneos C. 2008. Utilization of steel slag for Portland cement clinker production, *J. Hazard. Mater*. **152**, (2) 805–811.

Xue Y, Wu S, Hou H, Zha J. 2006. Experimental investigation of basic oxygen furnace slag used as aggregate in asphalt mixture. *Journal of Hazardous Materials.* **B138**, 261–268.